A Refined Chronology for the Middle–Upper Paleolithic Transition at Kozarnika Cave (Bulgaria) 40–50,000 Years Ago: New AMS Radiocarbon Dates and Implications for Early *Homo sapiens* in Europe

RACHEL HOPKINS
RLAHA, University of Oxford, Oxford, UNITED KINGDOM; and, Meow Wolf, Inc., 1352 Rufina Circle, Santa Fe, NM 87507, USA; rja.hopkins@protonmail.com

JEAN-LUC GUADELLI*
PACEA-UMR 5199 CNRS, Université de Bordeaux, Allée Geoffroy St Hilaire, Bâtiment B2, CS 50023, 33615 Pessac cedex, FRANCE; jean-luc.guadelli@u-bordeaux.fr

DUSTIN WHITE
Department of Chemistry, University of York, UNITED KINGDOM; dustin.white@york.ac.uk

CHRIS STRINGER
Natural History Museum, Cromwell Road, London, UNITED KINGDOM; c.stringer@nhm.ac.uk

EMESE VÈGH
Department of Evolutionary Anthropology, University of Vienna, University Biology Building, Djerassiplatz 1, A-1030 Vienna; and, Human Evolution and Archaeological Science (HEAS) Network, Vienna, AUSTRIA; emese.vegh@univie.ac.at

MICHAEL BUCKLEY
Manchester Institute of Biotechnology, University of Manchester, M1 7DN, UNITED KINGDOM; M.Buckley@manchester.ac.uk

ALETA GUADELLI
Center for Underwater Archaeology, State Cultural Institute, Ministry of Culture, Str. Apollonia n°1, 8130 Sozopol, BULGARIA; aleta.guadelli@gmail.com

PHILIPPE FERNANDEZ
LAMPEA UMR 7269, CNRS, Aix Marseille Univ., Minist. Culture, MMSH, 5 Rue du Château de l'Horloge, F13094, Aix-en-Provence, FRANCE; philippe.fernandez@univ-amu.fr

NIKOLAI SIRAKOV
National Institute of Archaeology with Museum-Bulgarian Academy of Sciences, 2, Saborna Street, 1000, Sofia, BULGARIA; nikolaysirakov@gmail.com

TOM HIGHAM*
Department of Evolutionary Anthropology, University of Vienna, University Biology Building, Djerassiplatz 1, A-1030 Vienna; and, Human Evolution and Archaeological Science (HEAS) Network, Vienna, AUSTRIA; thomas.higham@univie.ac.at

*corresponding authors: Jean-Luc Guadelli; *jean-luc.guadelli@u-bordeaux.fr*; and Tom Higham; *thomas.higham@univie.ac.at*

submitted: 19 March 2025; revised 30 October 2025; accepted: 30 October 2025

Handling Editor in Chief: Karen Ruebens

ABSTRACT

The site of Kozarnika in Bulgaria is a key, deep (~6m) archaeological sequence spanning the Lower, Middle and Upper Paleolithic of Europe. In its latter phases, it documents the transition from a Neanderthal-dominated Europe to one in which only modern humans are present. The process of this transition is of major importance to understanding the timeline of hominin dispersals, extinctions and replacement in Europe. We obtained 37 new AMS radiocarbon dates to build a robust chrono-stratigraphy for the site through sampling humanly modified bones, artifacts and human remains. We focussed particularly on dating the Initial Upper Paleolithic phase of the occupation, in geological layer 6/7, because of its potential link with early dispersing *Homo sapiens* populations and the presence of co-mingled human remains in the layer itself. The latter phases of human occupation at Kozarnika comprised five distinct periods, dated between about 50–26,000 years ago. We found that the 6/7 phase ranged from 48,500–44,050 cal BP, probably starting from about 49,960 cal BP. The stone tool evidence from the layer contains some Levallois pieces with echoes of the earlier Middle Paleolithic. One possible scenario is that both Neanderthals and early modern humans alternated in their use of the site during this period. Aside from the evidence from Apidima (Greece) which has been argued to evidence *Homo sapiens* at about 210,000 years ago (Harvati et al. 2019), Kozarnika is the earliest site found in southeastern Europe from the last 100,000 years which contains evidence for the presence of modern humans.

INTRODUCTION

Between ~60–30,000 years ago, during the late Middle and early Upper Paleolithic periods, a dynamic and formative phase of human evolution takes place. Major expansions in the distribution of modern humans can be observed as they move into Eurasia; there is adaptation to new environments, the co-existence of hominin groups such as Neanderthals and Denisovans at regional and continental scales, and occasional genetic (and possibly cultural) admixture between them. Following the major and widespread dispersal of modern humans across Eurasia after 60,000 years ago, Neanderthals were replaced during the so-called Middle to Upper Paleolithic transition (Stringer 2022). Their disappearance has been estimated to have occurred in Western Europe between 41–39,000 years ago (Higham et al. 2014).

Dates of early modern human bone remains, and age estimates from archaeological sites, suggest that there must have been a considerable overlap between late Neanderthal and early human populations. Higham et al. (2014) estimated this at between ~2600–5400 years and subsequent work has confirmed this (Djakovic et al. 2022). Interbreeding has been identified between these modern humans and Neanderthals too (Fu et al. 2015; Green et al. 2010; Hajdinjak et al. 2018), raising the possibility of hybrid populations being present during this period. This suggests that linking biological populations with lithic remains from archaeological sites is likely to be extremely challenging and controversial. Recent findings, however, suggest that we might be able to address this. A combination of proteomics, genomics, and archaeology, for example, has shown that the early Upper Paleolithic "Lincombian-Ranisian-Jerzmanowician" (LRJ) technocomplex of northern Europe was probably made by modern humans (Mylopotamitaki et al. 2024). The LRJ from the Illsenhöhle site at the castle of Ranis dates to 47–45,000 cal BP (Mylopotamitaki et al. 2024). Previously, it was not known whether Neanderthals or modern humans were the authors, but ancient genomics confirms that it was the latter, albeit with some previous Neanderthal ancestry. Material from Initial Upper Paleolithic (IUP) contexts at the Bacho Kiro site (Bulgaria) was revealed in 2020 to be linked to *Homo sapiens* too, dating back as far as 46–45,000 cal BP (Hajdinjak et al. 2020; Hublin et al. 2020). In France, at the Grotte Mandrin, human remains associated with the IUP-like Neronian technocomplex are even earlier (~54,000 cal BP) (Slimak et al. 2022), although the case would be made stronger with additional genetic evidence. The notion of a mosaic-like distribution of hominins and a long overlap between them is an apt description of the situation (Higham et al. 2014).

Dating accuracy and precision is of paramount importance in studies of the Middle to Upper Paleolithic and its spatio-temporal pattern. Thankfully, there have been several improvements in chronometric dating recently, which means we are now in a strong position to provide reliable chronologies to what is a challenging period to date, particularly for the radiocarbon method (Devièse et al. 2018; Fewlass et al. 2017; Higham 2011; Higham et al. 2006). The latest iteration of the INTCAL calibration curve, INTCAL20, enables calibration back to 55,000 cal BP (Reimer et al. 2020), in turn enabling the application of Bayesian statistical approaches and the building of chronometric models combining radiocarbon and other age estimates. These new approaches and developments have significantly improved the reliability of dating the ancient past. In this paper we apply these methods to Kozarnika, where a deep stratigraphic sequence provides the crucial 'prior' framework for the Bayesian modelling we undertake.

THE ARCHAEOLOGICAL SITE OF KOZARNIKA

Kozarnika is a site in northwestern Bulgaria (43.652 N, 22.702 E) (Figure 1). It is a 210m long cave (Figure 2) currently being excavated by a Bulgarian-French team (led by J.-L. G. and N. S.) (Sirakov et al. 2010). Four excavation sectors have been opened (see Figure 2), revealing Upper

Figure 1. Map of Middle and Upper Paleolithic sites mentioned in this paper. 1) Grotte Mandrin, 2) Ranis, 3) Koněprusy caves, 4) Tincova, 5) Kozarnika, 6) Samuilitsa, 7) Muselievo, 8) Bacho Kiro, 9) Apidima, 10) Kostenki IV.

(sectors I, II, and III), Middle (sectors I, II, and IV) and Lower Paleolithic (sectors I and II) occupation evidence, with almost 400,000 lithic and faunal remains. Important finds include the human skeletal remains from both modern humans and Neanderthals (Guadelli 2004), pieces of art (Guadelli 2004, 2011; Guadelli and Guadelli 2004; Tillier et al. 2017), as well as a new lamellar lithic industry and a key tephra marker layer in the Upper Paleolithic levels (Sirakov et al. 2007; Tsanova et al. 2012). Of particular interest to this paper are the terminal Mousterian, 'transitional' (Initial Upper Paleolithic), as well as the Early Upper Paleolithic or Kozarnikian levels, as they are known.

The stratigraphic sequence of Kozarnika has been divided into geological layers and archaeological levels (Fig-

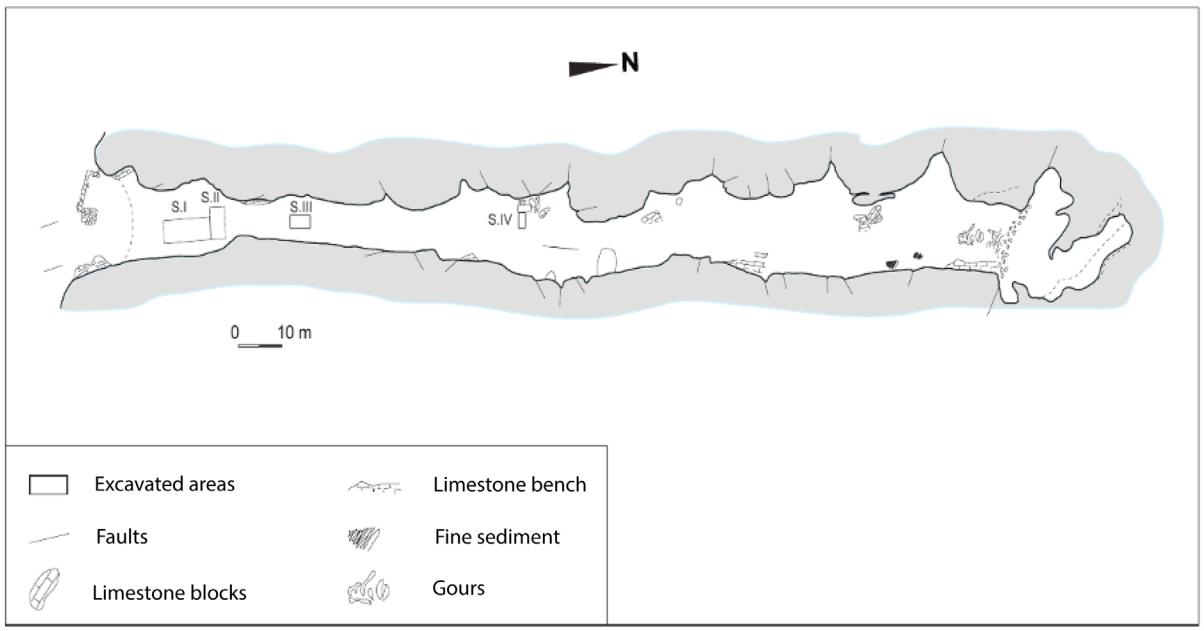

Figure 2. Kozarnika: map of cave with location of excavation sectors I, II, III, and IV (see Guadelli et al. 2025: Figure 3).

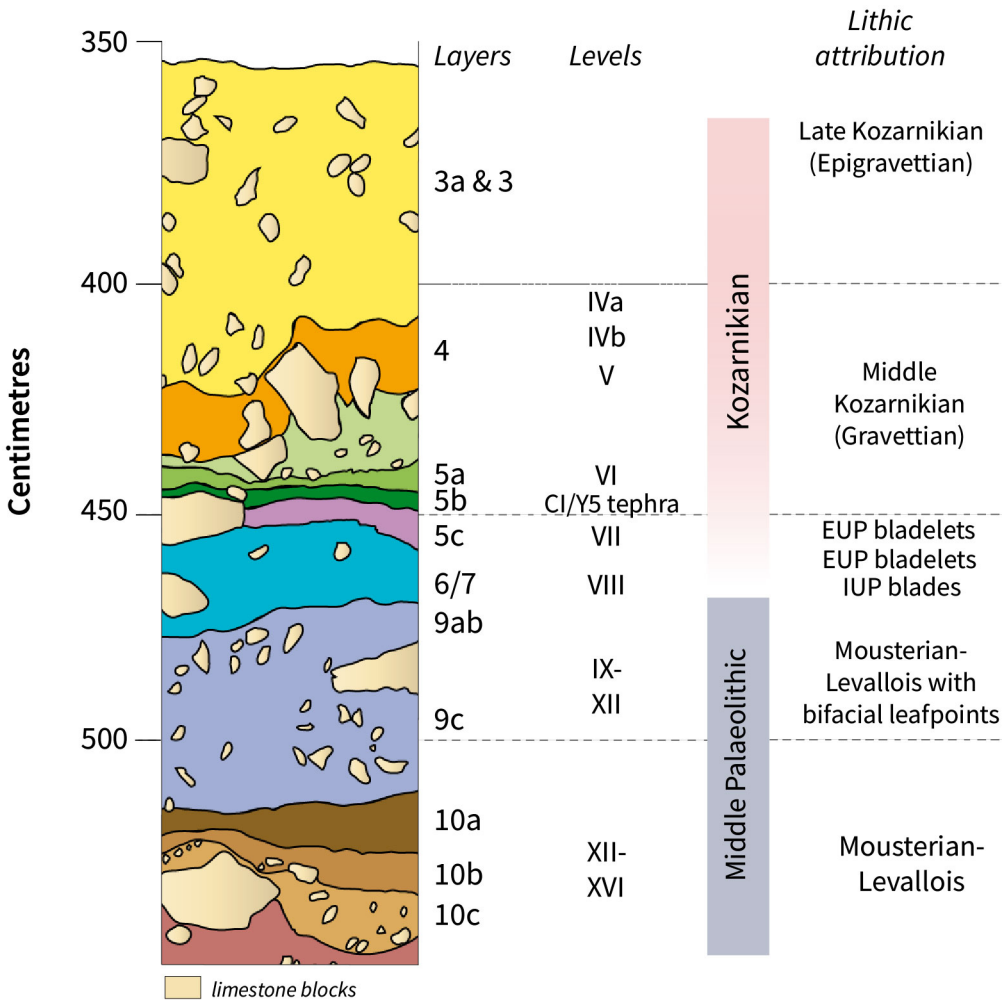

Figure 3. Stratigraphic sequence from Kozarnika (modified from Heydari et al. 2022 and Tsanova 2023).

ure 3). The former were labelled with Arabic numbers, the latter with Roman numerals. The layers most relevant to this paper are 3b to 5c (Upper Paleolithic), layer 6/7 (described previously as 'transitional' or very early Upper Paleolithic), and 9a (Middle Paleolithic). What was initially identified as layer 8, later excavation showed to be den infill, nonetheless, the original layer numbering was kept, meaning that the sequence passes from layer 7 directly to layer 9 (Sirakov et al. 2010). Both sectors I and II in the front of the cave have been extended and the stratigraphy connected, so they can be treated as one large excavation area. In contrast, sector III in the cave gallery cannot be correlated so readily.

The lithic remains from the site are impressive and the entirety of the lithic *chaîne opératoire* is represented. More than 70% of the lithics are made up of debris and lithic remains resulting from intermediary steps, while around a quarter of the material has typo-technological significance. Presently, little sign of mixing of lithics between archaeological levels has been identified (Guadelli 2004). Local raw material predominates. Flint was preferentially used, with quartz and quartzite being rare. Environmental processes, such as tectonic movement and repeated frost, cause the flint at the site to be fragile and cracked. The high number of geofacts requires that extra care is needed in identifying archaeological artifacts (Guadelli et al. 2005).

The uppermost Middle Paleolithic level found at Kozarnika is archaeological unit IX in Layer 9a (9a and 9b represent essentially the same horizon, one south of sector II (9a) and one south and east of sector II (9b)). It is dominated by tools made using Levallois methods, with centripetal or bipolar preferential debitage present. The cores are small to medium sized and often made on cortical flakes or nodule fragments. Retouched forms include denticulated flakes and scrapers. Mousterian points are rare, and some more typical leaf points (*pointes foliacées*) are present. In general, the Levallois Mousterian found in layer 9a is typical of the eastern Balkans and comparable to assemblages found at Muselievo and Samuilitsa (Guadelli et al. 2005). We link Layer 9a with Neanderthal groups based on the presence of their associated remains (Tillier et al. 2017).

Layer 6/7 is above 9a and contains a blade technology that echoes the Initial Upper Paleolithic (IUP) *sensu lato*. This layer (6/7) contains two distinct lithic technologies—laminar, which forms the IUP component, and lamellar, which finds its closest similarity in material in the overlying layer 5c (Tsanova 2023). In Figure 4a we show some of the

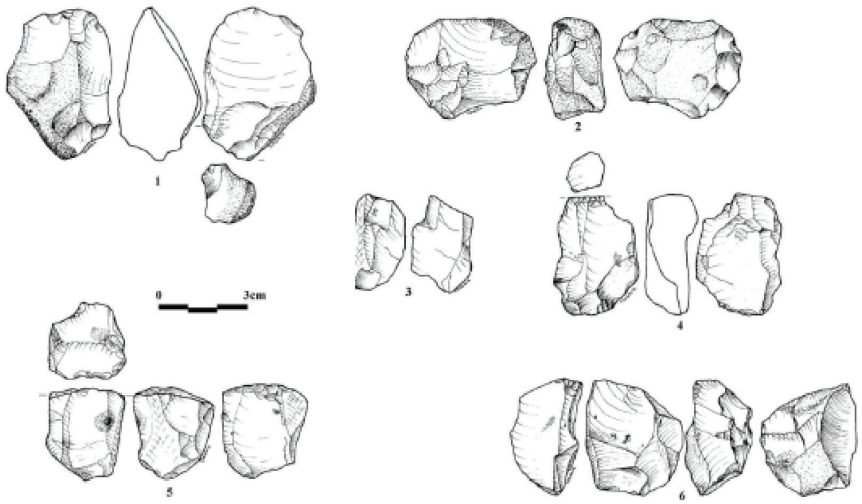

a)

b)

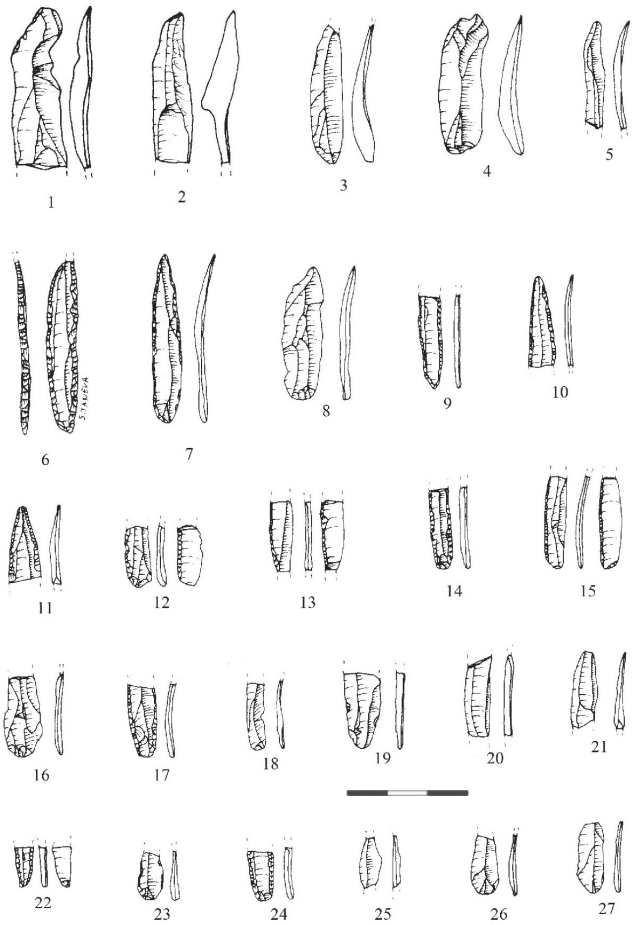

Figure 4a. Kozarnika. Upper Paleolithic lithics from layer 6/7 (1, 4, 5, 6: flake and bladelet nuclei with two striking planes; 2: Levallois nucleus with negatives of a reuse (?) on the narrow edge reminiscent of Gravettian debitage; 3: bladelet nucleus with one striking plane). Figure 4b. Kozarnika. Level VII, Early Kozarnikian. 1, 2, 3, 4, 8, 16, 19: rough bladelet; 5, 18, 20, 21, 25, 26, 27: rough microbladelet; 6, 7: backed points; 9, 22: fragments of bladelet or backed points; 10, 11: fragments of lamellar points regularized by fine to semi-abrupt bilateral retouch; 14, 17, 24: fragments of bladelet or points with fine to semi-abrupt bilateral retouch; 23: fragment of bladelet with partial fine retouch; 12, 13, 15: fragments of bladelet with fine to semi-abrupt alternate retouch.

Figure 5. (left) First phalanx of a human hand from layer 6/7 (F7-T467-F12). (right) Homo *sp., lower right P3 (E9 2944), found in layer 6/7 ls. (Photographs: A. Guadelli (l) and J.-L. Guadelli (r)).*

lithic materials from 6/7 (see also Supplementary Information (SI 1)) including the 3D X-Y-Z plots of bones and lithic artifacts from this level). There are some Levallois pieces that are like some of those found in the Mousterian layers below. This raises the possibility that Neanderthals might have also been present during this period. It is very likely that layer 6/7 is linked with *Homo sapiens* first and foremost, however, because a first phalanx (F7-T467-F12) of a human hand, a crown portion of I1-2 or canine (H7-T/469-F2), and a lower right *Homo sapiens* P3 (E9-2944, layer 6/7ls) (Figure 5), were found co-mingled in this layer. The application of sediment and ancient DNA methods may enable us to confirm more reliably whether there were other occupants of the cave during this key period. From the 2016 excavation season onwards, the separation of layer 6/7 into three subfacies—labelled 6/7 lb, 6/7 ls, and 6/7 lp—was possible for squares D7-9 and E7-9.

Taphonomy and geoarchaeology are key areas of importance in Paleolithic archaeology. A study of sediment microstructures undertaken by Ferrier et al. (2009) showed that gelifluction affected layer 6/7 (as well as 10a). The presence of a few frosted pebbles and the general grain size of the coarse fraction (with an average size of 1cm to 2cm), indicate the action of a secondary frost with a possible lateral redistribution of fine particles towards the south and north, an absence of any lithic or dental and bone gelifracts or evidence of major syn-sedimentary or post-depositional movements (Ferrier et al. 2009). This indicates that secondary frost was of minor importance. A forthcoming semi-quantitative study of the fauna (Guadelli et al. 2025) shows that, for layer 6/7, thermal conditions were colder than they are today, but were not the severe periglacial conditions that could have disturbed sediments, artifacts, and fauna. This conclusion contrasts with recent paleoclimatic work from the Middle to Upper Paleolithic layers (N1-K, N1-J and N1-I) at Bacho Kiro using oxygen isotopes. These horizons correspond more or less to layers 9c (MP), 6/7 (IUP), and 5c (Ancient Kozarnikian, i.e., AUP) at Kozarnika. Tooth $d^{18}O$ isotopic values suggested that temperatures were, on average, ~14°C lower than today, with the largest differences in summer and the smallest in winter (Pederzani et al. 2021). If reliable, these temperature estimates would imply episodes of deep frost processes leading to significant post-depositional disturbances such as polygonal and striated soils. However, to our knowledge, such formations have never been reported in Bulgaria. At Kozarnika, a semi-quantitative method based on the analysis of the climate preferences of large fauna indicates a clear cooling of the climate (approximately 6°C below the July average, 3—4°C above the January average and 2—3°C below the annual average), but not as low as implied at Bacho Kiro and closer to what one would currently find in parts of western Ukraine and Slovakia in terms of annual average temperatures (Guadelli et al. 2025). The fauna of Bacho Kiro and Kozarnika are similar, and they are geographically close, which would suggest we ought to expect a similar regional climate signal. Taken together, it is clear that local climate conditions were cooler than today, but more work is needed to reconcile the two approaches and obtain more robust and detailed data.

Layer 5c (in archaeological Level VII) is composed of a bladelet technology that appears to precede the Gravettian assemblages at the site typologically and technologically, but which is otherwise locally unknown. Layer 5c represents its oldest expression. The name 'Ancient Kozarnikian' (Kozarnikien *très ancien*) has been used to describe the lithic assemblage. It contains some backed-like pieces, which were usually formed by semi-abrupt retouch and become more frequent during the Middle Kozarnikian. Alternately or reversed retouched blades and bladelets are numerous and more common than in later phases. These include regular backed pieces as well as bladelets with a thin, abrupt or semi-abrupt, retouch (either bilaterally convergent or alternating). Scrapers with lateral retouch, often seen as 'Aurignacian' scrapers, are abundant, though Guadelli et al. (2005) and Sirakov et al. (2007) emphasize that such technology is not unique to the Aurignacian. Burins are rare and there is a small series of leaf points and bifacially retouched pieces. The few larger blades in Level VII are made from non-local flints. Since no cores fitting

these tools are present at the site, it can be concluded that they were manufactured elsewhere and retouched on site (Tsanova et al. 2012). No carinated scrapers or Aurignacian blades have been found. Tsanova et al. (2012) mention a series of Dufour bladelets identified in level VII but we do not subscribe to this interpretation. Overall, the technocomplex shows some overlap with the Proto-Aurignacian and Early Aurignacian industries. Teyssandier (2008) sees parallels with the Proto-Aurignacian found at Tincova (Romania). Sirakov et al. (2007) suggest there are analogies between the bladelet tools and the archaic Ahmarian from Levant, as well as the Proto-Aurignacian from southern Europe. Despite this, the Ancient Kozarnikian should be seen as an individual technocomplex until its relationship to the Proto-Aurignacian and Early Aurignacian is better understood, to avoid chronocultural schema developed in other regions from clouding the local archaeological record. In terms of time, the assemblage appears to occupy the relative chronostratigraphic position that the Early Aurignacian would normally hold in central and western European sites. We show some of the lithic remains from Level VII in Figure 4b.

We identified the remains of *Homo sapiens* in this level and those above it, providing strong evidence that they were the probable authors of the industry. Three cranial fragments have been identified in layer 5c (H6-T/855-F49, G5-1048, H3-1199) and a third phalanx (H5-H6-T/833-F1343) in layer 5b. Finally, while cleaning fallen sediments from a profile, a right upper M1 (D-E7-10-K/3329-F1) was recently found. It may be attributed to the Upper Paleolithic, but in addition to its morphometric study, direct dating and DNA analysis are required. Other human remains have been found at Kozarnika (see SI 1) but some of these were from clandestine excavations and therefore have problematic context.

The boundary between level VII to level VI is disturbed by cryoturbation. A chronological gap observed during previous dating efforts is not detectable in the stratigraphic record. There are no signs of erosion, and the period of nearly 10k years was deemed too long for no sedimentation to occur. Nonetheless, from a lithic perspective, levels V and VI seem to be more closely connected to level VII, below, than to level IV, above. Level IV in layer 4 is characterized by backed blades and a specific type of broad and straight point (like the shape of a dart) of type 'Kozarnika.' In addition, IVb produced Gravettian points (Tsanova 2003). Neither of these artifact types were found in the layers below. Similarities between the backed bladelets from the Middle and Recent Kozarnikian (Kozarnikien *moyen* and Kozarnikien *supérieur*) prompted a comparison between the Kozarnikian and the Gravettian (Sirakov et al. 2007). While many similarities were found, it was noted that the dimensions observed at Kozarnika were significantly smaller, and the retouch more abrupt than observed at Gravettian sites in France.

A tephra horizon visible in layer 5b has been identified as the Campanian Ignimbrite tephra eruption (CI or Y5 when found in ocean archives), a key marker in the Balkans and eastern Mediterranean (Lowe et al. 2012).

Kozarnika is rich in osseous worked objects and artifacts. The most common tools are punches and retouchers from the Upper Paleolithic sequence (Guadelli 2009; 2011; Tsanova et al. 2012). Some significant pieces of artistic expression have been found, including portable art and ornaments. The oldest examples are two engraved bones found in layer 12 (Guadelli 2004; Guadelli and Guadelli 2004; Sirakov et al. 2010). Fragments of portable art from Level 6/7 lp and ls depict carved animals. In layer 6/7 two pendants were found that were made on fox canine teeth. Starting with level VII, pierced teeth and shells appear, some of which show traces of ochre. Delicate beads of ca. 2cm length made of thin bones have also been found (Guadelli 2011). Together with awls, the pendants present the diagnostic features of the osseous industry from the early Kozarnikian. Another noteworthy find is an anthropomorphic figure from level V, which shows similarities with those found at Kostenki IV (SI 1 Figure S19).

The archaeological record in sector III is more modest. Despite this, an ochre rich band—layer A—is of interest since it yielded a fragment of a possible Mladeč point. The only other osseous point from the site came from contact zone VII/VIII and may represent a split-based point (Guadelli 2004: Figure 20-1). Without a stratigraphic connection from the area to sector I/II, the precise relationship to the industries found at the front of the cave remains uncertain. Another remarkable find—the fragmented remains of a Venus figurine (Kz-57 in SI 1 Table S3)—was discovered in the debris left behind by illicit excavation work and therefore has no secure context. Unfortunately, the first attempt at direct dating was a failure and only a new attempt direct at dating would allow some temporal classification.

METHODS AND MATERIALS

Prior to our work, two separate radiocarbon dating campaigns were undertaken—one focusing on the age of the archaeological levels in which samples were dated at the French laboratory at Gif-sur-Yvette, and one in relation to the analysis of tephra at the site with samples dated at the ORAU (Guadelli et al. 2002 and Tables S1 and S2). Ten reliable radiocarbon measurements and 7 possible minimum age estimates on charcoal were obtained ultimately, as well as a securely identified CI tephra as a chronological marker in layer 5b. However, there was some dating variability and uncertainty in the age ascribed to layer 6/7 (SI 1 Tables S1 and S2). The results of some experimental work comparing ABOx and ABA pretreatments showed that, in the main, there was no significant contamination present in the charcoal samples being dated.

To refine the chronology, we sampled a total of 109 bone fragments for radiocarbon dating in 2015 and 2016. This included 99 securely and 7 potentially anthropogenically modified faunal fragments. From these, 43 samples were chemically pretreated for radiocarbon analysis (SI 1 Table S3). Thirty-three of these samples were anthropogenically modified faunal material from sector I/II (layers 3b to 6/7) (SI 1). In layer 6/7, preference was given to samples col-

lected in 2016, when three distinct subunits were identified during excavation, as outlined previously. This provided an opportunity to increase dating precision at the lower end of the Upper Paleolithic sequence. In general, preference was given to dating samples with full coordinates (over those with only square and depth information), and with acceptable biomolecular preservation.

We selected three human remains for dating that were found without secure archaeological context in the area that later became excavation sector III. This was the same location as the Venus figurine fragment (Kz-57) for which direct radiocarbon dating was the only method available to provide temporal context. The samples comprised a juvenile tibia (Kz-53) and an adult femur (Kz- 54), as well as a cranial fragment. We used ZooMS (Zooarchaeology by Mass Spectrometry) to show that this fragment was in fact *Ursus* sp. (Kz-55) and not human.

We screened bones for collagen content using %N measurements on 2–3mg of drilled bone powder. Bone with %N >0.76% is associated with an ~85% collagen extraction success rate (Brock et al. 2010). We used ZooMS to identify bones to species/genus based on peptide mass spectra (Buckley et al. 2009). We took sub-samples of bone, decalcified them with 0.6 M HCl and ultrafiltered the acid-soluble collagen into 50mM ammonium bicarbonate which was then treated with 0.2µg trypsin (sequencing grade; Promega, UK) and incubated at 37°C for 18 h. The trypsinized samples were further purified using C18 solid-phase extraction cartridges into a 50:50 acetonitrile:MQ 0.1% trifluoroacetic acid (TFA) solution, dried to completion, and resuspended with 20µl 0.1% TFA. One µl of the resulting peptide solutions were mixed with a matrix solution of 1µl α -cyano-4-hydroxycinnamic acid solution (10mg/mL in 50% acetonitrile [ACN]/0.1% TFA). The solutions were spotted and crystalized onto a ground steel target plate (Bruker MTP 384 Target Plate 8280784). We used a Bruker Ultraflex II (Bruker Daltonics, Bremen) MALDI-Tof/Tof mass spectrometer to analyze the mass spectrum of the peptides from each spotted sample. The mass spectra were matched to a reference library of published peptide markers by FlexAnalysis software (Buckley et al. 2009). We also used SpecieScan, an automated identification workflow (Végh and Douka 2024), with spectra preprocessed through Savitzky-Golay smoothing, baseline removal, and total ion current (TIC) normalization. The signal-to-noise ratio (SNR) threshold was visually optimized to SNR=3.5 based on representative spectra. Spectra exhibiting fewer than 39 or more than 70 detected peaks were excluded as low-quality outliers following qualitative assessment. We also assessed contamination using SpecieScan and the results showed only common laboratory contaminants and human keratin contamination (SI 1).

All samples were AMS dated at the University of Oxford (Oxford Radiocarbon Accelerator Unit, ORAU). We extracted and purified bulk bone collagen using an ultrafiltration protocol (Brock et al. 2010). The ultrafiltered collagen samples were then combusted with an automated carbon and nitrogen elemental analyzer (Carlo Erba EA1108) coupled with a continuous-flow isotope monitoring mass spectrometer (Europa Geo 20/20) using helium as a carrier gas. We obtained $d^{15}N$ and $d^{13}C$ values, %carbon values, and C:N atomic ratios, using VPDB as the $d^{13}C$ standard and AIR for $d^{15}N$. We produced graphite via a reaction over an iron catalyst in an excess atmosphere of hydrogen at 560°C (Dee and Ramsey 2000). AMS determinations were made according to the conventions in Stuiver and Polach (1977) and Bronk Ramsey et al. (2004). Bone determinations were background corrected using the established ORAU method (Wood et al. 2010).

We used OxCal 4.4 (Bronk Ramsey 2009a) and the IntCal20 calibration curve (Reimer et al. 2020) to build Bayesian chronometric models. We used the boundary command in OxCal to delineate the beginning of one Phase and the start of another, and two Boundary commands to identify a sterile layer. We used the Interval command to quantify the span of time represented in a specific Phase or between different parameters. We built eight stratigraphic Phase models to compare age estimates for boundary transitions between different archaeological horizons and test the sensitivity of different model parameters (SI 1 Methods). This included comparing our dataset against the OSL age estimates of Heydari et al. (2022). We also used the KDE_Model method in OxCal for visualizing the shape of the underlying distribution of a dataset using a non-parametric approach (Bronk Ramsey 2017). Three KDE models were run to test the different datasets in relation to identifying the timing of human activity at the cave (see below and SI 1 Methods).

For all models, duplicate samples were combined using the R_Combine function. We used the General outlier model for assessing whether individual radiocarbon dates and combined dates were outliers within the constraints of the model, and the Ssimple outlier model for radiocarbon dates in R_Combine (Bronk Ramsey 2009b). Prior sample outlier probability was set at 5%. The radiocarbon dates were sorted into Phases separated by single boundaries and placed into a Sequence according to their archaeological level or geological layer attribution. The Campanian Ignimbrite age estimate from Giaccio et al. (2017) was placed within layers 5c/5b (levels VII/VI contact) to represent the age of the CI eruption. The Date command was used to calculate the duration of phases. The CQL code used in all models is given in the SI 1.

RESULTS

Bone preservation at Kozarnika initially appeared encouraging with 77% of the radiocarbon samples yielding %N>0.7 (Table 1). Despite this, 8 of the 43 samples treated had insufficient collagen preservation for radiocarbon dating. This left 37 successful radiocarbon measurements from 35 bone samples (see Table 1). Unfortunately, two samples that failed in pretreatment were Kz-57 and Kz-58—the Venus figurine and the osseous point from sector III. One further artifact and 4 faunal samples were also not AMS dated, as a direct result of their low collagen yield (SI 1). Samples Kz-54 and Kz-55 were dated despite insufficient collagen

TABLE 1. KOZARNIKA: NEW AMS RADIOCARBON DATES ON ANTHROPOGENICALLY MODIFIED BONE (ref-no 3–38) FROM SECTOR I WITH ARCHAEOLOGICAL CONTEXT INFORMATION AND PRE-TREATMENT RESULTS.*

Ref-no.	Species	Sq.	Layer	Depth (cm)	%N	Treat.	Yield (mg)	Yield (wt.%)	%C	$d^{15}N$ (‰)	$d^{13}C$ (‰)	C:N	Lab-no	$F^{14}C$	±	^{14}C (BP)
Kz-03	Bovinae	D7	3b = III	380–385	0.49	AG	8.88	0.99	40.4	8.4	-19.7	3.2	OxA-35417	0.05541	0.00126	23240±180
Kz-06	Large ungulate	E9	4 = IVa	390–393	1.71	AF	9.23	1.60	43.0	7.9	19.6	3.2	OxA-33834	0.03057	0.00109	28020±290
Kz-07	*Equus*	D8	4 = IVa	395–400	1.54	AF	7.84	2.18	43.3	7.7	-19.6	3.2	OxA-34767	0.03741	0.00105	26400±220
Kz-08	*Bos/Bison*	E9	4 = IVa	393–395	1.92	AF	14.43	2.51	43.0	8.5	-19.4	3.2	OxA-34768	0.03309	0.00102	27380±250
Kz-10	Large ungulate	E7	4 = IVa	393–395	2.03	AF	19.32	3.17	45.3	6.3	-20.7	3.3	OxA-33546	0.03330	0.00109	27330±260
Kz-14	*Equus*	E7	4 = IVb	410–415	1.37	AF	30.34	3.42	42.0	4.5	-21.4	3.2	OxA-35230	0.03768	0.00105	26340±220
Kz-15	Large ungulate	E10	4 = IVb	410–415	0.48	AG	7.92	0.94	–	–	–	–	P-39504	–		–
Kz-19	Bovinae	E9	4 = IVb	410–415	2.91	AF	33.46	5.16	42.8	6.8	-19.8	3.2	OxA-33547	0.04030	0.00110	25800±220
Kz-23	Large artiodactyl	D10	4 = IVb	405–410	3.05	AF	25.78	4.47	43.0	5.8	-20.1	3.2	OxA-33548	0.04983	0.00115	24090±180
Kz-24	Large ungulate	F10	5a = V	420–425	2.20	AF	14.51	2.76	43.5	6.6	-19.3	3.2	OxA-33549	0.03346	0.00111	27290±270
Kz-25	Large ungulate	F10	5a = V	425–430	2.27	AF	24.84	4.17	43.3	6.2	-20.8	3.2	OxA-33550	0.03246	0.00109	27540±270
Kz-38	Rhinocerotidae	F9	5b = VI	435–440	0.91	AG	4.54	0.75	–	–	–	–	P-39527	–		–
Kz-39	*Ursus* cf. *spelaeus*	F8	5b = VI	430–435	3.01	AF	35.63	8.71	42.9	2.6	-21.7	3.2	OxA-33551	0.01696	0.00105	32750±500
Kz-45	*Equus*	F10	5b = VI	440–445	0.87	AG	6.96	1.26	40.8	8.1	-19.5	3.2	P-39534	–	-	–
Kz-43	*Cervus elaphus*	G5	5c = VII	440–443	1.37	AF	20.25	3.24	42.9	8.2	-19.4	3.2	OxA-33552	0.01000	0.00102	37000±800
Kz-47	No id	F8	5c = VII	445–450	1.97	AF	27.77	4.59	42.9	8.9	-20.7	3.2	OxA-33835	0.00940	0.00101	37500±900
Kz-48‡	*Ovis/Capra*	G5	5b/c = VI/VII	443	1.68	AF	38.30	7.75	42.6	7.3	-19.6	3.2	OxA-34769	0.01054	0.00098	36550±750
Kz-49	No id	G7	5c = VII	450–455	1.01	AF	16.13	2.68	43.1	6.8	-19.3	3.2	OxA-33553	0.01021	0.00103	36800±800
Kz-50	No id	G11	5b = VI	450–455	2.18	AF	17.40	3.64	43.0	6.9	-21.9	3.1	OxA-33554	0.01513	0.00108	33650±550
Kz-79	*Equus*	E10	5a = V	415–420	3.00	AF	15.15	2.61	42.6	6.6	-21.2	3.2	OxA-34822	0.04237	0.00108	25400±200
Kz-88	*Cervus/Saiga/Gazella*	D9	5b = VI	445–448	1.83	AF	25.95	3.39	40.3	9.1	-18.7	2.9	OxA-35575	0.0313	0.00104	27830±270
Kz-90	No id	D9	5b = VI	443–445	2.08	AF	21.74	2.88	41.0	7.4	-20.8	3.1	OxA-35576	0.03061	0.00105	28010±280
Kz-85	*Equus*	D7	5c = VII	445-448	0.33	AF	36.22	5.34	43.2	8.2	-20.6	3.2	OxA-34824	0.00926	0.00099	37600±900
Kz-87*f*	*Bos/Bison*	E9	5c = VII	450–453	2.62	AF	59.29	7.00	43.8	9.2	-19.2	3.2	OxA-35234	0.00954	0.00098	37400±800
Kz-44	Large ungulate	F7	6/7 = VIII	460–465	0.66	AG	3.40	0.64	-	-	-	-	P-39533	-	-	-
Kz-52	Large ungulate	F5	6/7 = VIII	453–455	1.96	AF	17.00	2.76	43.1	8.5	-19.5	3.2	OxA-33555	0.00432	0.00101	43700±1900
Kz-93	*Equus*	E9	6/7lp = VIII	455–458	0.91	AF	20.03	2.46	43.2	6.5	-21.4	3.2	OxA-34825	0.00427	0.00098	43800±1800
Kz-80	*Bos/Bison*	D8	6/7lp = VIII	458–459	2.15	AF	53.15	5.44	43.1	7.9	-19.9	3.2	OxA-34823	0.00423	0.00097	43900±1800
Kz-81	*Bos/Bison*	E8	6/7ls = VIII	458–459	0.44	AG	2.43	0.28	–	–	–	–	P-42170	–		–
Kz-82	Cervidae/Bovidae	E8	6/7ls = VIII	458–459	0.90	AF	6.63	0.77	42.8	8.4	-19.9	3.2	OxA-X-2699-11	0.00481	0.001	42900±1700

TABLE 1. KOZARNIKA: NEW AMS RADIOCARBON DATES ON ANTHROPOGENICALLY MODIFIED BONE (ref-no 3–38) FROM SECTOR I WITH ARCHAEOLOGICAL CONTEXT INFORMATION AND PRE-TREATMENT RESULTS (continued).*

Ref-no.	Species	Sq.	Layer	Depth (cm)	%N	Treat.	Yield (mg)	Yield (wt.%)	%C	$d^{15}N$ (‰)	$d^{13}C$ (‰)	C:N	Lab-no	$F^{14}C$	±	^{14}C (BP)
Kz-83	*Bos/Bison*	E7	6/7ls = VIII	461–462	–	AG	2.02	0.27	–	–	–	–	P-42116	–		–
Kz-109	Ursidae/Felidae	D7	6/7lb = VIII	461–462	2.51	AF	78.72	8.57	43.1	3.5	-20.9	3.2	OxA-34826	0.00702	0.00098	39800±1100
Kz-109	No id	D7	6/7lb = VIII	461–462	2.51	AF	71.05	8.02	43.0	3.3	-20.9	3.2	OxA-34827	0.00614	0.00098	40900±1300
Kz-110¶	*Bos/Bison*	E7	6/7 lp,ls* = VIII	464–465	1.02	AF	20.21	2.20	43.0	8.6	-19.2	3.2	OxA-34828	0.00417	0.00097	44000±1900
Kz-111	*Equus*	G30	A2	540–545	3.2	AF	90.94	9.82	43.5	8.0	-20.4	3.2	OxA-34829	0.01053	0.00098	36600±750
Kz-112	*Equus*	G30	A1	545–550	0.88	AF	24.18	2.56	43.2	10.3	-20.2	3.2	OxA-34830	0.00901	0.00102	37800±900
Kz-114	*Capra/Rangifer*	F29	D2	550–555	2.49	AF	44.78	6.31	40.5	5.0	-20.9	3.1	OxA-35577	0.00031	0.00099	> 48900
Kz-115	*Equus caballus*	F30	C	540–545	1.12	AF	12.65	1.68	41.4	5.2	-22.7	3.1	OxA-35578	0.00246	0.001	48300±3300
Kz-116	*Equus*	F29	D2	545–550	2.33	AF	38.41	5.99	40.8	5.9	-21.7	3.1	OxA-35579	0.00423	0.00099	43900±1900
Kz-116	*Equus*	F29	D2	545–550	2.33	AF	35.48	6.91	40.1	6.6	-20.1	2.9	OxA-35580	0.00473	0.00098	43000±1700
Kz-53	*Homo sapiens*	–	–	–	0.86	AF	31.90	4.95	43.3	8.3	-19.1	3.2	OxA-33472	0.73025	0.00249	2525±27
Kz-54	*Homo sapiens*	–	–	–	0.80	AG	12.01	2.53	38.5	10.6	-18.0	3.2	OxA-33473	0.73636	0.00258	2458±28
Kz-55	*Ursus* sp.	–	–	–	0.58	AG	8.70	1.67	42.0	9.3	-23.9	3.2	OxA-33474	0.00253	0.00117	48000±3700
Kz-57	No id	–	–	–	0.69	AG	0.00	0.00	–	–	–	–	P-39546	–		–
Kz-58	No id	F30	6/7?	504	0.21	AG	0.00	0.00	–	–	–	–	P-39547	–		–

*Samples Kz-53 to Kz-58 and Kz-111 to Kz-116 are from sector III, the rest from sector I/II. AMS radiocarbon dates are on anthropogenically modified bone and humans. Kz-15 is a retoucher, Kz 53 and 54 are human bones, Kz-55 was thought to be human bone, but was identified later using ZooMS as an Ursid, Kz-57 and 58 are the Venus figurine and the osseous spear point, respectively, Kz-79 is a sample from an anthropomorphic figurine. Samples were identified using either archaeozoological methods or ZooMS. Failed samples are in grey. Ref-no. = our reference numbers. %N = nitrogen weight content before chemical pre-treatment. Treat. = Pretreatment protocols used: AG = ORAU acid-base-acid pretreatment, AF = ORAU ultrafiltration protocol. Yield = sample left after chemical pre-treatment (both in mg and wt.%). %C = carbon yield on combustion. C:N = carbon to nitrogen atomic ratio of combusted collagen sample. $F^{14}C$ = fraction modern carbon. ^{14}C (BP) = conventional radiocarbon age Before Present. Both $F^{14}C$ and ^{14}C ages (BP) are given with a ±1 sigma error.

Notes:

¶Kz-110 was originally labelled on site as belonging to layer 6/7 lb. Looking at the planum drawing from just above (depth: 460cm), the location is marked as 6/7 lp, while the one from just below (depth: 465cm) shows 6/7 ls. In addition, the sample shows patina consistent with other samples from layer 6/7 lp, but not with layer 6/7 lb. It can be concluded that the sample belongs to either layer 6/7 lp or 6/7 ls. The radiocarbon age of 44,000±1900 BP (OxA-34828) is consistent with such an attribution.

*f*Kz-87 was originally attributed to 5c. The find location is marked by very uneven layer limits, which leave an alternating pattern between layer 6/7 and 5c when cut horizontally. The patina differs from other artifacts from layer 5c in that sector and shows signs of heating, consistent with an origin in the 'fireplace' layer below 5c, i.e., at the top of layer 6/7. Consequently, the layer attribution was changed from 5c to 6/7.

‡Kz-48 was bagged as coming from layer 5b, however, the excavation documentation leaves attribution somewhat ambiguous. Both layers 5b and 5c were found in the vicinity of the sample, judging by planar drawings. As a result, both layer attributions were tested during Bayesian modelling.

yield for ultrafiltration. They were believed to be human remains. We found that Kz-54 dated to 2458±28 BP (OxA-33473) while Kz-55 resulted in an age of 48,000±3700 BP (OxA-33474). We used ZooMS to later identify the sample as *Ursus* sp., and in the absence of any identifiable anthropogenic modifications, this no longer has a connection to human activity.

Twenty-eight radiocarbon results from sector I/II were obtained that are directly connected to human activity and suitable for Bayesian modelling, including 26 ultrafiltered humanly modified faunal remains, 1 ultrafiltered anthropomorphic figurine (Kz-79), and a non-ultrafiltered humanly modified faunal fragment. In addition, there are 6 dates on ultrafiltered faunal remains from sector III to provide an initial assessment of the chronological placement of layers A, C and D.

We built eight Bayesian models that included different sets of data and tested small changes in the parameters for their sensitivity (SI 1). The Bayesian model we favor is Model 8, which comprises all the new AMS determinations (Figure 6). We prefer it to Model 7 (which included previous charcoal and bone dates from earlier dating campaigns) and other models, because it has fewer outliers, higher agreement indices, and more robust convergence values following sensitivity testing (SI 1). It differs somewhat from the previous models in that we make a stratigraphic separation of level 6/7 into three sub-levels (6/7 lb, 6/7 ls, and 6/7 lp). As mentioned earlier, from excavation season 2016 onwards, separation of layer 6/7 into these three sub-facies was possible for squares D7-9 and E7-9, therefore, the Bayesian model reflects the reality of the archaeological succession.

When we included the OSL data of Heydari et al. (2022) in the models we observe that the OSL estimates for levels 6/7 and 5c are significantly younger than the radiocarbon chronology, so we set these to one side for the time being (SI 1). This is unfortunate because Layer 9 is essentially undated in our chosen model. Further work is therefore needed to generate reliable data that could constrain further the start boundary of 6/7.

The CI tephra, with its independent age, is an important tie-point in any Bayesian model. There is, however, a degree of spread in the identified CI tephra within level VI which influences its precise assignation within a Bayesian model. The tephra shard count peaks across the level but are shards are also found at lower counts in the uppermost part of layer 5c as well as the lower most part of 5a. This probably evidences some mixing of material in these contact zones. The CI age fits well within the Bayesian age model when placed at the start of layer 5b, with the eruption seeming to either coincide with the occupation phase dated by OxA-33551 (Kz-39) and OxA-33554 (Kz-50), or to just predate it. Both scenarios would be consistent with a spread of the identified tephra within level VI. The distribution of the radiocarbon ages in 5b suggests a hiatus of several thousand years. All Bayesian models had similar patterns. It seems parsimonious to conclude that layer 5b contains some material belonging to layers 5a and 5c. OxA-35575 and OxA-33576, for example, overlap with the dates obtained above in layer 5a. Caution may be advised, therefore, when analyzing the lithic and osseous industries found within layer 5b. Below this, phases 5c and 6/7 yielded more consistent series results, with no outliers. Overall, Model 8 was robust with only three outliers and a consistency in the age-depth relationship.

We now consider the main boundaries and date ranges in the model.

Phase 6/7 at Kozarnika is of crucial importance because it corresponds with the onset of the IUP at the site and, we argue, the possible onset of modern human occupation. The start boundary of this phase ranges between 50,020–44,880 cal BP (95.4% prob.). The date of the phase corresponds with a range spanning 48,500–44,030 cal BP.

The start of Layer 5c, representing the Kozarnikien *très ancien* (Ancient Kozarnikian) ranges between 43,330–41,530 cal BP (95.4% prob.) and the entire phase covers a date range between 42,810–40,800 cal BP. This overlaps quite closely with the earliest Aurignacian in much of western Europe (Frouin et al. 2022; Higham et al. 2012; Szmidt et al. 2010). Analogies can be drawn in terms of the lithic technology with the archaic Ahmarian from the Levant, as well as the Proto-Aurignacian from southern Europe, albeit with diagnostic elements absent (e.g., carinated scrapers, Aurignacian blades, and Dufour bladelets) (Tsanova et al. 2012). Layer 5b has material within it that dates to two quite different periods, as already mentioned above, and by 32,030–31,310 cal BP (95.4%) it gives way to Level 5a, where we find Middle Kozarnikian archaeology. Layer 4 ranges from 31,550–28,120 cal BP.

KDE models are useful in summarizing distributions of radiocarbon measurements. The KDE model we favor (KDE 1 see SI 1 Methods) largely reflects the same pattern observed for the Bayesian phase models, and shows five discrete human occupation events corresponding to peaks in the KDE distribution at: (1) 48–44 ka cal BP, (2) 44–40 ka cal BP, (3) 39–36 ka cal BP, (4) 33–30 ka cal BP, and (5) 29–26 ka cal BP (SI 1 Figure S14). These fit with the human occupations within layers 6/7 ls/lp (level VIII), 5c (VII), the middle section of 5b (VI), 5a (V) and 4 (IV), and 3b (III), respectively. The KDE approach illustrates how important it is to undertake targeted radiocarbon sampling to focus on only humanly modified substrates and thereby build models that reflect human activity rather than reflecting taphonomic influences or fauna. The agreement between the results of the KDE model and the stratigraphic models is evidence for a largely intact and well identified stratigraphic sequence at Kozarnika. The only notable challenges are found within layer 5b as noted earlier.

We compared the PDF for the Date estimate of 6/7 with the Bacho Kiro dataset, since it is the most relevant, considering its nearness to Kozarnika (Fewlass et al. 2020). We generated a Date estimate for the N1-I layer at Bacho Kiro with Kozarnika in Figure 7. The two PDFs show an offset with the Kozarnika distribution slightly earlier. We note, however, that in the upper part of N1-J, which is below the IUP-associated N1-I level, the excavators identify the

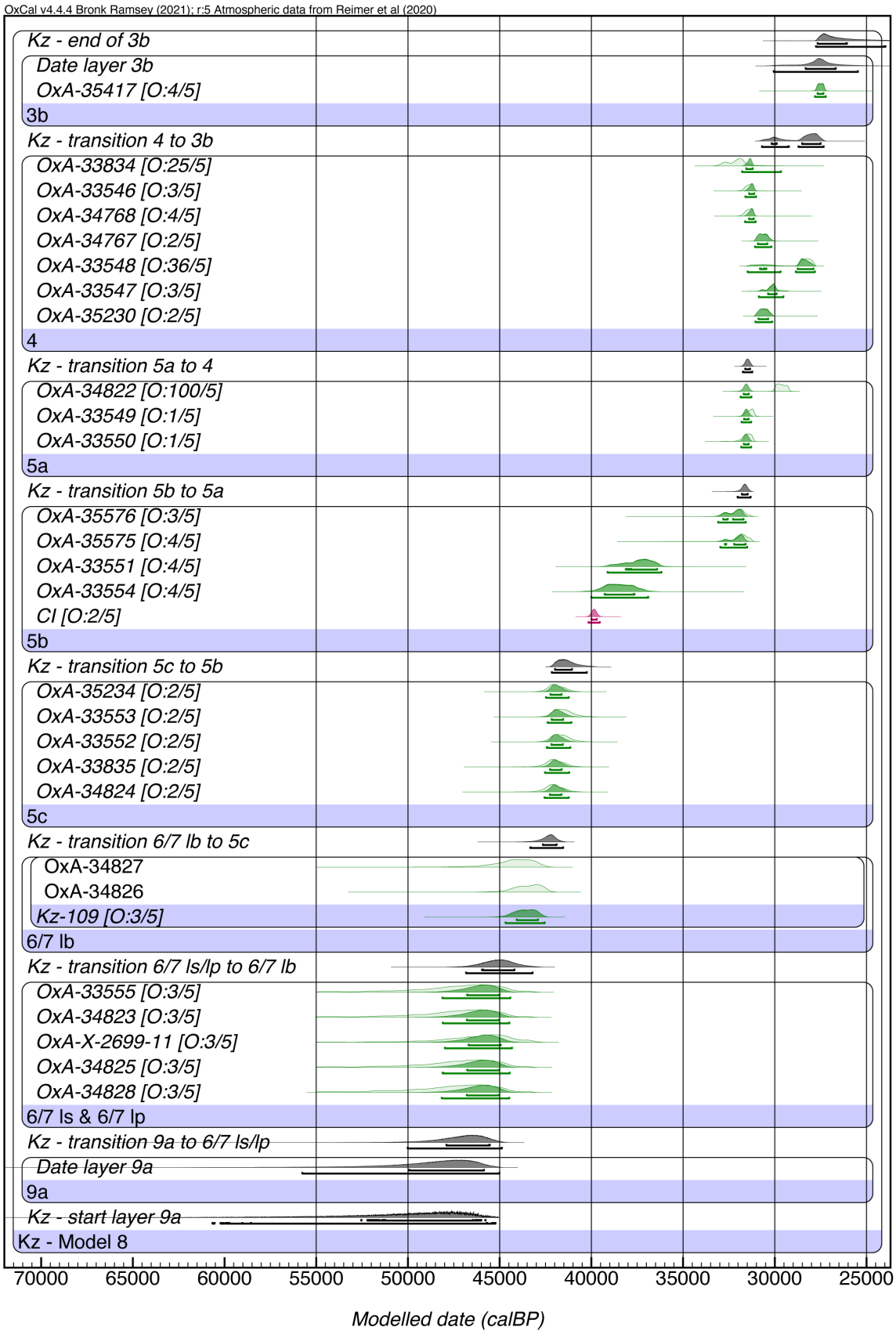

Figure 6. Final Bayesian age model from the Kozarnika site. The green posterior probability distributions are determinations on humanly modified bone. Outlier probabilities (O: posterior/prior) *are given next to the date information. All were set to 5%. There is one major outlier of significance (OxA-34822 at 100%) and two others which have an outlier posterior probability that is higher than the prior. See text for details.*

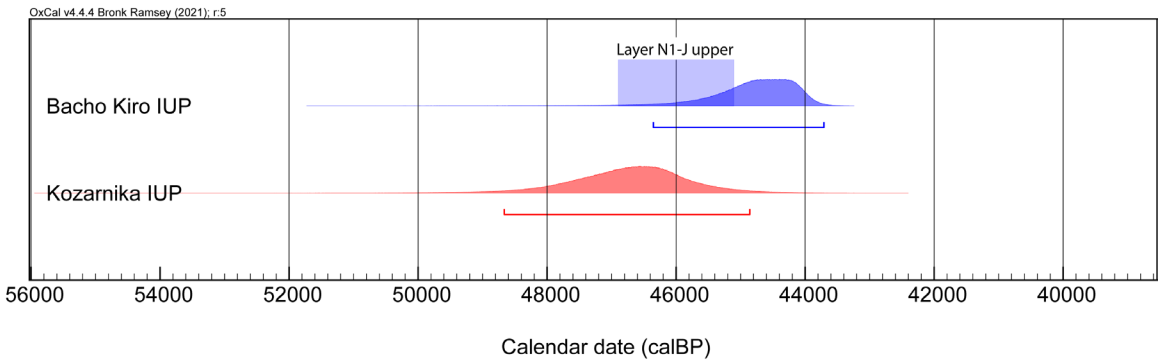

Figure 7. Comparison of the Date command outputs from Kozarnika and Bacho Kiro. The dark blue Bacho Kiro PDF is the Date estimate for the N1-I layer, while the opaque blue box indicates the likely range of the IUP back to the middle of that layer, as outlined by Fewlass et al. (2020). The comparison shows that there is a high degree of overlap between the range distributions.

presence of IUP artifacts that are similar in their techno-typological characteristics to those from N1-I. Therefore, they suggest that the IUP probably starts earlier than the Date distribution of N1-I would imply (Fewlass et al. 2020). Two AMS determinations from this upper locus span from 45,690–44,390 cal BP. When we place this range onto the Bacho Kiro PDF we observe that there is good agreement with the Kozarnika range, suggesting the two occupations likely overlap in time (see Figure 7).

We compared the Kozarnika start and end Boundary distributions with those from other sites dating to the IUP or early Upper Paleolithic (Figure 8). We observe that other IUP boundaries overlap significantly, spanning from 44-45,000 cal BP, back to almost 50,000 cal BP. Mandrin is the exception and sits earlier (Slimak et al. 2022), while the Bohunician result is limited by poor precision and should be treated with caution. Taken together, the deeper antiquity of modern human presence in Europe raises intriguing questions regarding the extent to which Neanderthals overlapped with moderns generally, and perhaps more specifically in the sites themselves. Ancient DNA evidence from Bacho Kiro shows that the early modern humans ana-

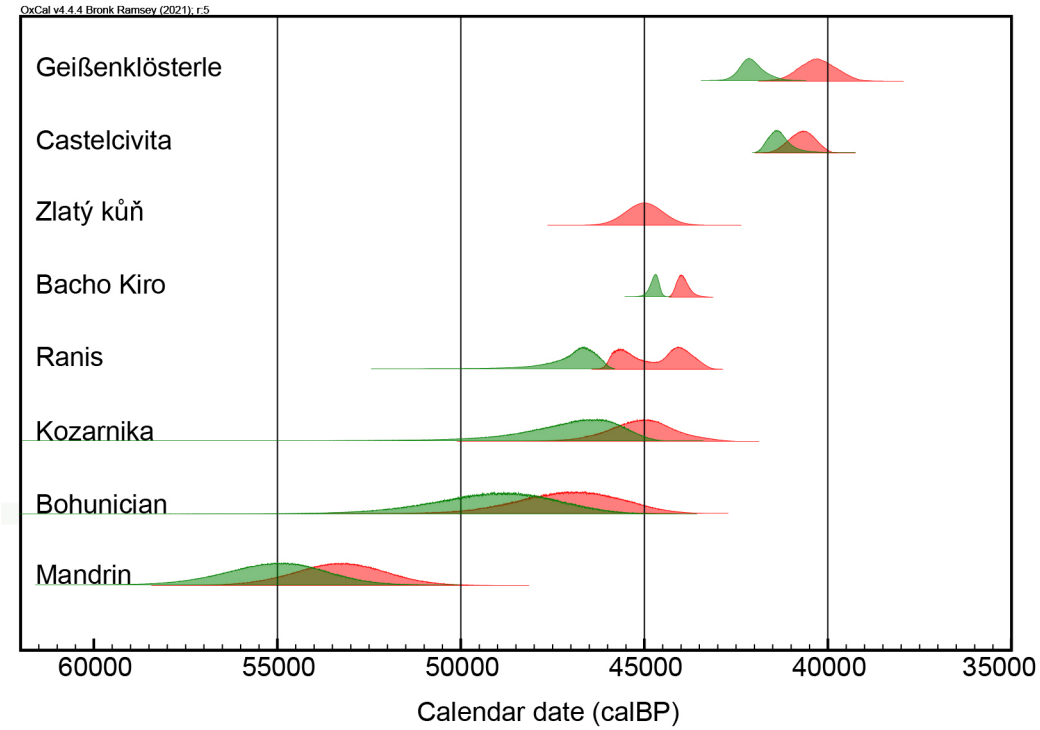

Figure 8. Comparisons between the start (green) and end (red) boundaries for key Early and Initial Upper Paleolithic sites in Europe. Zlatý kůň is an estimated age based on genetic estimates (Prüfer et al. 2021) and may be a minimum age. (see SI 1 Figure S16 for the equivalent image with Date ranges).

lyzed from the IUP levels there had recent Neanderthal ancestry, less than six generations back in one instance, and in two others, intervals of ten and seventeen generations, respectively (Hajdinjak et al. 2021). Similarly, the Zlatý kůň female, found in the Koněprusy caves in the Czech Republic, yielded evidence for Neanderthal ancestry in her genome (3.2%) and an estimated age (based on Bayesian tip dating) of >45,000 cal BP (Prüfer et al. 2021). This confirms the presence of admixed modern humans in central Europe probably in the period prior to 45,000 cal BP at sites with IUP and LRJ technologies such as Kozarnika, Ranis, and Bacho Kiro.

CONCLUSIONS

Radiocarbon data from the upper parts of the sequence at the site of Kozarnika, coupled with Bayesian modelling, have yielded a robust chronometric sequence with few outliers. This supports a well-preserved stratigraphy. The start of Phase 6/7 (ls/lp) is dated from ~50–45 ka cal BP. We think the most likely occupants at this time are modern humans, as evidenced by the remains of *Homo sapiens* co-mingled securely within the same context. If the 'transitional/IUP' industry found within this horizon is solely the result of modern human presence, this boundary would also mark the end of Neanderthal occupation at Kozarnika. However, there are hints of more complexity. The similarity of the Levallois pieces in 6/7 to some of those found in the Mousterian layers below suggest that Neanderthals might have been present during this time too. More detailed work on the lithic assemblage from layer 6/7 is needed as well as the application of sediment DNA analyses. In the Near East, the IUP technocomplex is increasingly brought up in connection with Eurasian sites and seen as a genuine modern human cultural expression (Slimak 2023; Tsanova 2023). This, and other work, suggests that modern human presence in Europe substantially predates 45,000 cal BP, and a long overlap with Neanderthal groups across Europe implies the great potential for genetic and cultural interaction between the two groups, which is indeed seen in the genomes sequenced thus far. Identifying and dating further occurrences of early IUP-like industries in European sites is key if we are to establish the spatio-temporal spread of these early hominins.

ACKNOWLEDGEMENTS

Kozarnika cave fieldwork and post-excavation work is funded by the National Institute of Archaeology and Museum of the Bulgarian Academy of Sciences (N. Sirakov) and UMR5199 CNRS PACEA (J.-L. Guadelli), financially supported by the Advisory Committee of the Archaeological Research abroad of the French Ministry of Foreign Affairs (Mission Paléolithique de Bulgarie directed by J.-L. Guadelli). The bulk of the radiocarbon component of the research leading to these results was based on funding from the European Research Council under the European Union's Seventh Framework Programme (FP7/2007-2013); ERC grant 324139 "PalaeoChron" awarded to T. Higham. Other radiocarbon measurements were obtained as part of the RESET (Response of Humans to Abrupt Environmental Transitions) project funded by the Natural Environment Research Council (NERC) of the UK. The research of C. Stringer is supported by the Calleva Foundation (Grant Number SDV17014) and the Human Origins Research Fund. This paper is a contribution to the NHM's Evolution of Life research theme. We thank the excavation teams of the Kozarnika site and the staff of the Oxford Radiocarbon Accelerator Unit at the University of Oxford for their work.

DATA AVAILABILITY STATEMENT

The authors declare that all data is available in Supplementary Information 1 (text, references, tables, figures, models, and CQL code) and 2 (datasets) to the paper and within the text. ZooMS spectra are available at https://figshare.com/articles/dataset/Palaeolithic_Kozarnika_ZooMS/30074632.

The authors declare no competing interests.

REFERENCES

Brock, F., Higham, T.F.G., Bronk Ramsey, C., 2010. Prescreening techniques for identification of samples suitable for radiocarbon dating of poorly preserved bones. J. Archaeol. Sci. 37(4), 855–865.

Brock, F., Higham, T., Ditchfield, P., Bronk Ramsey, C., 2010. Current pretreatment methods for AMS radiocarbon dating at the Oxford Radiocarbon Accelerator Unit (ORAU). Radiocarbon 52(1), 103–112.

Bronk Ramsey, C., 2009a. Bayesian analysis of radiocarbon dates. Radiocarbon 51(1), 337–360.

Bronk Ramsey, C., 2009b. Dealing with outliers and offsets in radiocarbon dating. Radiocarbon 51(3), 1023–1045.

Bronk Ramsey, C., 2017. Methods of summarizing radiocarbon datasets. Radiocarbon 59, 1809–33.

Bronk Ramsey, C., Higham, T., Leach, P., 2004. Towards high-precision AMS: progress and limitations. Radiocarbon 46(1), 17–24.

Buckley, M., Collins, M., Thomas-Oates, J., Wilson, J.C., 2009. Species identification by analysis of bone collagen using matrix-assisted laser desorption/ionisation time-of-flight mass spectrometry. Rapid Commun. Mass Spectrom., 23(23), pp.3843-3854.

Dee, M., Ramsey, C.B. 2000. Refinement of graphite target production at ORAU. Nucl. Instrum. Methods Phys. Res. B 172(1-4), 449–453.

Devièse, T., Comeskey, D., McCullagh, J., Ramsey, C.B., Higham, T., 2018. New protocol for compound specific radiocarbon analysis of archaeological bones. Rapid Commun. Mass Spectrom. 32, 373–79.

Djakovic, I., Key, A., Soressi, M. 2022. Optimal linear estimation models predict 1400-2900 years of overlap between *Homo sapiens* and Neandertals prior to their disappearance from France and northern Spain. Sci. Rep. 12(1), 15000.

Ferrier, C., Leblanc, J.-C., Berthet, A. L., Delfour, G., 2009. La Grotte Kozarnika (Gara Oreshets, Bulgarie): données stratigraphiques, géologiques et sédimentologiques. In: Gatsov, I., Guadelli, J.L. (Eds.), Saxa Loquuntur ! "The Stone Will Speak": sbornik včest na 65-godišninata na Nikolay Sirakov. Avalon Publishing, Sofia, pp. 13–27.

Fewlass, H., Talamo, S., Tuna, T., Fagault, Y., Kromer, B., Hoffmann, H., Pangrazzi, C., Hublin, J.J., Bard, E., 2017. Size matters: radiocarbon dates of < 200 μg ancient collagen samples with AixMICADAS and its gas ion source. Radiocarbon 60(2), 425–439.

Fewlass, H., Talamo, S., Wacker, L., Kromer, B., Tuna, T., Fagault, Y., Bard, E., McPherron, S.P., Aldeias, V., Maria, R., Martisius, N.L., 2020. A ^{14}C chronology for the Middle to Upper Palaeolithic transition at Bacho Kiro Cave, Bulgaria. Nat. Ecol. Evol. 4(6), 794–801.

Frouin, M., Douka, K., Dave, A.K., Schwenninger, J-L, Mercier, N., Murray, A.S., Santaniello, F., Boschian, G., Grimaldi, S., Higham, T.F.G., 2022. A refined chronology for the Middle and early Upper Paleolithic sequence of Riparo Mochi (Liguria, Italy). J. Hum. Evol.169, 103211.

Fu, Q., Hajdinjak, M., Moldovan, O. T., Constantin, S., Mallick, S., Skoglund, P., Patterson, N., Rohland, N., Lazaridis, I., Nickel, B., Viola, B., Prufer, K., Meyer, M., Kelso, J., Reich, D., Pääbo, S., 2015. An early modern human from Romania with a recent Neanderthal ancestor. Nature 524, 216–219.

Giaccio, B., Hajdas, I., Isaia, R., Deino, A., Nomades, S., 2017. High–precision ^{14}C and ^{40}Ar/^{39}Ar dating of the Campanian Ignimbrite (Y-5) reconciles the time-scales of climatic-cultural processes at 40ka. Sci. Rep. 7, 45940.

Green, R.E., Krause, J., Briggs, A.W., Maricic, T., Stenzel, U., Kircher, M., Patterson, N., Li, H., Zhai, W., Fritz, M.H.Y., Hansen, N.F., 2010. A draft sequence of the Neandertal genome. Science 328(5979), 710–722.

Guadelli, A. 2004. Étude des incisions du plus ancien os gravé découvert dans la Grotte Kozarnika (Bulgarie du Nord-Ouest). Une preuve de l'existence du symbolisme au Paléolithique inférieur. Arch. Bulg. 3, 1–7.

Guadelli, A., 2009. Bone artifacts from the Paleolithic in Bulgaria. Dissertation for awarding the educational and scientific degree "Doctor". National Archaeological Institute and Museum Bulgarian Academy of Sciences. Part One: Exposition, pp. 378, 183 Figs., 37 Plates. Part Two: Catalogue.

Guadelli, A. 2011. Les artefacts en matières dures animales du paléolithique en Bulgarie. Ph.D. dissertation. Institut National d'Archéologie, Académie Bulgare des Sciences, Sofia.

Guadelli, A., Guadelli, J.-L. 2004. Une expression « symbolique » sur os dans le Paléolithique inférieur: étude préliminaire de l'os incisé de la grotte Kozarnika, Bulgarie du Nord-Ouest. In: Otte, M. (Ed.), Actes du colloque international "La spiritualité". U.I.S.P.P. VIIIème Commission: Paléolithique supérieur. Liège, 10-11-12 décembre 2003. ERAUL 106, Liège, pp. 87–95.

Guadelli, J.-L., Sirakov, N., Anastassova, E., Berry, G., Berthet, A.-L., Delfour, G., Delpech, F., Dimitrova, I., Djabarska, N., Fernandez, P., Ferrier, C., Fontugne, M., Guadelli, A., Iordanova, D., Iordanova, N., Ivavona, S., Kovatcheva, M., Krumov, I., Leblanc, J.-C., Mallye, J.-B., Marinska, M., Miteva, V., Popov, V. V., Sirakova, S., Spassov, R., Taneva, S., Tisnérat-Laborde, N., 2002. Rapport de la Mission Préhistorique française en Bulgarie du Nord « Les plus anciennes manifestations de la présence humaine dans les Balkans » (MAE). Projet de recherche conjoint CNRS-Univ. Bordeaux I / Institut d'Archéologie et Musée de l'Académie bulgare des Sciences.

Guadelli, J.-L., Sirakov, N., Delpech F., Dimitrova, I., Fernandez, P., Ferrier, C., Guadelli, A., Krumov, I., Leblanc, J.-Cl., Sirakova, S., Taneva, S., Tillier A.-M., 2025. Earliest dispersals and migrations to Europe via the Balkans in Lower to Upper Palaeolithic: evidence from Kozarnika Cave (Northern Bulgaria). In: Symposium: Évolution de la biodiversité depuis plus d'un million d'années et rapports entre l'Homme et son environnement sur le littoral méditerranéen. Nice 01-02 octobre 2020, pp. 390–457, Figures 247–273, Tables 30–49.

Guadelli, J.-L., Sirakov, N., Ivanova, S., Sirakova, S., Anastassova, E., Courtaud, P., Dimitrova, I., Djabarska, N., Fernandez, P., Ferrier, C., Fontugne, M., Gambier, D., Guadelli, A., Iordanova, D., Iordanova, N., Kovatcheva, M., Krumov, I., Leblanc, J.-Cl., Mallye, J.-B., Marinska, M., Miteva, V., Popov, V., Spasov, R., Taneva, S., Tisterat-Laborde, N., Tsanova, T., 2005. Une séquence du Paléolithique inférieur au Paléolithique récent dans les Balkans: la grotte Kozarnika à Oreshets (nord-ouest de la Bulgarie). In: Molines, N., Moncel, M-H., Monnier, J.-L. (Eds.), Les premiers peuplements en Europe. British Archaeological Reports, International Series 1364. Archaeopress, Oxford, pp. 87–103.

Hajdinjak, M., Fu, Q., Hübner, A., Petr, M., Mafessoni, F., Grote, S., Skoglund, P., Narasimham, V., Rougier, H., Crevecoeur, I., Semal, P., 2018. Reconstructing the genetic history of late Neanderthals. Nature 555(7698), 652–656.

Hajdinjak, M., Mafessoni, F., Skov, L., Vernot, B., Hübner, A., Fu, Q., Essel, E., Nagel, S., Nickel, B., Richter, J., Moldovan, O.T., Constantin, S., Endarova, E., Zahariev, N., Spasov, R., Welker, F., Smith, G.M., Sinet-Mathiot, V., Paskulin, L., Fewlass, H., Talamo, S., Rezek, Z., Sirakova, S., Sirakov, N., McPherron, S.P., Tsanova, T., Hublin, J.-J., Peter, B.M., Meyer, M., Skoglund, P., Kelso, J., Pääbo, S., 2021. Initial Upper Palaeolithic humans in Europe had recent Neanderthal ancestry. Nature *592*(7853), 253–257.

Harvati, K., Röding, C., Bosman, A.M., Karakostis, F.A., Grün, R., Stringer, C., Karkanas, P., Thompson, N.C., Koutoulidis, V., Moulopoulos, L.A., Gorgoulis, V.G., Kouloukoussa, M., 2019. Apidima Cave fossils provide earliest evidence of *Homo sapiens* in Eurasia. Nature 571, 500–504.

Heydari, M., Guérin, G., Sirakov, N., Fernandez, P., Ferrier, C., Guadelli, A., Leblanc, J.C., Taneva, S., Sirakova,

S., Guadelli, J.L., 2022. The last 30,000 to 700,000 years ago: unravelling the timing of human settlement for the Palaeolithic site of Kozarnika. Quatern. Sci. Rev. 291, 107645.

Higham, T.F.G., 2011. European Middle and Upper Palaeolithic radiocarbon dates are often older than they look: problems with previous dates and some remedies. Antiquity 85 (327), 235–249.

Higham, T.F.G., Basell, L., Jacobi, R.M, Wood, R., Bronk Ramsey, C., Conard, N.J., 2012. Testing models for the beginnings of the Aurignacian and the advent of figurative art and music: the radiocarbon chronology of Geißenklösterle. J. Hum. Evol. 62(6), 664-676.

Higham, T., Douka, K., Wood, R., Bronk Ramsey, C., Brock, F., Basell, L., Camps, M., Arrizabalaga, A., Baena, J., Barroso-Ruíz, C., Bergman, C., Boitard, C., Boscato, P., Caparrós, M., Conard, N.J., Draily, C., Froment, A., Galván, B., Gambassini, P., Garcia-Moreno, A., Grimaldi, S., Haesaerts, P., Holt, B., Iriarte-Chiapusso, M.J., Jelinek, A., Jordá Pardo, J.F., Maíllo-Fernández, J-M., Marom, A., Maroto, J., Menéndez, M., Metz, L., Morin, E., Moroni, A., Negrino, F., Panagopoulou, E., Peresani, M., Pirson, S., de la Rasilla, M., Riel-Salvatore, J., Ronchitelli, A., Santamaria, D., Semal, P., Slimak, L., Soler, J., Soler, N., Villaluenga, A., Pinhasi, R., Jacobi, R., 2014. The timing and spatio-temporal patterning of Neanderthal disappearance. Nature 512, 306–309.

Higham, T.F.G., Jacobi, R.M., Bronk Ramsey, C., 2006. AMS radiocarbon dating of ancient bone using ultrafiltration. Radiocarbon 48(2), 179–195.

Hublin, J.J., Sirakov, N., Aldeias, V., Bailey, S., Bard, E., Delvigne, V., Endarova, E., Fagault, Y., Fewlass, H., Hajdinjak, M., Kromer, B., 2020. Initial Upper Palaeolithic *Homo sapiens* from Bacho Kiro cave, Bulgaria. Nature 581(7808), 299–302.

Lowe, J., Barton, N., Blockley, S., Ramsey, C.B., Cullen, V.L., Davies, W., Gamble, C., Grant, K., Hardiman, M., Housley, R., Lane, C.S., Lee, S., Lewis, M., MacLeod, A., Menzies, M., Müller, W., Pollard, M., Price, C., Roberts, A.P., Rohling, E.J., Satow, C., Smith, V.C., Stringer, C.B., Tomlinson, E.L., White, D., Albert, P., Arienzo, I., Barker, G., Borić, D., Carandente, A., Civetta, L., Ferrier, C., Guadelli, J.-L., Karkanas, P., Koumouzelis, M., Müller, U.C., Orsi, G., Pross, J., Rosi, M., Shalamanov-Korobar, L., Sirakov, N., Tzedakis, P.C., 2012. Volcanic ash layers illuminate the resilience of Neanderthals and early modern humans to natural hazards. Proc. Nat. Acad. Sci. U.S.A. 109(34), 13532–7.

Mylopotamitaki, D., Weiss, M., Fewlass, H., Zavala, E.I., Rougier, H., Sümer, A.P., Hajdinjak, M., Smith, G.M., Ruebens, K., Sinet-Mathiot, V., Pederzani, S., 2024. *Homo sapiens* reached the higher latitudes of Europe by 45,000 years ago. Nature 626(7998), 341–346.

Pederzani, S., Britton, K., Aldeias, V., Bourgon, N., Fewlass, H., Lauer, T., McPherron, S., Rezek, Z., Sirakov, N, Spasov, R., Tran, N-an, Tsanova, T., Hublin, J-J., 2021. Subarctic climate for the earliest *Homo sapiens* in Europe. Sci. Adv. 7, eabi4642.

Prüfer, K., Posth, C., Yu, H., Stoessel, A., Spyrou, M.A., Deviese, T., Mattonai, M., Ribechini, E., Higham, T., Velemínský, P., Brůžek, J., Krause, J., 2021. A genome sequence from a modern human skull over 45,000 years old from Zlatý kůň in Czechia. Nat Ecol Evol 5, 820–825. https://doi.org/10.1038/s41559-021-01443-x

Reimer, P.J., Austin, W.E.N., Bard, E., Bayliss, A., Blackwell, P.G., Bronk Ramsey, C., Butzin, M., Cheng, H., Edwards, R.L., Friedrich, M., Grootes, P.M., Guilderson, T.P., Hajdas, I., Heaton, T.J., Hogg, A.G., Hughen, K.A., Kromer, B., Manning, S.W., Muscheler, R., Palmer, J.G., Pearson, C., van der Plicht, J., Reimer, R.W., Richards, D.A., Scott, E.M., Southon, J.R., Turney, C.S.M., Wacker, L., Adolphi, F., Büntgen, U., Capano, M., Fahrni, S.M., Fogtmann-Schulz, A., Friedrich, R., Köhler, P., Kudsk, S., Miyake, F., Olsen, J., Reinig, F., Sakamoto, M., Sookdeo, A., Talamo, S., 2020. The IntCal20 Northern Hemisphere Radiocarbon Age Calibration Curve (0–55 cal kBP). Radiocarbon 62(4), 725–757.

Sirakov, N., Guadelli, J.-L., Ivanova, S., Sirakova, S., Boudadi-Maligne, M., Dimitrova, I., Fernandez, P., Ferrier, C., Guadelli, A., Iordanova, D., Iordanova, N., Kovatcheva, M., Krumov, I., Leblanc, J.-C., Miteva, V., Popov, V. V., Spassov, R., Taneva, S., Tsanova, T., 2010. An ancient continuous human presence in the Balkans and the beginnings of human settlement in western Eurasia: a Lower Pleistocene example of the Lower Palaeolithic levels in Kozarnika cave (North-western Bulgaria). Quatern. Int. 223-224, 94–106.

Sirakov, N., Tsanova, T., Sirakova, S., Taneva, S., Krumov, I., Dimitrova, I., Kovatcheva, N., 2007. Un nouveau faciès lamellaire du début du Paléolithique supérieur dans les Balkans. PALEO 19, 131–144.

Slimak, L., 2023. The three waves: rethinking the structure of the first Upper Paleolithic in Western Eurasia. PLoS One 18(5), e0277444. https://doi.org/10.1371/journal.pone.0277444

Slimak, L., Zanolli, C., Higham, T., Frouin, M., Schwenninger, J.L., Arnold, L.J., Demuro, M., Douka, K., Mercier, N., Guérin, G., Valladas, H. 2022. Modern human incursion into Neanderthal territories 54,000 years ago at Mandrin, France. Sci. Adv. 8(6), eabj9496.

Stringer, C., 2022. The development of ideas about a recent African origin for *Homo sapiens*. J. Anthropol. Sci. 100, 5–18.

Stuiver, M., Polach, H.A., 1977. Discussion: Reporting of C-14 data. Radiocarbon 19, 355–363.

Szmidt, C.C., Normand, C., Burr, G.S., Hodgins, G.W., LaMotta, S., 2010., AMS ^{14}C dating the Protoaurignacian/Early Aurignacian of Isturitz, France. Implications for Neanderthal–modern human interaction and the timing of technical and cultural innovations in Europe. J. Archaeol. Sci. 37(4), 758–768.

Teyssandier, N., 2008. Revolution or evolution: the emergence of the Upper Paleolithic in Europe. World Archaeol. 40(4), 493–519.

Tillier, A.-M., Sirakov, N., Guadelli, A., Fernandez, P., Sirakova, S., Dimitrova, I., Ferrier, C., Guérin, G., Heidari,

M., Krumov, I., Leblanc, J.-C., Miteva, V., Popov, V., Taneva, S., Guadelli, J.-L., 2017. Evidence of Neanderthals in the Balkans: the infant radius from Kozarnika Cave (Bulgaria). J. Hum. Evol. 111, 54–62.

Tsanova, T., 2003. Le Gravettien en Bulgarie du Nord: niveau IVb de la grotte Kozarnika. In: Tsonev, T., Kokelj, E.M. (Eds.), The Humanized Mineral Word: Towards Social and Symbolic Evaluation of Prehistoric Technologies in South Eastern Europe, Sofia, 3-6 Sept. 2003. ERAUL 103, 33–39.

Tsanova, T., 2023. Preliminary comparison and chronology of the lithic blade and bladelet assemblages at the onset of the Upper Palaeolithic from Bacho Kiro, Temnata and Kozarnika Caves in the Eastern Balkans (Bulgaria). Proc. British Acad. 258, 156–202.

Tsanova, T., Zwyns, N., Eizenberg, L., Teyssandier, N., Le Brun-Ricalens, F., Otte, M., 2012. Le plus petit dénominateur commun: réflexion sur la variabilité des ensembles lamellaires du Paléolithique supérieur ancien d'Eurasie. Un bilan autour des exemples de Kozarnika (Est des Balkans) et Yafteh (Zagros central). L'Anthropologie 116(4), 469–509.

Végh, E., Douka, K., 2024. SpecieScan: semi-automated taxonomic identification of bone collagen peptides from MALDI-ToF-MS. Bioinformatics 40(3), btae054.

Wood, R.E., Bronk Ramsey, C., Higham, T.F.G., 2010. Refining the ultrafiltration bone pretreatment background for radiocarbon dating at ORAU. Radiocarbon 52(2–3), 600–611.

Supplement 1 to A Refined Chronology for the Middle–Upper Paleolithic Transition at Kozarnika Cave (Bulgaria) 40–50,000 Years Ago: New AMS Radiocarbon Dates and Implications for Early *Homo sapiens* in Europe

RACHEL HOPKINS
RLAHA, University of Oxford, Oxford, UNITED KINGDOM; and, Meow Wolf, Inc., 1352 Rufina Circle, Santa Fe, NM 87507, USA; rja.hopkins@protonmail.com

JEAN-LUC GUADELLI
PACEA-UMR 5199 CNRS, Université de Bordeaux, Allée Geoffroy St Hilaire, Bâtiment B2, CS 50023, 33615 Pessac cedex, FRANCE; jean-luc.guadelli@u-bordeaux.fr

DUSTIN WHITE
Department of Chemistry, University of York, UNITED KINGDOM; dustin.white@york.ac.uk

CHRIS STRINGER
Natural History Museum, Cromwell Road, London, UNITED KINGDOM; c.stringer@nhm.ac.uk

EMESE VÈGH
Department of Evolutionary Anthropology, University of Vienna, University Biology Building, Djerassiplatz 1, A-1030 Vienna; and, Human Evolution and Archaeological Science (HEAS) Network, Vienna, AUSTRIA; emese.vegh@univie.ac.at

MICHAEL BUCKLEY
Manchester Institute of Biotechnology, University of Manchester, M1 7DN, UNITED KINGDOM; M.Buckley@manchester.ac.uk

ALETA GUADELLI
Center for Underwater Archaeology, State Cultural Institute, Ministry of Culture, Str. Apollonia n°1, 8130 Sozopol, BULGARIA; aleta.guadelli@gmail.com

PHILIPPE FERNANDEZ
LAMPEA UMR 7269, CNRS, Aix Marseille Univ., Minist. Culture, MMSH, 5 Rue du Château de l'Horloge, F13094, Aix-en-Provence, FRANCE; philippe.fernandez@univ-amu.fr

NIKOLAI SIRAKOV
National Institute of Archaeology with Museum-Bulgarian Academy of Sciences, 2, Saborna Street, 1000, Sofia, BULGARIA; nikolaysirakov@gmail.com

TOM HIGHAM
Department of Evolutionary Anthropology, University of Vienna, University Biology Building, Djerassiplatz 1, A-1030 Vienna; and, Human Evolution and Archaeological Science (HEAS) Network, Vienna, AUSTRIA; thomas.higham@univie.ac.at

SUPPLEMENT 1

This supplement contains: Supplementary text, Supplementary Tables S1–S5, Supplementary Figures S1–S20, selected images of modified bones for AMS dating, Supplementary references, and CQL codes.

Supplementary Methods

Table of Contents

The Kozarnika site

Kozarnika is in north-west Bulgaria, close to the Danube plains in the pre-Balkans and sits at 481m a.s.l. at 43.652 N, 22.702 E (Sirakov et al. 2010) (Figure 1). The cave comprises a 210m long gallery, divided into three main sections (Figure 2). The front of the cave averages 11m wide and the vault ceiling 3.5m above the modern floor level. The boundary from this entrance section to the gallery (second section) is marked by a narrowing of the walls to ~5m width and 2m height. The gallery widens again towards the rear of the cave, reaching 18.5m width and 5m height at the point at which it leads to the last section, the salle terminal (the 'rear hall'). The rear of the cave formed because of a fracture in the same direction as some of the fractures visible in the gallery (Guadelli et al. 1998; 2016). During the Middle Ages and modern period, the cave was used for various agricultural purposes. The name Kozarnika means the 'goat herding cave'. In the past, the site has also been known as the 'dry cave' (Sirakov et al. 2010).

Kozarnika was first identified as an archaeological site by R. Popov in 1931 (Popov 1933). However, no extensive archaeological work took place until much later. In the 1960s the site was turned into a nuclear fallout shelter—the remains of the brick wall enclosing the entrance were still in place in 1994, when N. Sirakov, H. Laville, and S. Ivanova returned to the site for archaeological prospections (Guadelli and Sirakov 1996). Subsequently, a Bulgarian-French collaboration led by J.-L. Guadelli and N. Sirakov, started archaeological excavations at Kozarnika in 1996 (ongoing), and revealed an extensive stratigraphy.

Stratigraphic units at the excavation were independently labelled with Latin letters and Arabic numbers. A is of special interest because it yielded material from the early Upper Paleolithic. Layers 10a–5a are around 1.2–1.5m thick and are "characterized by a finely powdered beige silty fraction, probably of aeolian origin "(Sirakov et al. 2010: 96). The coarse fraction, calcareous gravel and heterometric pebbles, are derived from fragmentation of walls and ceiling. Their abundance decreases through the sequence, with the highest concentrations found in layer 10a. In most areas of excavation, layers 6 and 7 were too similar to separate, resulting in the designation 6/7 for the combined unit. Sirakov et al. (2010) describes it as "silty sediment (3–5cm thick), light brown (layer 7) to light gray (layer 6), containing rare calcareous gravels as well as charcoal". More recent work has shown a range in thickness covering 3–15cm. In some cases, the layer turns into a thin charcoal horizon (Ferrier et al. 2009). Layers 4–3a are 1.14m thick with often strongly deformed limits. It is "composed of calcareous gravel in a light brown to whitish powdered silty matrix with a lamellar structure" (Sirakov et al. 2010: 97). Sediment origin is the same as for the layers below, though their relative concentration has changed—cave wall and ceiling fractions outweigh aeolian sediment. Both the lamellar structure and evidence of cryoturbation indicate repeated frost/thaw processes post-sedimentation. The latter is strongest in layer 4, which also contains a significant number of fallen rocks (Sirakov et al. 2007; 2010).

Layer 6/7

Layer 6/7 is the key archaeological horizon at Kozarnika which references the earliest inferred presence of modern humans. From excavation season 2016 onwards, separation of this layer into three sub-facies was possible. These were labelled 6/7 lb, 6/7 ls, and 6/7 lp, in squares D7-9 and E7-9. In the upper and middle parts of layer 6/7, there are three sedimentological facies: 6/7 lp (powdery silt); 6/7 ls (sandy silt); 6/7 lb (brown silt - more clayey) which result from local sedimentological and partly post-sedimentological processes, within the same lithostratigraphic unit 6/7; these facies are present in almost the entire thickness of the layer without inferring any stratigraphic order. Details of the 3D plotted lithics and faunal remains are shown in Figures S1–S3.

As outlined in the main paper, gelifluction influenced layer 6/7. A soon-to-be-published study of the fauna of the site shows that the minimum thermal parameters for January place Kozarnika in present-day conditions close to those prevailing in the Lviv region and that the thermal parameters values of July (maximum of July) place Kozarnika in present-day conditions close to those prevailing in the region of Budapest. As for the post-depositional conditions for layers 5c to 5a, the thermal parameter values of January (minimum of January) place Kozarnika in current conditions close to those prevailing in the Stockholm region (5c), Berlin region (5b) and Warsaw region (5a) and the thermal parameters values of July (maximum of July) place again Kozarnika in current conditions close to those prevailing in the Budapest region (5c, 5b, 5a). Clearly, then, this suggests that at the latitude of Kozarnika, thermal conditions were colder than they are today, which is understandable for a Late Pleistocene, especially with colder winters, but not near severe periglacial conditions.

Figure S1. Y-Z projection for lithics and faunal remains from layer 6/7 Kozarnika.

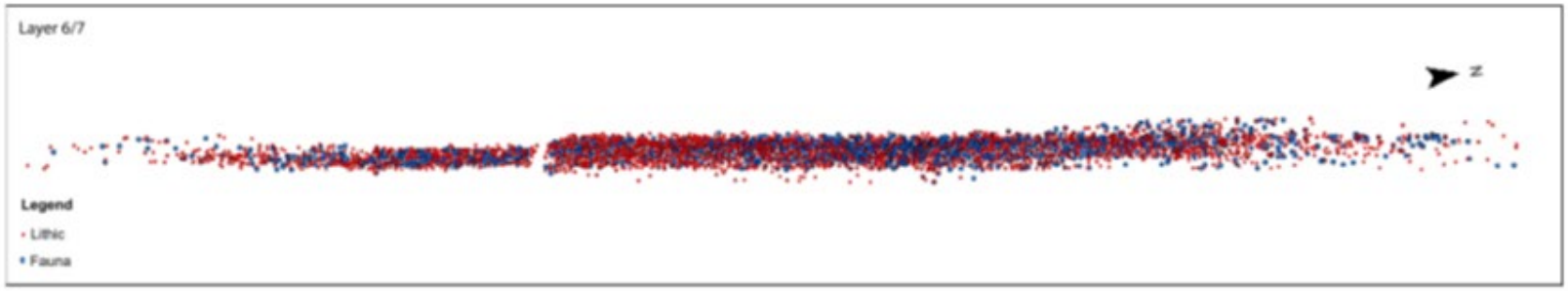

Figure S2. A 3D X-Y-Z projection for lithics and faunal remains from layer 6/7 Kozarnika.

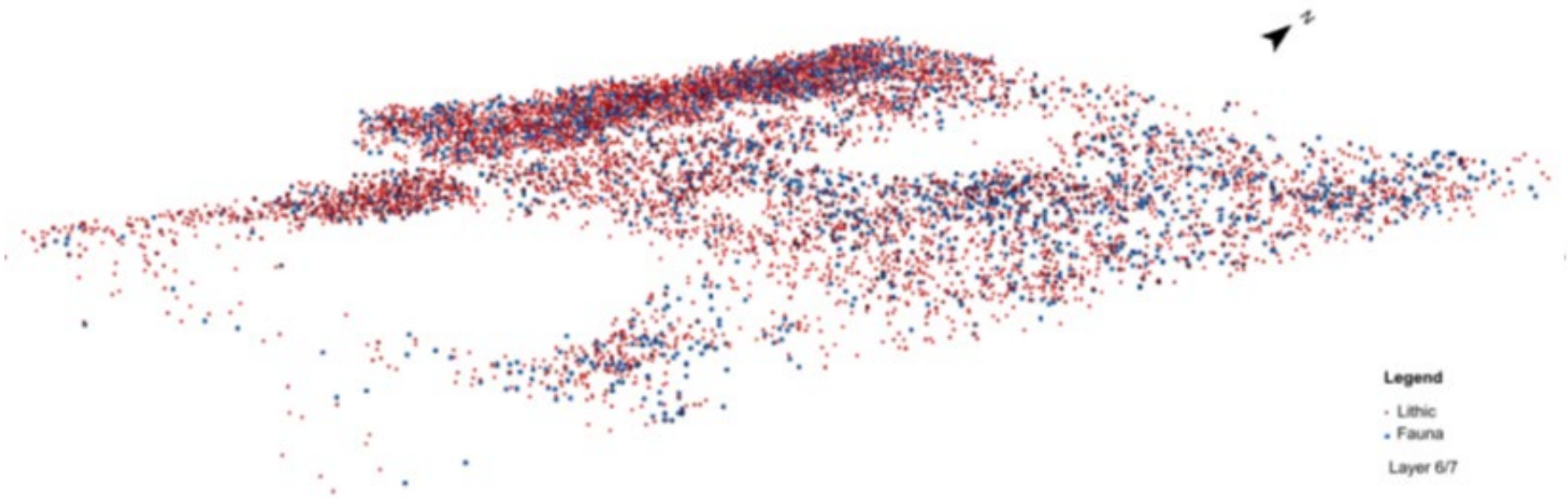

Figure S3. Plan X-Y showing lithics, charcoal and faunal remains from layer 6/7 Kozarnika.

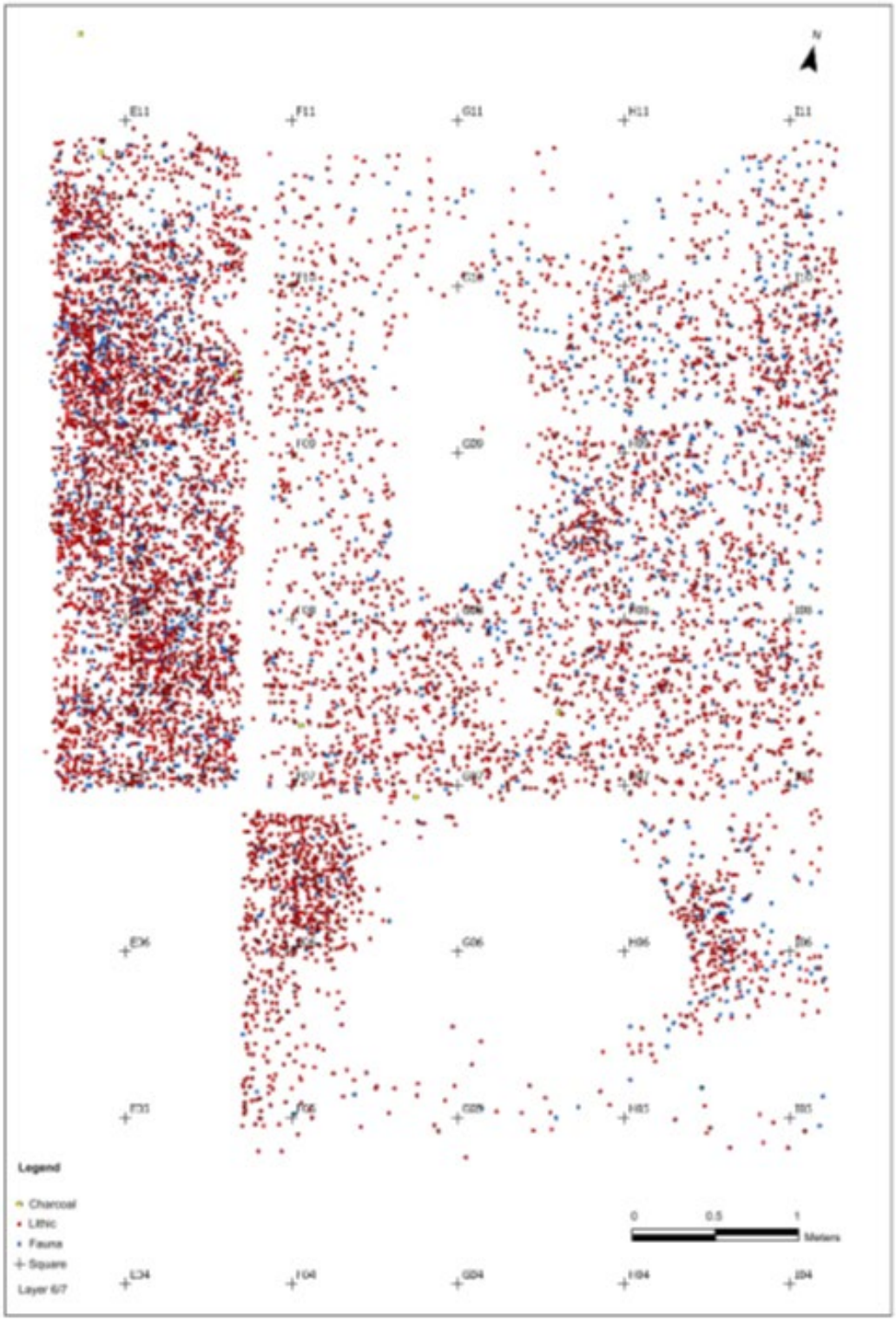

Fifty-one human remains have been identified in Kozarnika of which 33 come from Paleolithic levels. Unfortunately, some of these were found following an analysis of sediment disturbed by clandestine excavations. Several skeletal fragments were found in sector I/II. In the Lower Paleolithic layer 13, a cranial fragment (D13-T/1022-F2) was discovered. Further up, an upper right DI1 (E15-T/651-F4) was unearthed in layer 12. Presently, they have only been identified as '*Homo* sp'. Also identified as '*Homo* sp' we have in the Lower Paleolithic levels a very damaged metapodium* (G7-5430, layer 11b), a cranial part of cervical vertebra 1* (F8-2608-F1, layer 10b-11a), a part of left ulna shaft (H7-3606, c.10b-11a) and in the Middle Paleolithic levels, a damaged upper ID1 (D7-2685, layer 10a) and a small fragment of cranium* (D8-E8-T/2281-F2, layer 10a-fm). In contrast, a left radius (G10-2249, G10-2248) found in layer 10b, and published in Ref. 20, clearly belonged to an infant Neanderthal. In the Initial Upper Paleolithic layer 6/7, the first phalanx (F7-T467-F12) of a human hand (Figure 4a), a crown portion of I1-2 or Canine (H7-T/469-F2) and a lower right *Homo sapiens* P3 (E9-2944, layer 6/7ls) (Figure 4b) were retrieved. In addition, 9 fragments (pisiform*, metacarpal 1* and 2*, phalange 2* and vertebrae*)[1] are undoubtedly attributable to *Homo* (juvenile and adult). From *Homo sapiens*, 3 skull fragments* were discovered in layer 5c (H6-T/855-F49, G5-1048, H3-1199) and a third phalanx (H5-H6-T/833-F1343) in layer 5b. Finally, while cleaning fallen sediments from a profile, we recently found a right upper M1 (D-E7-10-K/3329-F1). It may be attributed to the Upper Paleolithic, but in addition to its morphometric study, direct dating and DNA analysis are required.

In sector III, the situation is more complex, as in addition to the Paleolithic levels, there were probably Protohistoric burials here, and the 20 human bones initially discovered from illicit excavations therefore have no reliable archaeological context.

Previous dating work at Kozarnika

Prior to our work, two separate radiocarbon dating campaigns were undertaken: one focusing on the age of the archaeological levels, and one in relation to the analysis of tephra at the site. The locations for previous radiocarbon sampling are illustrated in Figure S4 and compared to the squares sampled for this project.

An initial radiocarbon dating program, covering all Upper Paleolithic layers, resulted in radiocarbon measurements from 12 charcoals, 1 charred earth sample, 2 plant remains, and 1 faunal bone fragment (Guadelli et al. 2002) (Table S1). The samples were all processed at the Laboratoire des Sciences du Climate et de l'environment in Gif-sur-Yvette (UMR 8212, France), except for five dated using proportional gas counting (PGC) at the Laboratoire Souterrain de Modane (UMR 6417, France).

[1] Note: the small size of the fragments with "*" (less than 2cm) means that these determinations will have to be confirmed by DNA or ZooMS analysis.

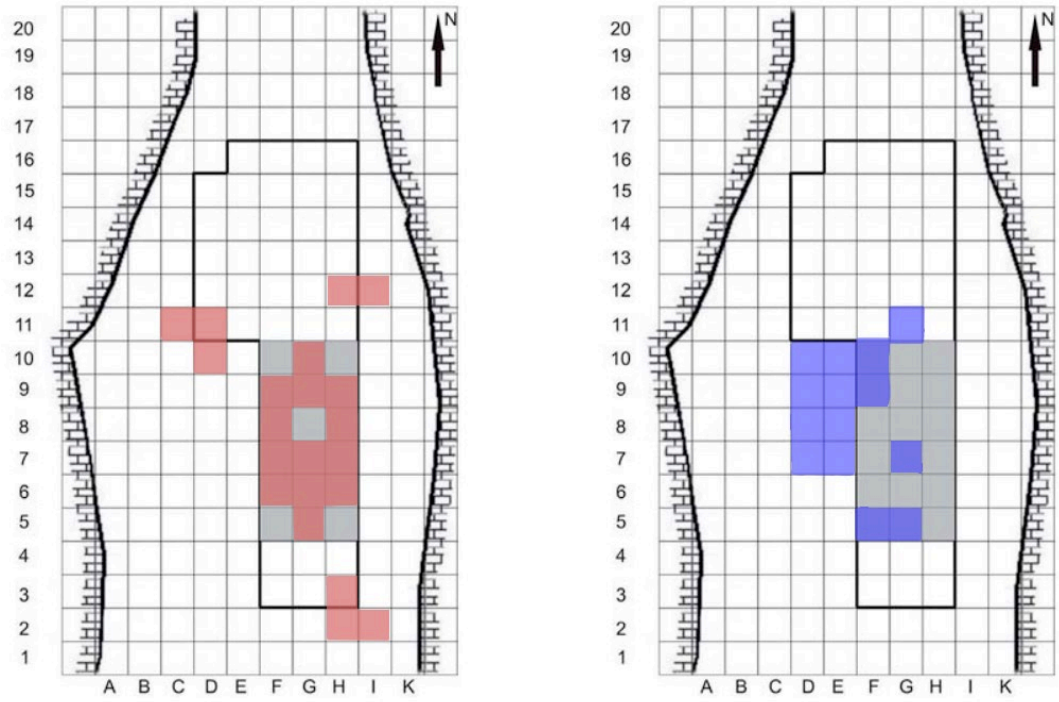

Figure S4: Kozarnika: Location of radiocarbon sampling highlighted in Kozarnika with co-ordinate system in sector I/II with previous dating in red (left) and new ones in blue (right), this paper.

Unfortunately, most of the samples dated cannot be securely connected to human activity at the site. Some (e.g., GifA-99662) have an ambiguous context attribution, referred to coming from both from layer 5c, and from level VIII. Three further samples (Gif-10673, GifA-101050, GifA-101052) were collected in contact zones. Without clear level attribution, the resulting radiocarbon ages are, therefore, unsuitable for Bayesian modelling. The remaining measurements suggested an early appearance of the Upper Paleolithic at Kozarnika. However, the four dates of most interest (covering layers 5c and 6/7) might be underestimating the true age of the samples, because the charcoal samples were only prepared using a less rigorous ABA pre-treatment. Experience has shown at an oxidation treatment is required to produce accurate dates on charcoal older than ~25,000 BP.

Date code	Sample no	Material	Layer	Square	Depth (cm)	Treat-ment	^{14}C age BP	±	δ^{13}C (per mille)
GifA-98345	7	charcoal	3a=0I	H2-I2	300-310	ABA	11550	100	
GifA-98346	1	charred earth	3a=0I	H2-I2	300-310	ABA	11490	120	
GifA-97285	9	vegetation	3a=I	G6/G5	330-334	ABA	7840	70	
Gif-10674	8	charcoal	3b+III	F6-G6	372-389	ABA	19770	270	-23.61
Gif-10673	4	charcoal	3b/4=III/Iva	H8	387-389	ABA	19890	270	-22.67
GifA-97286	11	vegetation	4=IVa	H7	391-393	ABA	26010	270	
Gif/LSM-10677	14	charcoal	4=Ivb	F7	402-405	ABA	26120	100	-23.29

Gif-10992	19	charcoal	5a=V	F7	425-431	ABA	25650	730	-23.42
GifA-99044	20	charcoal	5b=VI	F8	431-434	ABA	26490	270	-23.98
Gif/LSM-10994	*21*	*charcoal*	*5c=VII*	*F7*	*450-452*	*ABA*	*38700*	*1400*	*-24.2*
GifA-99706	*33*	*charcoal*	*5c=VII*	*F8*	*455*	*ABA*	*36200*	*540*	
GifA-101050	34	charcoal	5c-6/7=VII	D10-D11	447-451	ABA	37170	700	
GifA-99662	32	fauna	5c=VIII	F8	457-461	ABA	39310	100	
GifA-101052	36	charcoal	6/7-9=VIII	G7	470-473	ABA	42700	1000	
GifA-101051	*35*	*charcoal*	*6/7=VIII*	*D11-C11*	*458-460*	*ABA*	*43600*	*1200*	
GifA-101048	*30*	*charcoal*	*6/7=VIII*	*F8*	*457-461*	*ABA*	*29310*	*320*	

Table S1: Previously obtained radiocarbon dates from the Laboratoire des Sciences du Climate de l'environment in Gif-sur-Yvette (Guadelli et al., 2002, p. 211-215). "GifA-" dates were measured by AMS at Gif-sur-Yvette, the remaining dates by proportional gas counting (PGC) at the Laboratoire Souterrain de Modane. Geological layer given in Arabic numbers, archaeological levels in Roman numerals. Conventional radiocarbon ages Before Present are shown with $\pm$ 1 standard error. Grey rows – radiocarbon ages are considered unsuitable for modelling based on sample type, pretreatment and location; italic – ^{14}C dates >30k BP from charcoal samples treated with ABA only must be treated with caution.

Previous dates from the "RESET" project

The second dating effort was undertaken through the RESET (Response of Humans to Abrupt Environmental Transitions) project, which focused on the impact of volcanic ash layers (tephra) on the archaeology of the Middle to Upper Paleolithic transition. While some of the AMS measurements are reliable, some are experimental in nature (Table S2). In addition to dating, a bulk tephra horizon observed in layer 5b (21) was able to be correlated to the CI (Y5) eruption (Lowe et al. 2012), now dated to 39.85$\pm$0.14 ka cal BP (Giaccio et al. 2017). Further microtephra bands were found in layer 9a and 9c. Their similarities could indicate that they resulted from the same eruption, though it could not be excluded that they represent two separate events. The origin of this older tephra is presently undetermined.

Twenty AMS radiocarbon measurements were obtained on "single entity" samples covering the Upper Paleolithic layers 4 to 6/7. The two main pre-treatments used were ORAU's standard ABA protocol for charcoals (labelled ZR), and ABOx (coded XR) as described by Brock et al. (2010). Four samples (no. KZ-09, 28, 50, 55 and 58) were split, one fraction treated with ZR, the other with XR. A comparison of the results shows higher sample loss typical when applying the more rigorous ABOx treatment, as well as resulting higher %C on combustion. With charcoal samples older than 30,000 BP, we often see that XR treated fractions result in older radiocarbon ages, confirming the need for caution when dealing with ABA treated charcoal samples from this period. This is work, only one of the XR dates was older than the ABA result, suggesting contamination was low in its impact. Three results were dated using experimental, 'non-routine chemistry' (NRC) protocols, which refer to experiments using the ABOx method. OxA-X-2443-7 and OxA-X- 2416-47 were tested using CuO under vacuum method. OxA-X-2443-8 had an initial reaction under vacuum.

Date code	Sample no.	Layer	Square	Depth (cm)	PCode	Yield (mg)(wt.%)	%C	fM	fM ±	^{14}C age BP	±	δ^{13}C (per mille)
OxA-25184	48	4=IVb	F9	412-419	ZR	11.8 (42.2)	62.9	0.03315	0.00078	27370	190	-23.4
OxA-X-2443-7	KZ-09	4=IVb	H12-I12	421-423	NRC	5.69 (6.1)	78.3	0.04091	0.00069	25680	140	-22
OxA-X-2443-8	KZ-09	4=IVb	H12-I12	421-423	NRC	6.71 (7.2)	76.8	0.03926	0.00066	26010	140	-22
OxA-25355	KZ-09	4=IVb	H12-I12	421-423	XR	3.98 (4.3)	75.8	0.04041	0.00069	25770	140	-21.9
OxA-24786	25	5a=V	-	-	ZR	3.95 (18.9)	63.5	0.03775	0.00089	26320	190	-23.7
OxA-24865	56	5b=VI	H6	441-443	XR	3.35 (4)	80.5	0.02923	0.00064	28380	170	-23.4
OxA-22914	73	5b=VI	H3	443-444	ZR	24.2 (27.9)	60	0.01094	0.00062	36250	450	-23.7
OxA-24059	58	5b=VI	G5	445-448	XR	4.24(14.7)	70.5	0.01044	0.00060	36650	450	-23.3
OxA-22913	58	5b=VI	G5	445-448	ZR	34.8 (42.8)	65.2	0.01116	0.00056	36100	400	-23.5
OxA-24080	29	5c=VII	F7/G7	450-453	XR	7.51 (6.4)	77.8	0.01083	0.00057	36350	400	-23.2
OxA-22915	50	5c=VII	G9	449-451	ZR	22.7 (25.6)	60.8	0.01168	0.00060	35750	400	-23.6
OxA-24802	50	5c=VII	G9	449-451	XR	8.07 (7.4)	68.2	0.00923	0.00060	37650	500	-23.4
OxA-25405	51	5c=VII	F9	449-451	XR	8.83 (8.4)	89.9	0.01009	0.00054	36900	450	-23
OxA-25406	52	5c=VII	G9	451-452	XR	6.8 (6.3)	80.1	0.00926	0.00057	37600	500	-22.8
OxA-24058	55	5c=VII	G10	460	XR	8.85 (5.6)	79.2	0.01787	0.00058	32330	260	-22.4
OxA-X-2416-47	55	5c=VII	G10	460	NRC	7.79 (4.9)	83.7	0.01734	0.00057	32570	260	-22.7
OxA-23975	28	5c=VII	F8	445-446	XR	4.63 (19.4)	77.2	0.00879	0.00054	38050	500	-24.3
OxA-22916	28	5c=VII	F8	445-446	ZR	29.9 (41.3)	61.2	0.00986	0.00061	37100	500	-25.3
OxA-22842	66	6/7=VIII	F6	468-470	ZR	11.1 (52.6)	61	0.00599	0.00058	41100	750	-23.2
OxA-24083	69	6/7=VIII	H9	486-487	XR	3.31 (5.5)	70.9	0.00950	0.00059	37400	500	-24

Table S2: Previously obtained AMS radiocarbon dates from charcoal samples, measured under the RESET project (unpublished). Geological layer given in Arabic numbers, archaeological level in Roman numerals. ZR = ABA pre-treatment on charcoals; XR = ABOx pre-treatment on charcoal (see Brock et al. 2010); NRC = non-routine chemistry, see text for details. Grey rows – radiocarbon ages unsuitable for modelling based on pre-treatment chemistry. Italic text denotes ^{14}C dates >30k BP from charcoal samples treated with ABA only, these must be treated with caution.

In summary, the initial radiocarbon efforts from Kozarnika provided 13 radiocarbon age estimates on charcoal that we consider reliable and 7 that are potentially problematic due to a combination of less robust pretreatment and context problems, implying that in some instances these are minimum age estimates, as well as a securely identified CI tephra as a chronological marker in layer 5b. However, there was substantial dating variability and uncertainty in layer 6/7, potentially caused by using charcoal samples towards the limit of the radiocarbon method without robust pretreatment methodologies to remove trace contamination. We built a Bayesian model to show the results we think are most robust from this earlier work (Figure S17). This shows that, while the results from 6/7 appear to be underestimates of the age determined following the results outlined in this paper, those from 5c appear to be in good agreement with the results presented here.

Additional context details:

During the archaeological excavation in sector III, an ochre layer (layer A) containing an osseous fragment (Kz-58) – believed to be the base of a Mladeč point – was uncovered. Unfortunately, this sector is presently not physically connected to sectors I and II. On the basis of lithic industries and faunal associations A. Guadelli has proposed an "archaeological" correlation between sector III and the vestibule (sectors I and II): from bottom to the top, the industries of layers D and C would correspond to those of level VIII (layer 6/7 or one of its facies), layer A would have no archaeological equivalent and the archaeological content of layer U1 (not discussed here) would be the equivalent of level VII (layer 5c). Of course, even if the dates seem *pro parte* to support this hypothesis, only a direct stratigraphic connection between sectors III and I/II will validate or invalidate it. By sampling material from within an adjacent layer A, the age of layer A could be further constrained, thus allowing at least for a chronological comparison. However, no layers above were left *in situ* and no other securely anthropogenically modified faunal remains had been found. Instead, 7 samples (covering layers A, C and D) not securely connected to human activity (i.e., only showing possible anthropogenic cut marks) were sampled to provide some temporal understanding of sector III.

After obtaining the radiocarbon measurements, some discrepancies between radiocarbon age and layer attribution prompted a thorough re-checking of the archaeological contexts of all dated samples. While the information found in excavation journals and site drawings was consistent with those found in sample bags and bone fragments for most samples, in the cases below they were not:

1. Kz-110 was originally labelled on site as belonging to layer 6/7 Ib. Looking at the planum drawing from just above (depth: 460cm), the location is marked as 6/7 Ip, while the one from just below (depth: 465cm) shows 6/7 Is. In addition, the sample shows patina consistent with other samples from layer 6/7 Ip, but not with layer 6/7 Ib. It can be concluded that the sample belongs to either layer 6/7 Ip or 6/7 Is. The radiocarbon age of 44,000 BP (OxA-34828) is consistent with such an attribution.
2. Kz-87 was originally attributed to 5c. The find location is marked by very uneven layer limits, which leave an alternating pattern between layer 6/7 and 5c when cut horizontally. The patina differs from other artefacts from layer 5c in that sector and shows signs of heating, consistent with an origin in the 'fireplace' layer below 5c, i.e. at the top of layer 6/7. Consequently, the layer attribution was changed from 5c to 6/7. The label on the bag for Kz-87 had the following information written on it when radiocarbon sampling was conducted: "E9-2452, E9, 5b, 443-445 cm". However, the excavation journal has no sample E9-2452 listed at that depth. Instead, E9-2452 is featured on the sample list for spit 450-453cm. As the bone fragment has the number E9-2452 clearly written on it, the depth on the bag was undoubtedly a clerical error. The location of sample E9-2452 on the planum drawing is well within layer 5c. This information is more secure than the sample list noting layer 6/7, as misspelling a layer number is significantly more likely than missing a layer in a drawing.
3. Kz-48 was bagged as coming from layer 5b, however, the excavation documentation leaves attribution somewhat ambiguous. Both layers 5b and 5c were found in the vicinity of the sample, judging by plana drawings. As a result, both layer attributions were tested during Bayesian modelling.

Ref. no	Item	Excavation year	Sample no.	Sq.	Layer	x(m)	y(m)	z(m)	weight (mg)
Kz-03	faunal	2013	D7-92	D7	3b	194.55	1498.1	-3.84	894
Kz-06	faunal	2013	E9-343	E9	4 (IVa)	195.33	1500.47	-3.9	577
Kz-07	faunal	2014	D8-270	D8	4 (IVa)	194.94	1499.45	-3.99	360
Kz-08	faunal	2013	E9-477	E9	4 (IVa)	195.53	1500.43	-3.94	575
Kz-10	faunal	2013	E7-306	E7	4 (IVa)	195.02	1498.06	-3.93	610
Kz-14	faunal	2014	E7-744	E7	4 (IVb)	195.59	1498.69	-4.12	888
Kz-15	retoucher	2014	E10-471	E10	4 (IVb)	195.26	1501.32	-4.11	841
Kz-19	faunal	2014	E9-1045	E9	4 (IVb)	195.02	1500.71	-4.11	649
Kz-23	faunal	2014	D10-300	D10	4 (IVb)	194.82	1501.71	-4.1	577
Kz-24	faunal	2001	F10-n469	F10	5a	196.08	1501.03	-4.23	525
Kz-25	faunal	2001	F10-549	F10	5a	196.65	1501.77	-4.29	595
Kz-38	faunal	1997	F8-1169	F8	5b	196.11	1499.83	-4.39	608
Kz-39	faunal	1997	F8-1146	F8	5b	196.64	1499.98	-4.32	409
Kz-43	faunal	2002	G5-498	G5	5c	197.82	1496.37	-4.41	626
Kz-44	faunal	1999	F7-1955	F7	6/7	196.36	1498.89	-4.63	530
Kz-45	faunal	2001	F10-754	F10	5b	196.24	1501.74	-4.43	555
Kz-47	faunal	1997	F8-1327	F8	5c	196.63	1499.13	-4.48	605
Kz-48	faunal	2002	G5-588	G5	5c (5b*)	197.93	1496.13	-4.42	494
Kz-49	faunal	1997	G7-1793	G7	5c	197.78	1498.71	-4.51	601
Kz-50	faunal	1999	K844	G11	5b	197.4	1560.69	-4.55	478
Kz-52	faunal	2002	F5-1949	F5	6/7(5c*)	196.38	1496.14	-4.54	615
Kz-79	venus'	2014	E10-683	E10	5a	-	-	-4.15-4.2	581
Kz-80	faunal	2016	D8-1517	D8	6/7lp	-	-	-4.58-4.59	977
Kz-81	faunal	2016	E8-2385	E8	6/7ls	-	-	-4.58-4.59	859
Kz-82	faunal	2016	E8-2387	E8	6/7ls	-	-	-4.58 -4.59	864
Kz-83	faunal	2016	E7-2241	E7	6/7ls	-	-	-4.61-4.62	737
Kz-85	faunal	2015	D7-887	D7	5c	-	-	-4.45-4.48	679
Kz-87	faunal	2015	E9-2452	E9	5c\(6/7*)	-	-	-4.5-4.53	847
Kz-88	faunal	2016	D9-990	D9	5b	-	-	-4.45-64.48	766
Kz-90	faunal	2015	D9-988	D9	5b	-	-	-4.43-4.45	756
Kz-93	faunal	2016	E9-2712	E9	6/7lp	-	-	-4.55-4.58	815
Kz-109	faunal	2016	D7-1390	D7	6/7lb	-	-	-4.61-4.62	918, 885
Kz-110	faunal	2016	E7-2484	E7	6/7 lp/ls (6/7 lb*)	-	-	-4.64-4.65	919

Ref-no.	Item	Excav.	Sample- no	Sq.	Layer	x(m)	y(m)	z(m)	Weight (mg)
Kz-53	human	-	K/1509-1	-	-	-	-	-	645 mg
Kz-54	human	-	K/1509	-	-	-	-	-	474 mg
Kz-55	faunal	-	K/3322-7	-	-	-	-	-	522 mg
Kz-57	venus	2014	K/3360	-	-	-	-	-	318 mg
Kz-58	point	-	x150	F30	A?*	-	-	-5.04	279 mg
Kz-111	faunal	2016	G30-x160	G30	A2	-	-	-5.40-5.45	926 mg

Kz-112	faunal	2016	G30-x205	G30	A1	-	-	-5.45-5.50	943 mg
Kz-114	faunal	2016	F29-x1247	F29	D2	-	-	-5.50-5.55	709 mg
Kz-115	faunal	2016	F30-776	F30	C	-	-	-5.40-5.45	752 mg
Kz-116	faunal	2016	F29-x1150	F29	D2	-	-	-5.45-5.50	642, 514

Table S3: Kozarnika: Context details for samples selected for radiocarbon dating from sector I/III (above) and sector III (below). * for discussion of layer attribution see notes to Table 1.

ZooMS (Zooarchaeology by Mass Spectrometry)

The MALDI-ToF mass spectra processed using SpecieScan (Végh & Douka 2024) are given in the Supplementary Dataset 1 (Supplement 2). Contamination scanning (also assessed by SpecieScan) showing common laboratory contaminants and human keratin contamination is in Supplementary Dataset 2 (Supplement 3).

Images of selected modified bones for AMS dating

KZ-19

KZ-7

KZ-10

KZ-24

KZ-26

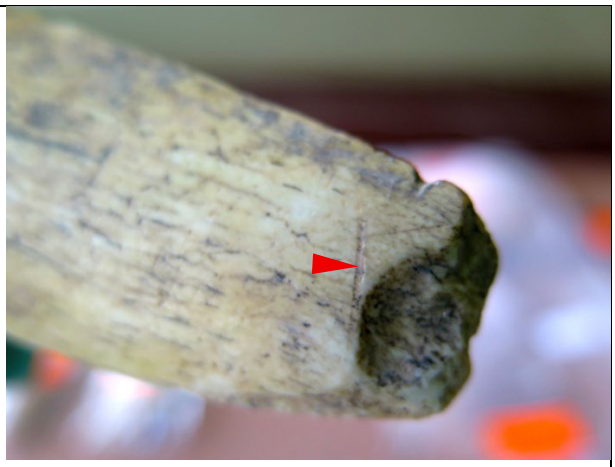

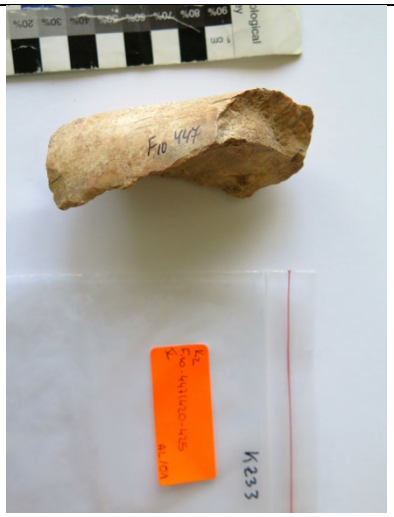
F10 447
K233

KZ-33


Geological
urvey
Kz '97
F8 (445-450)
VII
VM100

KZ-47


KlF8 1327

KZ-44

KZ-14

Bayesian modelling

Phase-Sequence models:
As outlined in the main paper, we ran several Bayesian models to test sensitivity and reproducibility, as well as the impact of different priors and radiocarbon likelihoods.

Model 0, using previously obtained radiocarbon data, represents the *status quo* prior to our work and aids as a comparison for the new results, both in terms of changes to the dating record and the influence of using different sample strategies.
Models 1–4 were all run on the newly obtained radiocarbon measurements. Contrasting Models 1/2 with Models 3/4 allows an assessment to be made of whether the subdivision of level IV into a and b can be supported by the dating record.
Contrasting Models 1/3 with Models 2/4 explores the effect of sample Kz-48 belonging to either layer 5c or 5b.

Models 5 and 6 use a combined old/new radiocarbon dataset to investigate the influence of charcoal dates on the age ranges and modelled transitions (considering charcoal samples are less securely connected to human activity and show added contamination complexity for samples older than 30k BP).
Model 7 uses the OSL age estimates of Heydari et al. (2022) to compare with the favored age model, Model 8 (see main paper).
Below we list the final model outputs for Model 8 (Table S4), as well as the Outlier results (Table S5). Note that Kz-48 was left out of this final Bayesian model due to the uncertainty over its precise context.
Each model is illustrated in Figures S5—S12.

The initial Bayesian models that were run showed that archaeological levels IVa and IVb were problematic, with high levels of outliers and results that were clearly not in agreement with the priors. Level IVa seemed to contain older radiocarbon results than IVb. The question of whether these are genuinely two separable strata is not at all clear. Layer 4 is a thin, discontinuous band with irregular layer boundaries and so it is perhaps not surprising that there is some variation in the results with respect to their assignation. Consequently, we considered it prudent to assign a single Phase IV (layer 4) for all determinations in later models. Following this, two dates remained outliers (OxA-33834 (Kz-06) and OxA-33548 (Kz-23)), but their chemical pretreatment was acceptable and so we think the age discrepancies could result from either intrusion, mixing of material, secondary depositioning, or misidentification of layer boundaries. The samples were both downweighted in the model using the outlier detection approaches.

The figurine we dated (OxA-34822 (Kz-79)) had a high outlier probability (99–100%), suggesting that it does not belong to layer 5a (level V) and must derive from a later period. Although the figurine was found in the top section of layer 5a, excavation documentation does not indicate that it could have been found within sediments associated with layer 4. The radiocarbon measurement appears reliable, placing the artifact in the later phases of the Middle Kozarnikian. We conclude that the figurine is most likely intrusive to 5a.

KDE Models:
The OxCal function `KDE_Model` was used to summarize three different radiocarbon datasets from Kozarnika. Their purpose was threefold: (1) to independently assess the structure of human activity observed and recorded during excavation; (2) to demonstrate the effect of sampling strategy on calculating periods of human activity; and (3) to illustrate the quality of the new radiocarbon dataset based on anthropogenically modified faunal remains. KDE 0 employs the previously obtained radiocarbon dataset on charcoal samples (Tables S1 and S2) and used in stratigraphic Model 0 (n=23) (see Figure S9). KDE 1 summarizes the new radiocarbon dataset on anthropogenically modified faunal remains from sector I/II (n=27) as used in stratigraphic Models 1–4 (Figure S10). KDE 2 combines the radiocarbon record from KDE 0 and KDE 1 (n=50)(Figure S11).

Bayesian model results:

In general, all stratigraphic models produced boundaries that are in good agreement with each other. Nonetheless, there are some differences that require discussion. The most notable exceptions are the higher `boundary` precisions (transitions 6/7 to 5c, and 5c to 5a) found in Model 5 and Model 6, and the younger `boundary` (transition 5c to 5a) in Model 0. Model 0 is likely underestimating the age of the transition, considering the limited charcoal data available for level IV. In the case of models 5 and 6, both include the previously obtained radiocarbon record on charcoal samples, which shows less age consistent data within a layer,

albeit not in direct disagreement with the chronostratigraphy of the site. Both models demonstrate how a larger age spread of radiocarbon dates within a `Phase` increases the precision of the adjacent transition `Boundary`. In contrast, more age consistent data within a `Phase`, which is also chronologically well separated from dates in adjacent units, reduces the `Boundary` precision.
There are two main scenarios to explain the higher age variation observed in charcoal samples. First, it may be caused by lower dating accuracy for charcoal samples closer to the radiocarbon detection limit. Second, it may be the result of charcoals representing a larger age range of sedimentation within a layer or level, in contrast to the more sporadic human occupation recorded by dating anthropogenically modified bones. Consequently, higher precision does not necessarily reflect (higher) accuracy.

While the charcoal data increased precision in the stratigraphic models, their effect on KDE modelling outcomes was the opposite. The charcoal data in KDE 0 obscures the anthropogenic signal at the site, producing less discrete events. In the model, there are only three main occupation events discernible, and the occupation appears to decrease over time. When using dates on anthropogenically modified bone (KDE 1), however, a minimum of five discrete human occupation events becomes apparent: (1) 50–44k cal BP, (2) 44–40k cal BP, (3) 39–36 cal BP, (4) 33–30k cal BP, and (5) 29–26 cal BP. They largely correspond to the human occupations within layers 6/7 Is/Ip (level VIII), 5c (VII), middle section of 5b (VI), 5a (V) and 4 (IV), and 3b (III). These results imply an increase in occupation frequency/intensity during the Middle Kozarnikian. As the archaeological material of this period can be found in distinct geological units, it can be concluded that an increase in occupation frequency is likely to be the main contributing factor.

KDE 2 illustrates how important question tailored radiocarbon sampling is. Despite the large number of anthropogenically modified bone dates in the model, the charcoal samples manage to sufficiently blur discrete occupation events for the model to revert to a near complete bimodal distribution.

The good agreement between the results of KDE 1 and the stratigraphic models is evidence for a largely intact and well identified stratigraphic sequence at Kozarnika. The only notable challenges are found within layer 5b. Therefore, Model 3 probably best reflects the stratigraphy at the site by being more conservative in boundary calculations – including OxA-34669 (Kz-48) in layer 5b for Model 4 may instil a false sense of accuracy by providing a higher precision boundary for the transition from layer 5c to 5b, and Stratigraphic Models 0, 1, 3, 5, and 6 have already been deemed less representative (see above).

Sector III
The modelled dates for each layer and their transitions in sector I/II can be compared to the radiocarbon results obtained from sector III. The unmodified faunal remains from layer C and D are significantly older than the ages from layer A, and are thus unable to further constrain the age of layer A. Therefore, the inter-sector comparison focused on layer A, represented by OxA-34829 (Kz-110) and OxA-34830 (Kz-112), and layers 6/7 until the transition to 5a, represented by Model 3.

While there is some overlap in the age probability distributions between layer A and layers 6/7 Ib and layer 5b, respectively, best agreement is found with the occupation in layer 5c. It remains to be seen whether these two units correspond to the same occupation, or to at least two distinct events (activity or cultures) using different sections of the cave in possibly short succession.

Bayesian models:

Model 0:
This uses previously obtained radiocarbon dates deemed suitable for modelling and the CI age proposed by Giaccio et al. (2017). The events were sorted according to their archaeological levels: VIII, VII, VI, V, IV, III, and 0I.

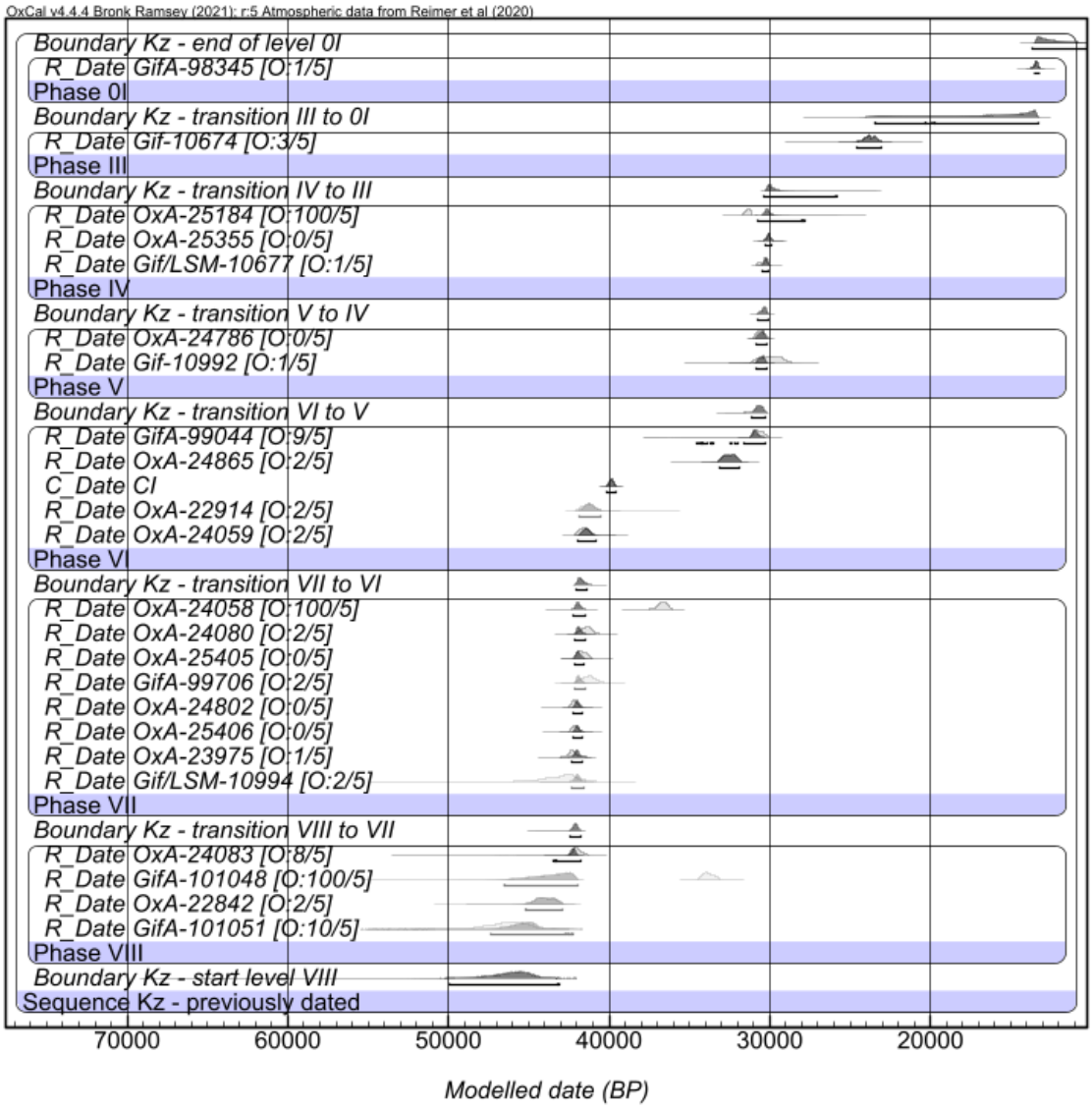

Figure S5: Bayesian model 0.

Model 1:

This incorporates all new radiocarbon dates on anthropogenic modified bone samples from sector I/II (see Table 1 in the main paper) and the CI age estimate. The events were sorted according to geological layers with Kz-48 featuring in 5c. Layer 6/7 Ip and 6/7 Is were combined as (a) the stratigraphy was unclear as to which one of the two is younger, and (b) Kz-110 could belong to either of them (see notes to Table 1). Layer 4 was subdivided into level IVa and IVb. This resulted in the following phases: 6/7 Is/Ip, 6/7 Ib, 5c, 5b, 5a, 4(IVa), 4(IVa), 3b.

Figure S6: Bayesian model 1.

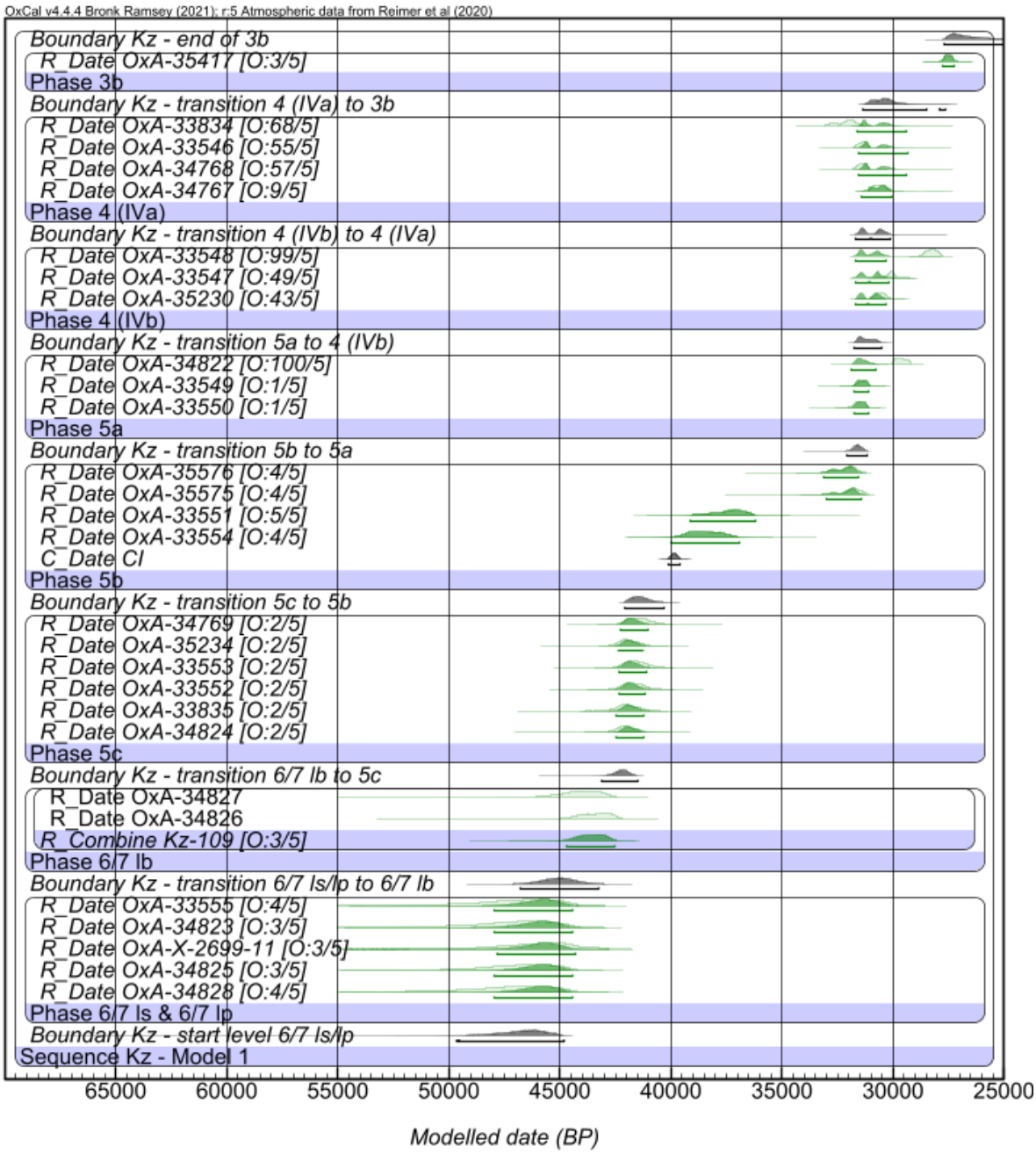

Model 2:

Model 2 (bone) incorporates the same radiocarbon dataset and `Phase` structure as Model 1, but Kz-48 is grouped under 5b.

Figure S7: Bayesian model 2.

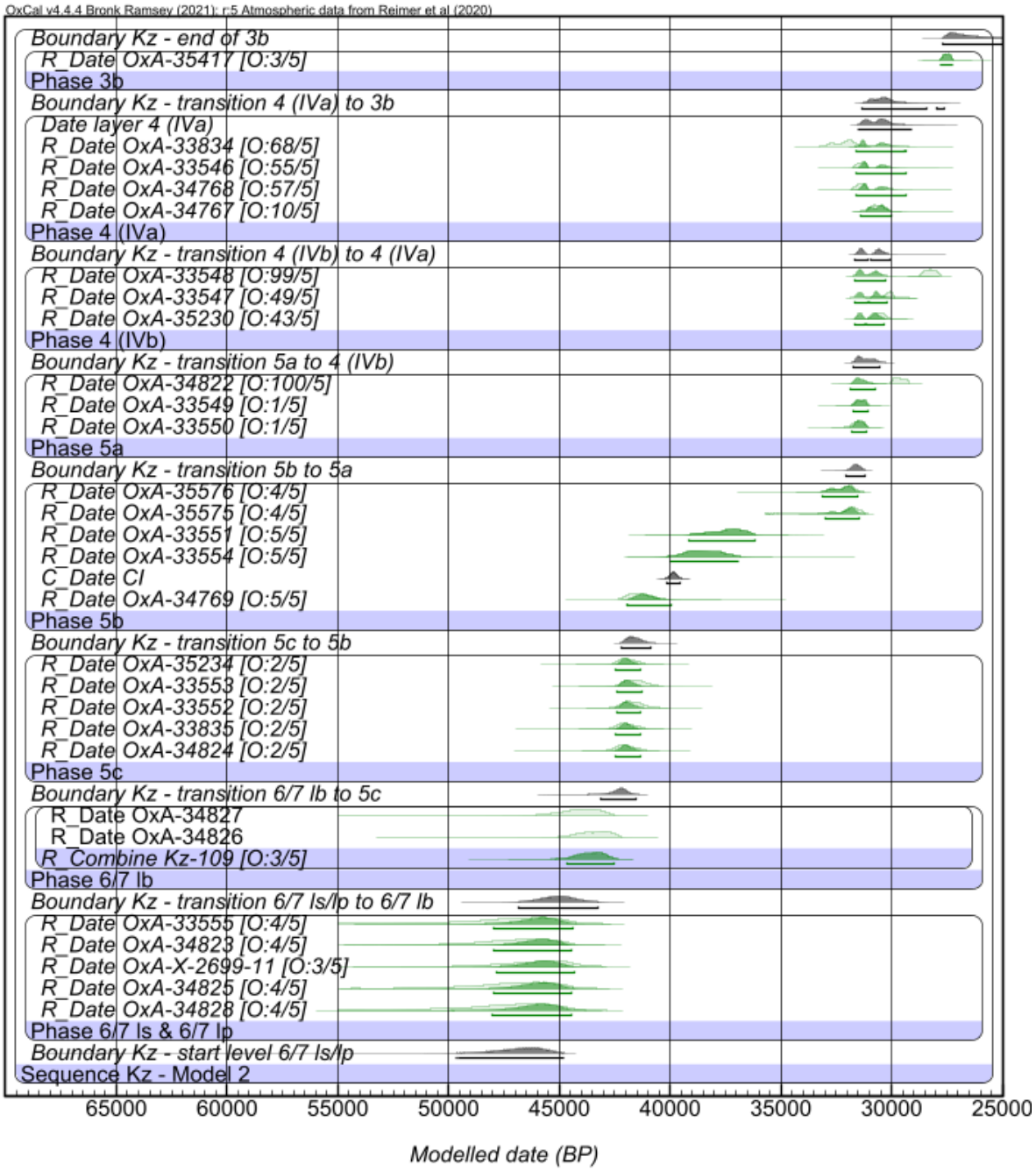

Model 3:

Model 3 (bone) employs the same radiocarbon data set as Model 1, with Kz-48 also attributed to layer 5c. However, layer 4 is not subdivided into IVa and IVb, giving the following phase structure: 6/7 Is/Ip, 6/7 Ib, 5c, 5b, 5a, 4, 3b.

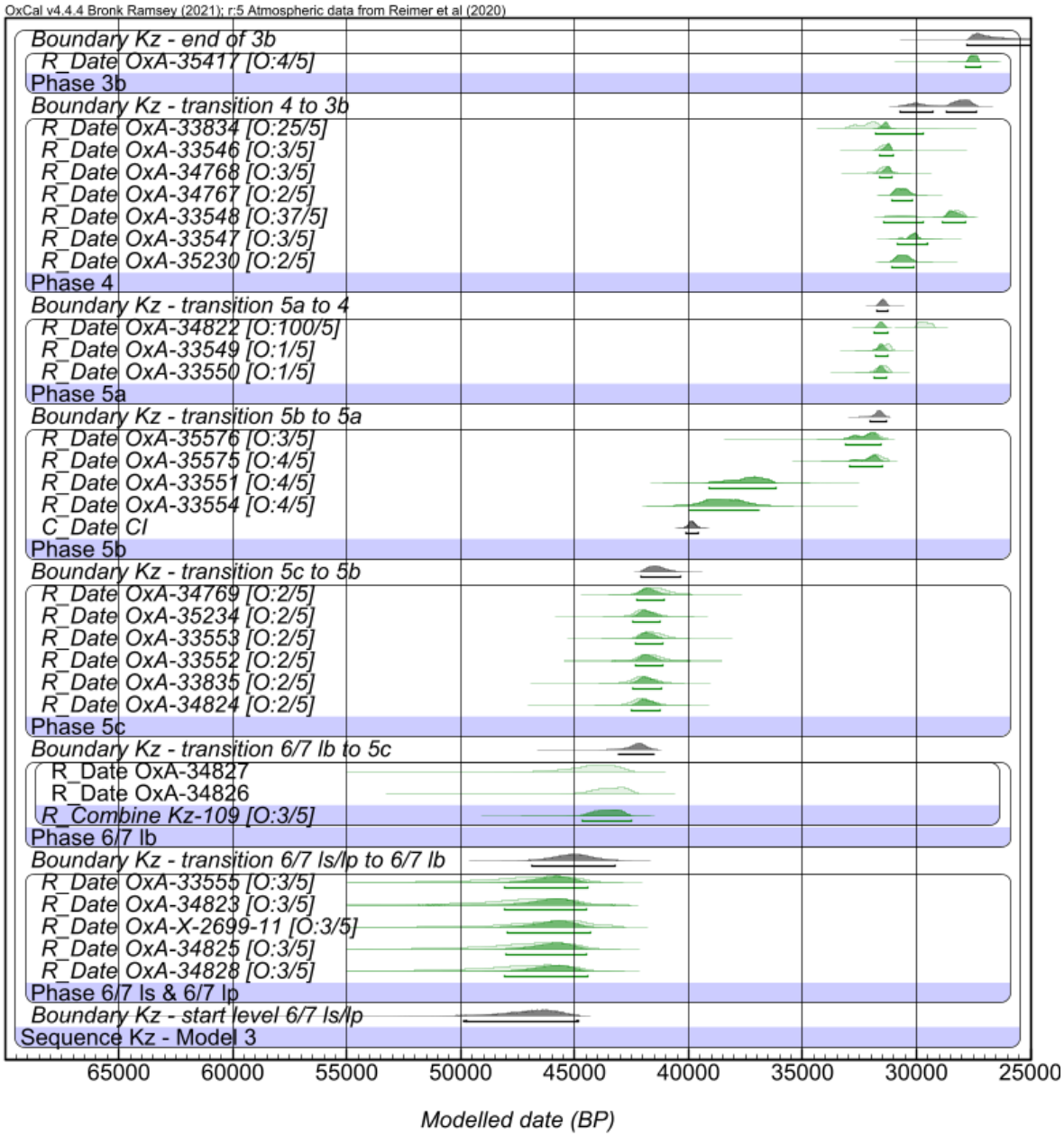

Figure S8: Bayesian model 3.

Model 4:

Model 4 (bone) runs the same radiocarbon data set as Model 2, with Kz-48 attributed to layer 5b, and the identical phase structure as Model 3.

Figure S9: Bayesian model 4.

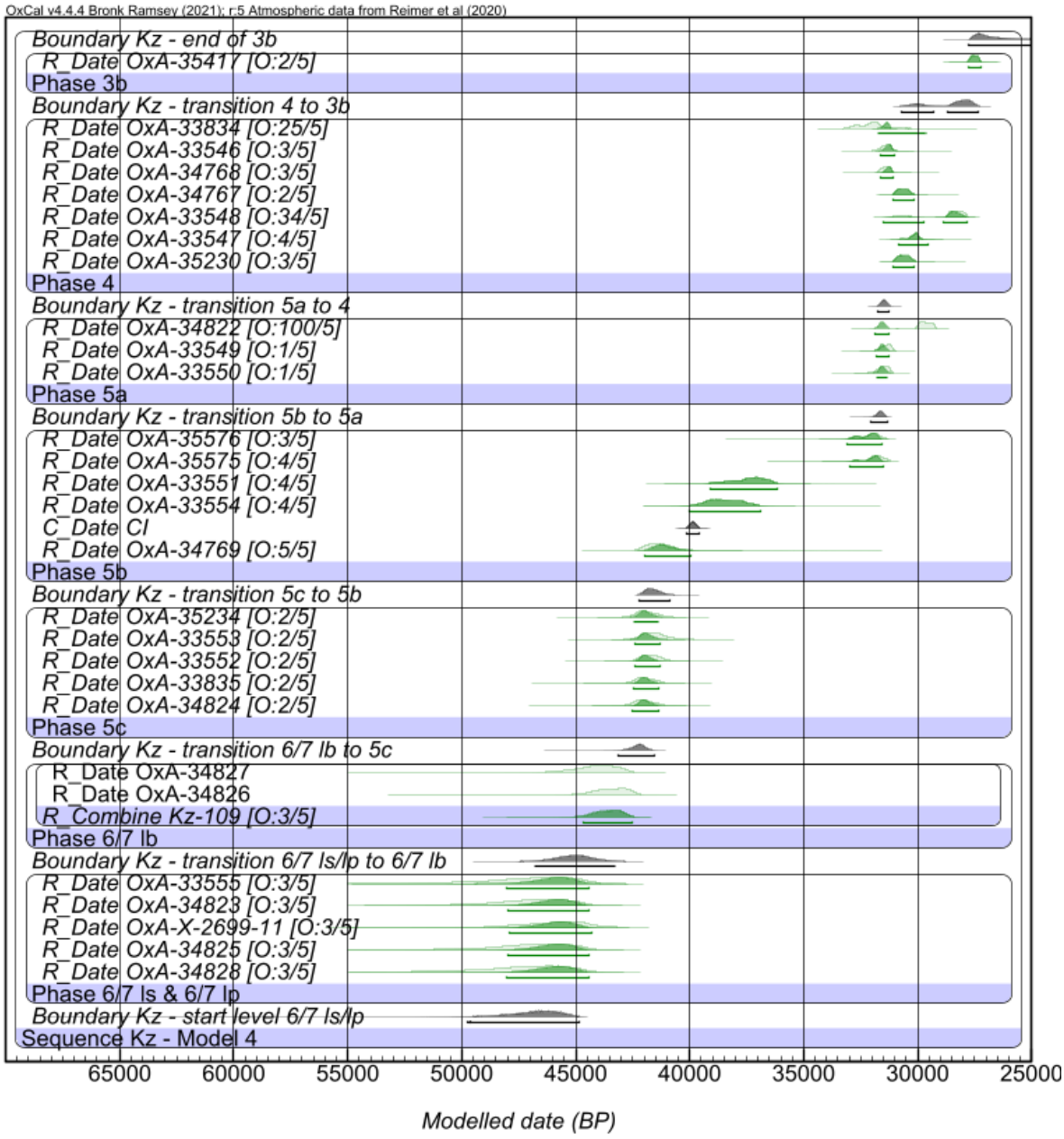

Model 5:

Model 5 (charcoal / bone) is based on Model 3 with the charcoal data from Model 0 added. Prior to 2015, layer 6/7 had not been subdivided. As a result, the phase structure had to be adjusted accordingly: 6/7, 5c, 5b, 5a, 4(IVa), 4(IVa), 3b.

Figure S10: Bayesian model 5.

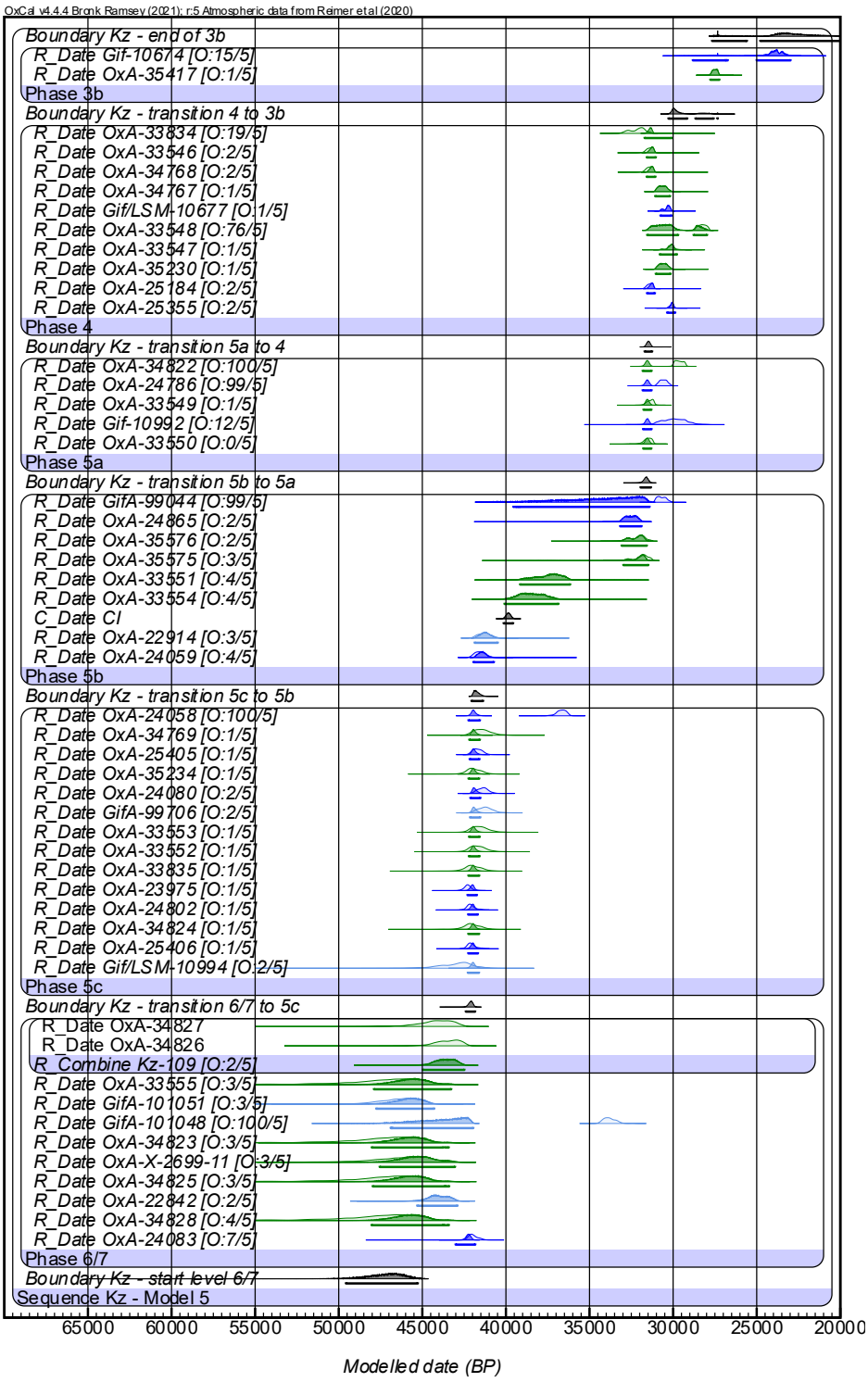

Model 6:

Model 6 (charcoal / bone) is based on Model 4 with the charcoal data from Model 0 added. Prior to 2015, layer 6/7 had not been subdivided. As a result, the phase structure had to be adjusted accordingly: 6/7, 5c, 5b, 5a, 4, 3b.

Figure S11: Bayesian model 6.

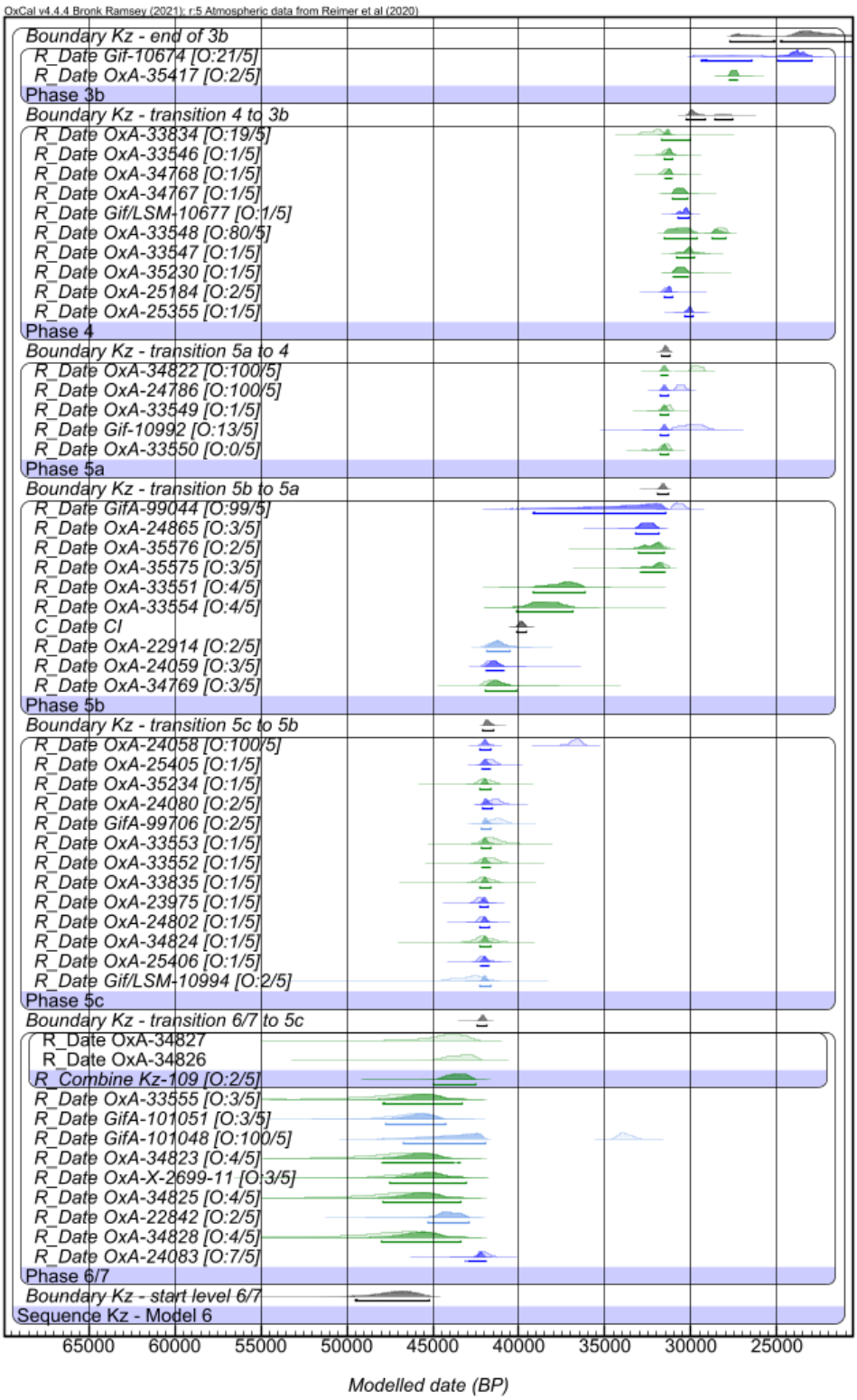

Model 7:

This model has the same underlying radiocarbon dataset and phase structure as Model 3. OSL results from Heydari et al. (2022) are included. These disclose high outlier probabilities in 3 cases.

Figure S12: Bayesian model 7.

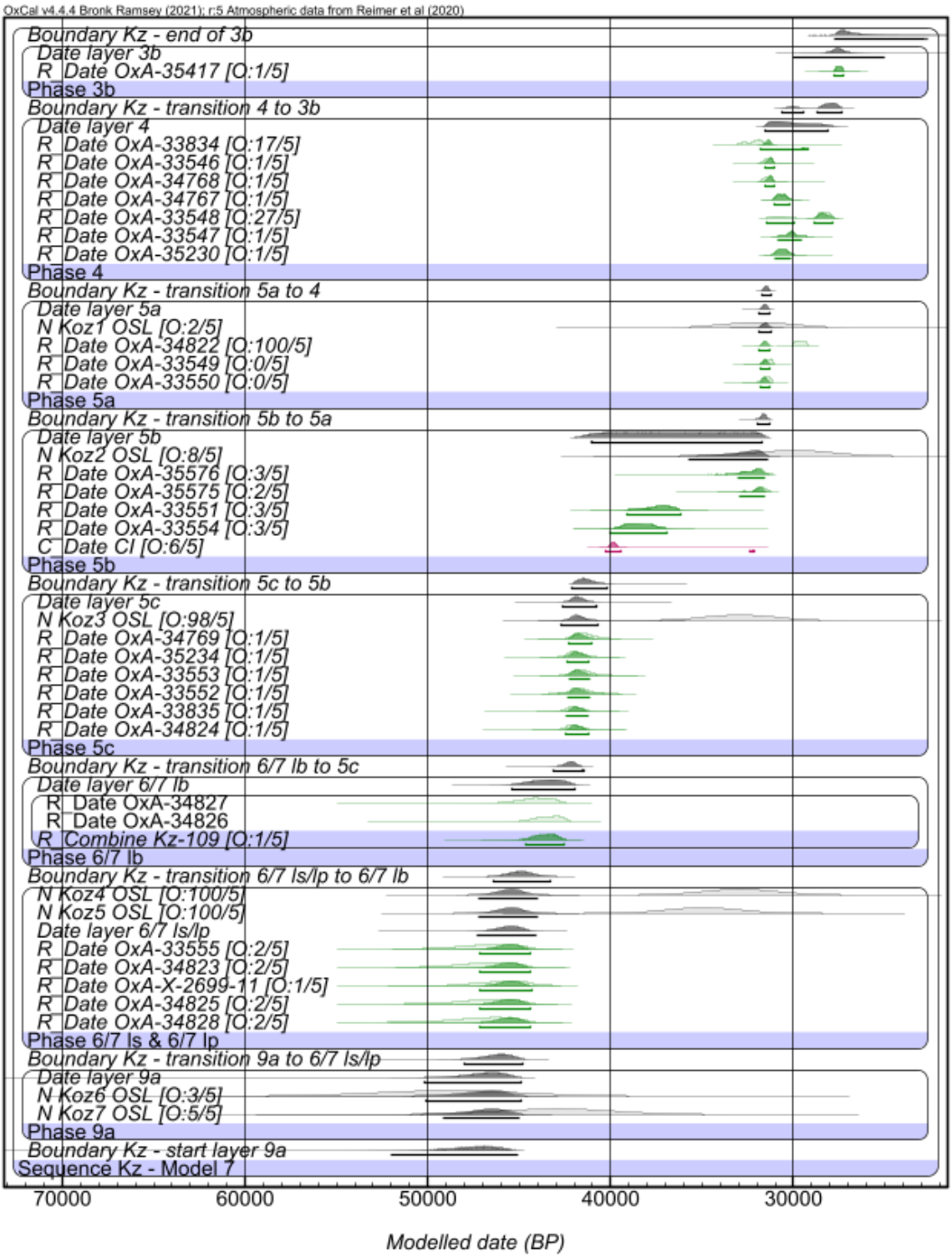

KDE Models:

As described above, KDE 0 employs the previously obtained radiocarbon dataset on charcoal samples (Tables S1 and S2) and used in stratigraphic Model 0 (n=23). KDE 1 summarises the new radiocarbon dataset on anthropogenically modified faunal remains from sector I/II (n=27) as used in stratigraphic Models 1–4. This KDE model is shown in the main paper.
KDE 2 combines the radiocarbon data from both KDE 0 and KDE 1 (*n*=50).

Figure S13: KDE model 0.

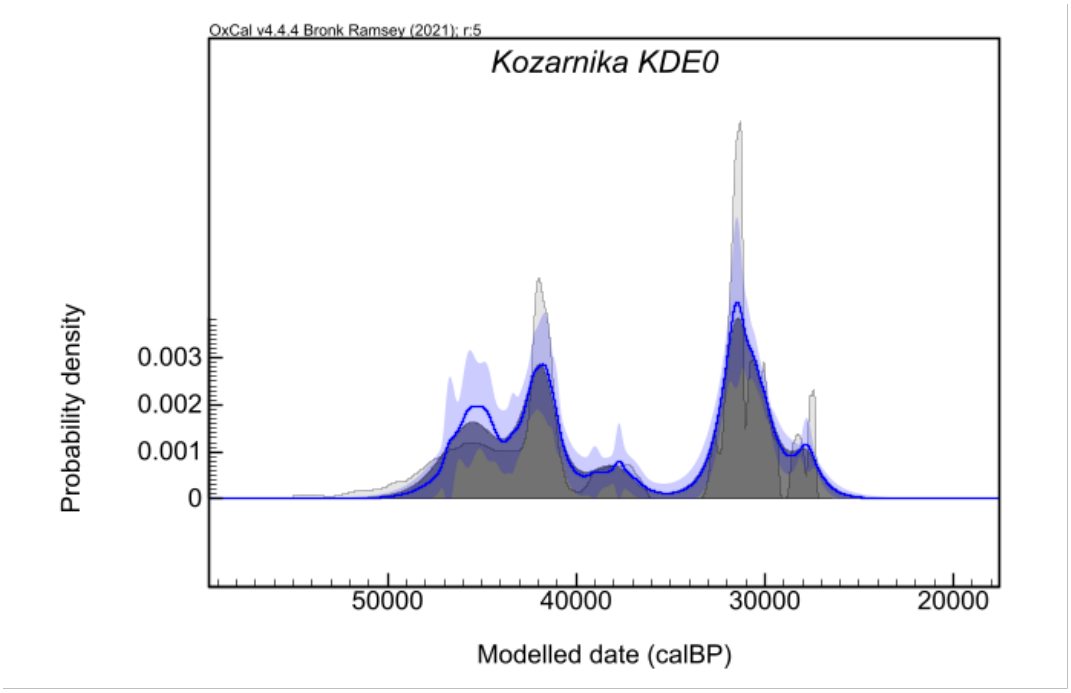

Figure S14: KDE model 1.

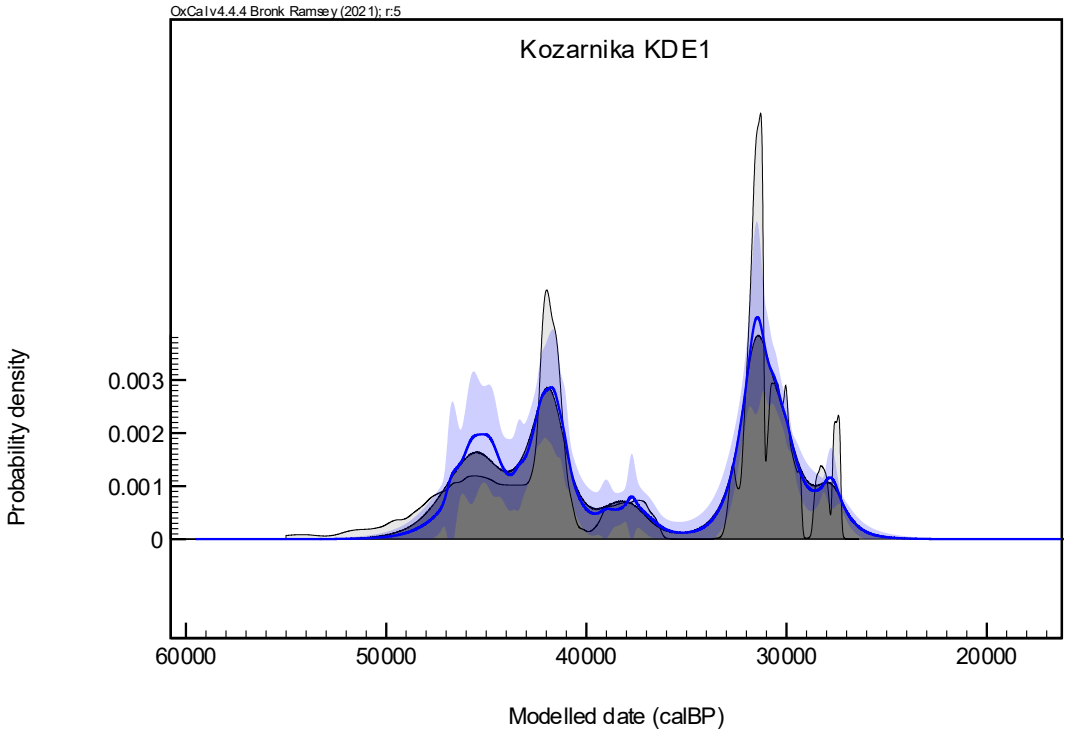

Figure S15: KDE model 2.

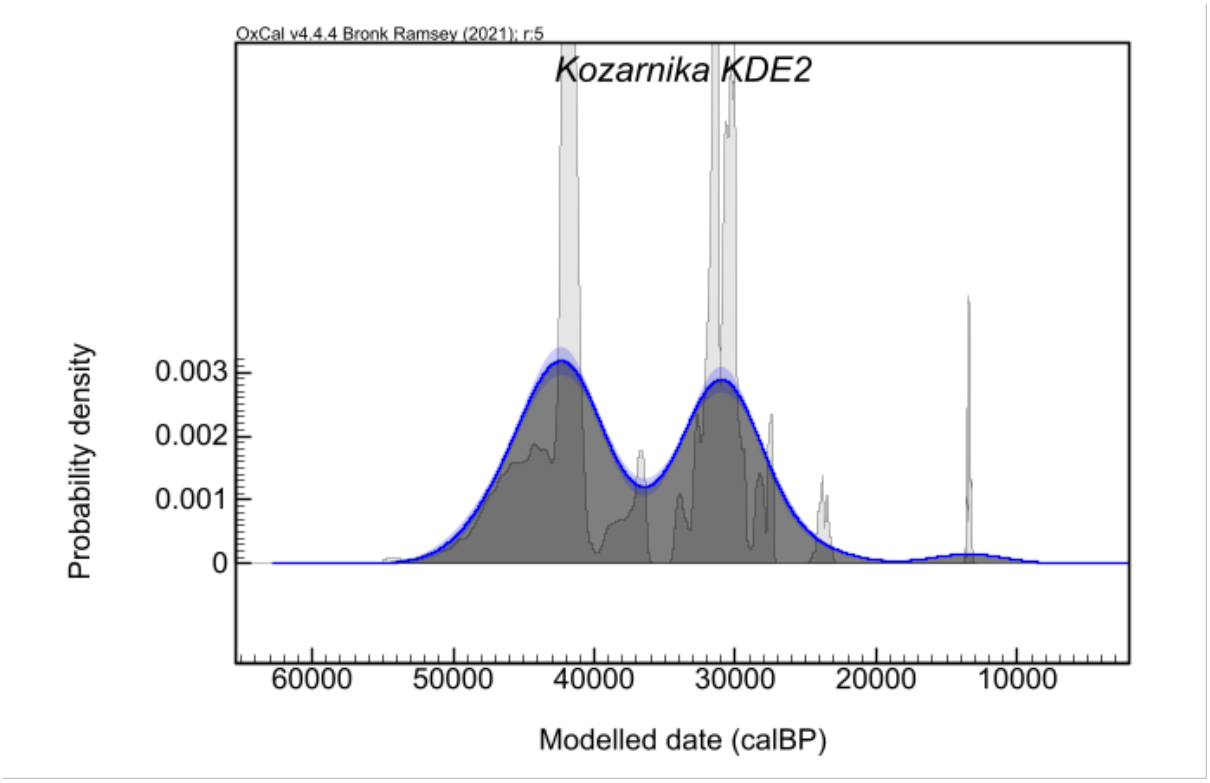

Figure S16: Comparisons between the start boundaries for for key Early and Initial Upper Palaeolithic sites in Europe. The shaded blue line is the estimate for Neanderthal disappearance based on Higham et al.'s (2014) estimates. Zlatý kůň is an estimated age, and is probably a minimum age based on genetic estimates[51]. The light blue box around Bacho Kiro accounts for the likely earlier spread of the IUP estimate to the layer below N1-I (Fewlass et al. 2020).

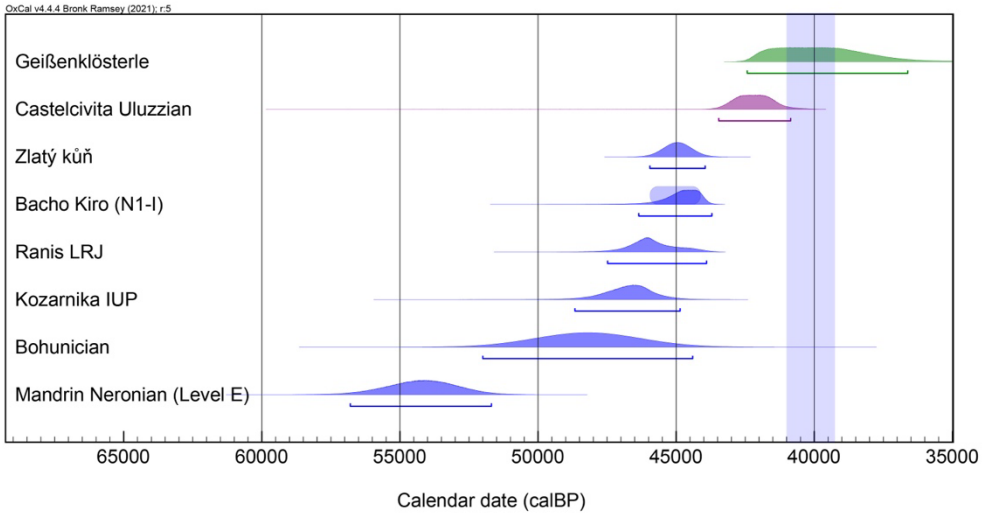

Figure S17: Bayesian model using data from Table S2.

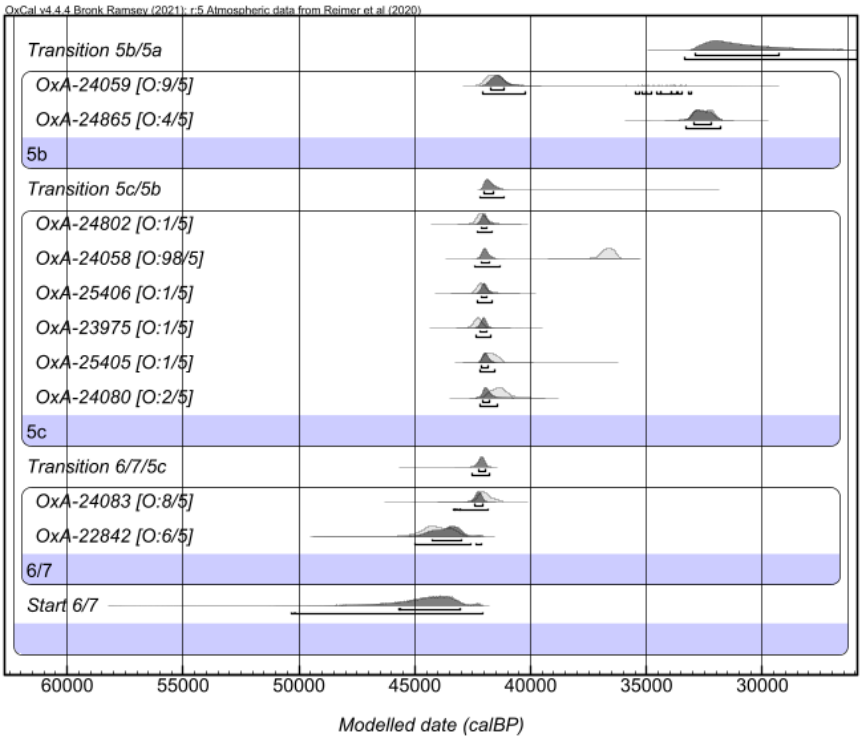

Anthropomorphic bone from 5a

A bone object found in Layer 5a is shown in Figure S18. We directly dated this (Kz-79) to 25,400 ± 200 BP. In terms of similar pieces, we note that it looks like one from Kostenki IV shown in Abramova (1962, 1967: Plate XIX 1,2 Figure S19). Similarly, the Kostenki-Avdeevo culture shows some parallels (see Goutas, 2013: Figure 4. 140). In Figure S20 we show two examples of mammoth rib bones from the sites of Avdeevo and Kostenki 1/1 respectively, which are probably more correctly termed 'spatulae'.

Figure S18: Anthropomorphic figurine from Level V.

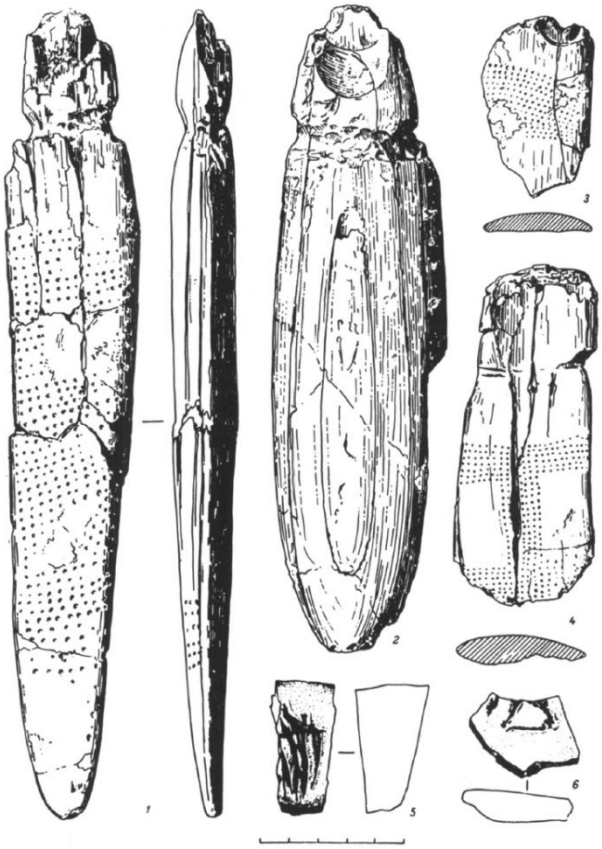

Figure S19: Kostenki IV upper horizon (after Abramova 1962; 1967).

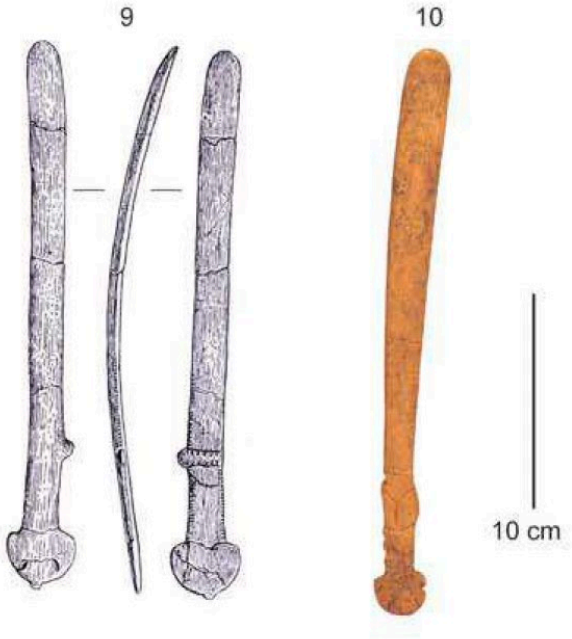

Figure S20: Two artefacts from Avdeevo (9) and Kostenki 1/1, complex 2 (9) which show some similarities with the Kozarnika artefact above (picture from Goutas 2013). They are made from half a mammoth rib.

Supplementary references:

Abramova, Z.A. 1962. Paleolititcheskoe iskousstvo na territorii SSSR. Akad. Nauk SSSR, Inst. Archeologii, Moskva, A 4–3.

Abramova, Z.A. 1967. Palaeolithic movable art in the USSR. [s.n.] 99–125, pl. XVXXIII.

Brock, F., Higham, T., Ditchfield, P., Bronk Ramsey, C., 2010. Current pretreatment methods for AMS radiocarbon dating at the Oxford Radiocarbon Accelerator Unit (ORAU). Radiocarbon 52(1), 103–112.

Ferrier, C., Leblanc, J.-C., Berthet, A. L., Delfour, G. 2009. La Grotte Kozarnika (Gara Oreshets, Bulgarie): Données stratigraphques, géologiques et d´edimentologiques. In *Saxa loquuntur*: sbornik včest na 65-godišninata na Nikolay Sirakov, pages 13–27. Avalon Publishing, Sofia: 13–27.

Fewlass, H., Talamo, S., Wacker, L., Kromer, B., Tuna, T., Fagault, Y., Bard, E., McPherron, S.P., Aldeias, V., Maria, R., Martisius, N.L. 2020. A 14C chronology for the Middle to Upper Palaeolithic transition at Bacho Kiro Cave, Bulgaria. Nat. Ecol. Evol. 4(6), 794-801.

Giaccio, B., Hajdas, I., Isaia, R., Deino, A., Nomades, S., 2017. High–precision ^{14}C and $^{40}Ar/^{39}Ar$ dating of the Campanian Ignimbrite (Y-5) reconciles the time-scales of climatic-cultural processes at 40ka. Sci. Rep. 7, 45940.

Goutas, N., 2013, September. New data on the osseous industry from Eastern Gravettian (Russia): Technological analyses and sociological perspectives. In *The Sound of Bones. 8th Meeting of the Worked Bone Research Group, Salzburg, August* (Vol. 29, pp. 133–154).

Guadelli, J.-L., Sirakov, N. 1996. *Rapport de la Mission Préhistorique française en Bulgarie du Nord « Les plus anciennes manifestations de la présence humaine dans les Balkans » (MAE)*. Projet de recherche conjoint CNRS-Univ. Bordeaux I / Institut d'Archéologie et Musée de l'Académie bulgare des Sciences. 9p.

Guadelli, J.-L., Sirakov, N., Anastassova, E., Berry, G., Berthet, A.-L., Delfour, G., Delpech, F., Dimitrova, I., Djabarska, N., Fernandez, P., Ferrier, C., Fontugne, M., Guadelli, A., Iordanova, D., Iordanova, N., Ivavona, S., Kovatcheva, M., Krumov, I., Leblanc, J.-C., Mallye, J.-B., Marinska, M., Miteva, V., Popov, V. V., Sirakova, S., Spassov, R., Taneva, S., Tisnérat-Laborde, N., 2002. Rapport de la Mission Préhistorique française en Bulgarie du Nord « Les plus anciennes manifestations de la présence humaine dans les Balkans » (MAE). Projet de recherche conjoint CNRS-Univ. Bordeaux I / Institut d'Archéologie et Musée de l'Académie bulgare des Sciences.

Guadelli, J.-L., Sirakov, N., Boyadzhiev, K., Dimitrova, I., Fontugne, M., Guadelli, A., Guérin, G., Heydari, M., Hopkins, R., Jacob, E., Kovacheva, M., Krumov, I., Monesi, E., Muttoni, G., Sirakova, S., Taneva, S., Tillier, A.-M., Tisnérat-Laborde, N., Yanakieva, K., Yordanova, D., Yordanova, N., and Zahariev, N. 2016. Les plus anciennes manifestations de la présence humaine dans les Balkans. Rapport de la Mission "Paléolithique de Bulgarie" (MAEDI) 2016, 122p.

Guadelli, J.-L., Sirakov, N., Christov, M., Courtaud, P., Crémades, M., Delpech, F., Ferrier, C., Fontugne, M., Gurova, M., Ivanova, S., Leblanc, J.-C., Marambat, L., Marinska, M., Popov, V., and Sirakova, S. 1998. Projet de recherche conjoint: "Les plus anciennes manifestations de la présence humaine en Bulgarie du Nord". Rapport de la Mission "Paléolithique de Bulgarie" (MAE), 217p.

Heydari, M., Guérin, G., Sirakov, N., Fernandez, P., Ferrier, C., Guadelli, A., Leblanc, J.C., Taneva, S., Sirakova, S., Guadelli, J.L., 2022. The last 30,000 to 700,000 years ago: unravelling the timing of human settlement for the Palaeolithic site of Kozarnika. Quatern. Sci. Rev. 291, 107645.

Higham, T., Douka, K., Wood, R., Bronk Ramsey, C., Brock, F., Basell, L., Camps, M., Arrizabalaga, A., Baena, J., Barroso-Ruíz, C., Bergman, C., Boitard, C., Boscato, P., Caparrós, M., Conard, N.J., Draily, C., Froment, A., Galván, B., Gambassini, P., Garcia-Moreno, A., Grimaldi, S., Haesaerts, P., Holt, B., Iriarte-Chiapusso, M.J., Jelinek, A., Jordá Pardo, J.F., Maíllo-Fernández, J-M., Marom, A., Maroto, J., Menéndez, M., Metz, L., Morin, E., Moroni, A., Negrino, F., Panagopoulou, E., Peresani, M., Pirson, S., de la Rasilla, M., Riel-Salvatore, J., Ronchitelli, A., Santamaria, D., Semal, P., Slimak, L., Soler, J., Soler, N., Villaluenga, A., Pinhasi, R., Jacobi, R. 2014. The timing and spatio-temporal patterning of Neanderthal disappearance. Nature 512, 306–309.

Lowe, J., Barton, N., Blockley, S., Bronk Ramsey, C., Cullen, V.L., Davies, W., Gamble, C. et al., 2012. Volcanic ash layers illuminate the resilience of Neanderthals and early modern humans to natural hazards. Proc. Nat. Acad. Sci. 109(34), 13532–13537.

Sirakov, N., Guadelli, J.-L., Ivanova, S., Sirakova, S., Boudadi-Maligne, M., Dimitrova, I., Fernandez, P., Ferrier, C., Guadelli, A., Iordanova, D., Iordanova, N., Kovatcheva, M., Krumov, I., Leblanc, J.-C., Miteva, V., Popov, V. V., Spassov, R., Taneva, S., Tsanova, T. 2010. An ancient continuous human presence in the Balkans and the beginnings of human settlement in western Eurasia: A Lower Pleistocene example of the Lower Palaeolithic levels in Kozarnika cave (North-western Bulgaria). Quatern. Int. 223-224, 94–106.

Sirakov, N., Tsanova, T., Sirakova, S., Taneva, S., Krumov, I., Dimitrova, I., Kovatcheva, N., 2007. Un nouveau faciès lamellaire du début du Paléolithique supérieur dans les Balkans. PALEO 19, 131–144.

Végh, E., Douka, K., 2024. SpecieScan: semi-automated taxonomic identification of bone collagen peptides from MALDI-ToF-MS. Bioinformatics 40(3), btae054.

Попов, . (1933). Пещерата МИРИЗЛИВКА. Приносъ къмъ дилувиалната фауна и културата на дилувиалния човькъ въ България (La grotte "Mirizlivka". Contribution à l'étude de la faune diluvienne et de la cutlure de l'homme quaternaire en Bulgarie). *Издания народния археологически музей, София (Cahier du musée national d'Archéologie, Sofia)*, 26:5–69.

CQL CODES:

Model 0.

```
Plot("Kz - previously dated")
 {
  Outlier_Model("General",T(5),U(0,4),"t");
  Sequence("Kz - previously dated")
  {
   Boundary("Kz - start level VIII");
   Phase("VIII")
   {
    R_Date("GifA-101051", 43600, 1200)
    {
     Outlier("General", 0.05);
     color="gray";
    };
    R_Date("OxA-22842", 41100, 750)
    {
     Outlier("General", 0.05);
     color="gray";
    };
    R_Date("GifA-101048", 29310, 320)
    {
     Outlier("General", 0.05);
     color="gray";
    };
    R_Date("OxA-24083", 37400, 500)
    {
     Outlier("General", 0.05);
    };
    Interval("Interval level VIII");
   };
   Boundary("Kz - transition VIII to VII");
   Interval("Interval transition VIII to VII");
   Phase("VII")
   {
    R_Date("Gif/LSM-10994", 38700, 1400)
    {
     Outlier("General", 0.05);
```

```
  color="gray";
 };
 R_Date("OxA-23975", 38050, 500)
 {
  Outlier("General", 0.05);
 };
 R_Date("OxA-25406", 37600, 500)
 {
  Outlier("General", 0.05);
 };
 R_Date("OxA-24802", 37650, 500)
 {
  Outlier("General", 0.05);
 };
 R_Date("GifA-99706", 36200, 540)
 {
  Outlier("General", 0.05);
  color="gray";
 };
 R_Date("OxA-25405", 36900, 450)
 {
  Outlier("General", 0.05);
 };
 R_Date("OxA-24080", 36350, 400)
 {
  Outlier("General", 0.05);
 };
 R_Date("OxA-24058", 32330, 260)
 {
  Outlier("General", 0.05);
 };
 Interval("Interval level VII");
};
Boundary("Kz - transition VII to VI");
Interval("Interval transition VII to VI");
Phase("VI")
{
 R_Date("OxA-24059", 36650, 450)
 {
  Outlier("General", 0.05);
 };
 R_Date("OxA-22914", 36250, 450)
 {
  Outlier("General", 0.05);
  color="gray";
 };
 C_Date("CI", -37900, 140);

 {
  Outlier("General", 0.05);
  color="magenta";
```

```
 };
 R_Date("OxA-24865", 28380, 170)
 {
  Outlier("General", 0.05);
 };
 R_Date("GifA-99044", 26490, 270)
 {
  Outlier("General", 0.05);
 };
 Interval("Interval level VI");
};
Boundary("Kz - transition VI to V");
Interval("Interval transition VI to V");
Phase("V")
{
 R_Date("Gif-10992", 25650, 730)
 {
  Outlier("General", 0.05);
 };
 R_Date("OxA-24786", 26320, 190)
 {
  Outlier("General", 0.05);
 };
 Interval("Interval level V");
};
Boundary("Kz - transition V to IV");
Interval("Interval transition V to IV");
Phase("IV")
{
 R_Date("Gif/LSM-10677", 26120, 100)
 {
  Outlier("General", 0.05);
 };
 R_Date("OxA-25355", 25770, 140)
 {
  Outlier("General", 0.05);
 };
 R_Date("OxA-25184", 27370, 190)
 {
  Outlier("General", 0.05);
 };
 Interval("Interval level IV");
};
Boundary("Kz - transition IV to III");
Interval("Interval transition IV to III");
Phase("III")
{
 R_Date("Gif-10674", 19770, 270)
 {
  Outlier("General", 0.05);
 };
```

```
    Interval("Interval level III");
   };
   Boundary("Kz - transition III to 0I");
   Interval("Interval transition III to 0I");
   Phase("0I")
   {
    R_Date("GifA-98345", 11550, 100)
    {
     Outlier("General", 0.05);
    };
    Interval("Interval level 0I");
   };
   Boundary("Kz - end of level 0I");
  };
 };
```

Model 1.

```
Plot()
 {
  Outlier_Model("General",T(5),U(0,4),"t");
  Outlier_Model("SSimple",N(0,2),0,"s");
  Sequence("Kz - Model 1")
  {
   Boundary("Kz - start level 6/7 ls/lp");
   Phase("6/7 ls & 6/7 lp")
   {
    R_Date("OxA-34828", 44000, 1900)
    {
     Outlier("General", 0.05);
     color="green";
    };
    R_Date("OxA-34825", 43800, 1800)
    {
     Outlier("General", 0.05);
     color="green";
    };
    R_Date("OxA-X-2699-11", 42900, 1700)
    {
     Outlier("General", 0.05);
     color="green";
    };
    R_Date("OxA-34823", 43900, 1800)
    {
     Outlier("General", 0.05);
     color="green";
    };
    R_Date("OxA-33555", 43700, 1900)
    {
     Outlier("General", 0.05);
```

```
  color="green";
 };
 Interval("Kz - Interval 6/7 ls lp");
 Date("Date layer 6/7 ls/lp");
};
Boundary("Kz - transition 6/7 ls/lp to 6/7 lb");
Interval("Kz - Interval transition 6/7 ls lp to 6/7 lb");
Phase("6/7 lb")
{
 R_Combine("Kz-109")
 {
  Outlier("General", 0.05);
  color="green";
  R_Date("OxA-34826", 39800, 1100)
  {
   Outlier("SSimple", 0.05);
   color="green";
  };
  R_Date("OxA-34827", 40900, 1300)
  {
   Outlier("SSimple", 0.05);
   color="green";
  };
 };
 Interval("Kz - Interval 6/7 lb");
 Date("Date layer 6/7 lb");
};
Boundary("Kz - transition 6/7 lb to 5c");
Interval("Kz - Interval transition 6/7 lb to 5c");
Phase("5c")
{
 R_Date("OxA-34824", 37600, 900)
 {
  Outlier("General", 0.05);
  color="green";
 };
 R_Date("OxA-33835", 37500, 900)
 {
  Outlier("General", 0.05);
  color="green";
 };
 R_Date("OxA-33552", 37000, 800)
 {
  Outlier("General", 0.05);
  color="green";
 };
 R_Date("OxA-33553", 36800, 800)
 {
  Outlier("General", 0.05);
  color="green";
 };
```

```
 R_Date("OxA-35234", 37400, 800)
 {
  Outlier("General", 0.05);
  color="green";
 };
 R_Date("OxA-34769", 36550, 750)
 {
  Outlier("General", 0.05);
  color="green";
 };
 Interval("Kz - Interval 5c");
 Date("Date layer 5c");
};
Boundary("Kz - transition 5c to 5b");
Interval("Kz - Interval transition 5c to 5b");
Phase("5b")
{
 C_Date("CI", -37900, 140);
 {
  Outlier("General", 0.05);
  color="#b7005c";
 };
 R_Date("OxA-33554", 33650, 550)
 {
  Outlier("General", 0.05);
  color="green";
 };
 R_Date("OxA-33551", 32750, 500)
 {
  Outlier("General", 0.05);
  color="green";
 };
 R_Date("OxA-35575", 27830, 270)
 {
  Outlier("General", 0.05);
  color="green";
 };
 R_Date("OxA-35576", 28010,280)
 {
  Outlier("General", 0.05);
  color="green";
 };
 Interval("Kz - Interval 5b");
 Date("Date layer 5b");
};
Boundary("Kz - transition 5b to 5a");
Interval("Kz - Interval transition 5b to 5a");
Phase("5a")
{
 R_Date("OxA-33550", 27540, 270)
 {
```

```
  Outlier("General", 0.05);
  color="green";
 };
 R_Date("OxA-33549", 27290, 270)
 {
  Outlier("General", 0.05);
  color="green";
 };
 R_Date("OxA-34822", 25400, 200)
 {
  Outlier("General", 0.05);
  color="green";
 };
 Interval("Kz - Interval 5a");
 Date("Date layer 5a");
};
Boundary("Kz - transition 5a to 4 (IVb)");
Phase("4 (IVb)")
{
 R_Date("OxA-35230", 26340, 220)
 {
  Outlier("General", 0.05);
  color="green";
 };
 R_Date("OxA-33547", 25800, 220)
 {
  Outlier("General", 0.05);
  color="green";
 };
 R_Date("OxA-33548", 24090, 180)
 {
  Outlier("General", 0.05);
  color="green";
 };
 Interval("Kz - Interval 4 (IVb)");
 Date("Date layer 4 (IVb)");
};
Boundary("Kz - transition 4 (IVb) to 4 (IVa)");
Interval("Kz - Interval transition 5a to 4 (IVb)");
Phase("4 (IVa)")
{
 R_Date("OxA-34767", 26400, 220)
 {
  Outlier("General", 0.05);
  color="green";
 };
 R_Date("OxA-34768", 27380, 250)
 {
  Outlier("General", 0.05);
  color="green";
 };
```

```
    R_Date("OxA-33546", 27330, 260)
    {
     Outlier("General", 0.05);
     color="green";
    };
    R_Date("OxA-33834", 28020, 290)
    {
     Outlier("General", 0.05);
     color="green";
    };
    Interval("Kz - Interval 4 (IVa)");
    Date("Date layer 4 (IVa)");
   };
   Boundary("Kz - transition 4 (IVa) to 3b");
   Interval("Kz - Interval transition 4 (IVa) to 3b");
   Phase("3b")
   {
    R_Date("OxA-35417", 23240, 180)
    {
     Outlier("General", 0.05);
     color="green";
    };
    Interval("Kz - Interval 3b");
    Date("Date layer 3b");
   };
   Boundary("Kz - end of 3b");
  };
 };
```

Model 2.

```
Plot()
 {
  Outlier_Model("General",T(5),U(0,4),"t");
  Outlier_Model("SSimple",N(0,2),0,"s");
  Sequence("Kz - Model 2")
  {
   Boundary("Kz - start level 6/7 ls/lp");
   Phase("6/7 ls & 6/7 lp")
   {
    R_Date("OxA-34828", 44000, 1900)
    {
     Outlier("General", 0.05);
     color="green";
    };
    R_Date("OxA-34825", 43800, 1800)
    {
     Outlier("General", 0.05);
     color="green";
    };
```

```
 R_Date("OxA-X-2699-11", 42900, 1700)
 {
  Outlier("General", 0.05);
  color="green";
 };
 R_Date("OxA-34823", 43900, 1800)
 {
  Outlier("General", 0.05);
  color="green";
 };
 R_Date("OxA-33555", 43700, 1900)
 {
  Outlier("General", 0.05);
  color="green";
 };
 Interval("Kz - Interval 6/7 ls lp");
 Date("Date layer 6/7 ls/lp");
};
Boundary("Kz - transition 6/7 ls/lp to 6/7 lb");
Interval("Kz - Interval transition 6/7 ls lp to 6/7 lb");
Phase("6/7 lb")
{
 R_Combine("Kz-109")
 {
  Outlier("General", 0.05);
  color="green";
  R_Date("OxA-34826", 39800, 1100)
  {
   Outlier("SSimple", 0.05);
   color="green";
  };
  R_Date("OxA-34827", 40900, 1300)
  {
   Outlier("SSimple", 0.05);
   color="green";
  };
 };
 Interval("Kz - Interval 6/7 lb");
 Date("Date layer 6/7 lb");
};
Boundary("Kz - transition 6/7 lb to 5c");
Interval("Kz - Interval transition 6/7 lb to 5c");
Phase("5c")
{
 R_Date("OxA-34824", 37600, 900)
 {
  Outlier("General", 0.05);
  color="green";
 };
 R_Date("OxA-33835", 37500, 900)
 {
```

```
  Outlier("General", 0.05);
  color="green";
 };
 R_Date("OxA-33552", 37000, 800)
 {
  Outlier("General", 0.05);
  color="green";
 };
 R_Date("OxA-33553", 36800, 800)
 {
  Outlier("General", 0.05);
  color="green";
 };
 R_Date("OxA-35234", 37400, 800)
 {
  Outlier("General", 0.05);
  color="green";
 };
 Interval("Kz - Interval 5c");
 Date("Date layer 5c");
};
Boundary("Kz - transition 5c to 5b");
Interval("Kz - Interval transition 5c to 5b");
Phase("5b")
{
 R_Date("OxA-34769", 36550, 750)
 {
  Outlier("General", 0.05);
  color="green";
 };
 C_Date("CI", -37900, 140);

 {
  Outlier("General", 0.05);
  color="#b7005c";
 };
 R_Date("OxA-33554", 33650, 550)
 {
  Outlier("General", 0.05);
  color="green";
 };
 R_Date("OxA-33551", 32750, 500)
 {
  Outlier("General", 0.05);
  color="green";
 };
 R_Date("OxA-35575", 27830, 270)
 {
  Outlier("General", 0.05);
  color="green";
 };
```

```
 R_Date("OxA-35576", 28010,280)
 {
  Outlier("General", 0.05);
  color="green";
 };
 Interval("Kz - Interval 5b");
 Date("Date layer 5b");
};
Boundary("Kz - transition 5b to 5a");
Interval("Kz - Interval transition 5b to 5a");
Phase("5a")
{
 R_Date("OxA-33550", 27540, 270)
 {
  Outlier("General", 0.05);
  color="green";
 };
 R_Date("OxA-33549", 27290, 270)
 {
  Outlier("General", 0.05);
  color="green";
 };
 R_Date("OxA-34822", 25400, 200)
 {
  Outlier("General", 0.05);
  color="green";
 };
 Interval("Kz - Interval 5a");
 Date("Date layer 5a");
};
Boundary("Kz - transition 5a to 4 (IVb)");
Phase("4 (IVb)")
{
 R_Date("OxA-35230", 26340, 220)
 {
  Outlier("General", 0.05);
  color="green";
 };
 R_Date("OxA-33547", 25800, 220)
 {
  Outlier("General", 0.05);
  color="green";
 };
 R_Date("OxA-33548", 24090, 180)
 {
  Outlier("General", 0.05);
  color="green";
 };
 Interval("Kz - Interval 4 (IVb)");
 Date("Date layer 4 (IVb)");
};
```

```
   Boundary("Kz - transition 4 (IVb) to 4 (IVa)");
   Interval("Kz - Interval transition 5a to 4 (IVb)");
   Phase("4 (IVa)")
   {
    R_Date("OxA-34767", 26400, 220)
    {
     Outlier("General", 0.05);
     color="green";
    };
    R_Date("OxA-34768", 27380, 250)
    {
     Outlier("General", 0.05);
     color="green";
    };
    R_Date("OxA-33546", 27330, 260)
    {
     Outlier("General", 0.05);
     color="green";
    };
    R_Date("OxA-33834", 28020, 290)
    {
     Outlier("General", 0.05);
     color="green";
    };
    Interval("Kz - Interval 4 (IVa)");
    Date("Date layer 4 (IVa)");
   };
   Boundary("Kz - transition 4 (IVa) to 3b");
   Interval("Kz - Interval transition 4 (IVa) to 3b");
   Phase("3b")
   {
    R_Date("OxA-35417", 23240, 180)
    {
     Outlier("General", 0.05);
     color="green";
    };
    Interval("Kz - Interval 3b");
    Date("Date layer 3b");
   };
   Boundary("Kz - end of 3b");
  };
 };
```

Model 3.

```
Plot()
 {
  Outlier_Model("General",T(5),U(0,4),"t");
  Outlier_Model("SSimple",N(0,2),0,"s");
  Sequence("Kz - Model 3")
  {
```

```
Boundary("Kz - start level 6/7 ls/lp");
Phase("6/7 ls & 6/7 lp")
{
 R_Date("OxA-34828", 44000, 1900)
 {
  Outlier("General", 0.05);
  color="green";
 };
 R_Date("OxA-34825", 43800, 1800)
 {
  Outlier("General", 0.05);
  color="green";
 };
 R_Date("OxA-X-2699-11", 42900, 1700)
 {
  Outlier("General", 0.05);
  color="green";
 };
 R_Date("OxA-34823", 43900, 1800)
 {
  Outlier("General", 0.05);
  color="green";
 };
 R_Date("OxA-33555", 43700, 1900)
 {
  Outlier("General", 0.05);
  color="green";
 };
 Interval("Kz - Interval 6/7 ls lp");
 Date("Date layer 6/7 ls/lp");
};
Boundary("Kz - transition 6/7 ls/lp to 6/7 lb");
Interval("Kz - Interval transition 6/7 ls lp to 6/7 lb");
Phase("6/7 lb")
{
 R_Combine("Kz-109")
 {
  Outlier("General", 0.05);
  color="green";
  R_Date("OxA-34826", 39800, 1100)
  {
   Outlier("SSimple", 0.05);
   color="green";
  };
  R_Date("OxA-34827", 40900, 1300)
  {
   Outlier("SSimple", 0.05);
   color="green";
  };
 };
 Interval("Kz - Interval 6/7 lb");
```

```
 Date("Date layer 6/7 lb");
};
Boundary("Kz - transition 6/7 lb to 5c");
Interval("Kz - Interval transition 6/7 lb to 5c");
Phase("5c")
{
 R_Date("OxA-34824", 37600, 900)
 {
  Outlier("General", 0.05);
  color="green";
 };
 R_Date("OxA-33835", 37500, 900)
 {
  Outlier("General", 0.05);
  color="green";
 };
 R_Date("OxA-33552", 37000, 800)
 {
  Outlier("General", 0.05);
  color="green";
 };
 R_Date("OxA-33553", 36800, 800)
 {
  Outlier("General", 0.05);
  color="green";
 };
 R_Date("OxA-35234", 37400, 800)
 {
  Outlier("General", 0.05);
  color="green";
 };
 R_Date("OxA-34769", 36550, 750)
 {
  Outlier("General", 0.05);
  color="green";
 };
 Interval("Kz - Interval 5c");
 Date("Date layer 5c");
};
Boundary("Kz - transition 5c to 5b");
Interval("Kz - Interval transition 5c to 5b");
Phase("5b")
{
 C_Date("CI", -37900, 140);
 R_Date("OxA-33554", 33650, 550)
 {
  Outlier("General", 0.05);
  color="green";
 };
 R_Date("OxA-33551", 32750, 500)
 {
```

```
  Outlier("General", 0.05);
  color="green";
 };
 R_Date("OxA-35575", 27830, 270)
 {
  Outlier("General", 0.05);
  color="green";
 };
 R_Date("OxA-35576", 28010,280)
 {
  Outlier("General", 0.05);
  color="green";
 };
 Interval("Kz - Interval 5b");
 Date("Date layer 5b");
};
Boundary("Kz - transition 5b to 5a");
Interval("Kz - Interval transition 5b to 5a");
Phase("5a")
{
 R_Date("OxA-33550", 27540, 270)
 {
  Outlier("General", 0.05);
  color="green";
 };
 R_Date("OxA-33549", 27290, 270)
 {
  Outlier("General", 0.05);
  color="green";
 };
 R_Date("OxA-34822", 25400, 200)
 {
  Outlier("General", 0.05);
  color="green";
 };
 Interval("Kz - Interval 5a");
 Date("Date layer 5a");
};
Boundary("Kz - transition 5a to 4");
Interval("Kz - Interval transition 5a to 4");
Phase("4")
{
 R_Date("OxA-35230", 26340, 220)
 {
  Outlier("General", 0.05);
  color="green";
 };
 R_Date("OxA-33547", 25800, 220)
 {
  Outlier("General", 0.05);
  color="green";
```

```
    };
    R_Date("OxA-33548", 24090, 180)
    {
     Outlier("General", 0.05);
     color="green";
    };
    R_Date("OxA-34767", 26400, 220)
    {
     Outlier("General", 0.05);
     color="green";
    };
    R_Date("OxA-34768", 27380, 250)
    {
     Outlier("General", 0.05);
     color="green";
    };
    R_Date("OxA-33546", 27330, 260)
    {
     Outlier("General", 0.05);
     color="green";
    };
    R_Date("OxA-33834", 28020, 290)
    {
     Outlier("General", 0.05);
     color="green";
    };
    Interval("Kz - Interval 4");
    Date("Date layer 4");
   };
   Boundary("Kz - transition 4 to 3b");
   Interval("Kz - Interval transition 4 (IVa) to 3b");
   Phase("3b")
   {
    R_Date("OxA-35417", 23240, 180)
    {
     Outlier("General", 0.05);
     color="green";
    };
    Interval("Kz - Interval 3b");
    Date("Date layer 3b");
   };
   Boundary("Kz - end of 3b");
  };
 };
```

Model 4.

```
{
Outlier_Model("General",T(5),U(0,4),"t");
Outlier_Model("SSimple",N(0,2),0,"s");
Sequence("Kz - Model 4")
```

```
{
Boundary("Kz - start level 6/7 ls/lp");
Phase("6/7 ls & 6/7 lp")
{
R_Date("OxA-34828", 44000, 1900)
{
Outlier("General", 0.05);
color="green";
};
R_Date("OxA-34825", 43800, 1800)
{
Outlier("General", 0.05);
color="green";
};
R_Date("OxA-X-2699-11", 42900, 1700)
{
Outlier("General", 0.05);
color="green";
};
R_Date("OxA-34823", 43900, 1800)
{
Outlier("General", 0.05);
color="green";
};
R_Date("OxA-33555", 43700, 1900)
{
Outlier("General", 0.05);
color="green";
};
Interval("Kz - Interval 6/7 ls lp");
Date("Date layer 6/7 ls/lp");
};
Boundary("Kz - transition 6/7 ls/lp to 6/7 lb");
Interval("Kz - Interval transition 6/7 ls lp to 6/7 lb");
Phase("6/7 lb")
{
R_Combine("Kz-109")
{
Outlier("General", 0.05);
color="green";
R_Date("OxA-34826", 39800, 1100)
{
Outlier("SSimple", 0.05);
color="green";
};
R_Date("OxA-34827", 40900, 1300)
{
Outlier("SSimple", 0.05);
color="green";
};
};
```

```
Interval("Kz - Interval 6/7 lb");
Date("Date layer 6/7 lb");
};
Boundary("Kz - transition 6/7 lb to 5c");
Interval("Kz - Interval transition 6/7 lb to 5c");
Phase("5c")
{
R_Date("OxA-34824", 37600, 900)
{
Outlier("General", 0.05);
color="green";
};
R_Date("OxA-33835", 37500, 900)
{
Outlier("General", 0.05);
color="green";
};
R_Date("OxA-33552", 37000, 800)
{
Outlier("General", 0.05);
color="green";
};
R_Date("OxA-33553", 36800, 800)
{
Outlier("General", 0.05);
color="green";
};
R_Date("OxA-35234", 37400, 800)
{
Outlier("General", 0.05);
color="green";
};
Interval("Kz - Interval 5c");
Date("Date layer 5c");
};
Boundary("Kz - transition 5c to 5b");
Interval("Kz - Interval transition 5c to 5b");
Phase("5b")
{
R_Date("OxA-34769", 36550, 750)
{
Outlier("General", 0.05);
color="green";
};
    C_Date("CI", -37900, 140);
{
Outlier("General", 0.05);
color="#b7005c";
};
R_Date("OxA-33554", 33650, 550)
{
```

```
Outlier("General", 0.05);
color="green";
};
R_Date("OxA-33551", 32750, 500)
{
Outlier("General", 0.05);
color="green";
};
R_Date("OxA-35575", 27830, 270)
{
Outlier("General", 0.05);
color="green";
};
R_Date("OxA-35576", 28010,280)
{
Outlier("General", 0.05);
color="green";
};
Interval("Kz - Interval 5b");
Date("Date layer 5b");
};
Boundary("Kz - transition 5b to 5a");
Interval("Kz - Interval transition 5b to 5a");
Phase("5a")
{
R_Date("OxA-33550", 27540, 270)
{
Outlier("General", 0.05);
color="green";
};
R_Date("OxA-33549", 27290, 270)
{
Outlier("General", 0.05);
color="green";
};
R_Date("OxA-34822", 25400, 200)
{
Outlier("General", 0.05);
color="green";
};
Interval("Kz - Interval 5a");
Date("Date layer 5a");
};
Boundary("Kz - transition 5a to 4");
Interval("Kz - Interval transition 5a to 4");
Phase("4")
{
R_Date("OxA-35230", 26340, 220)
{
Outlier("General", 0.05);
color="green";
```

```
};
R_Date("OxA-33547", 25800, 220)
{
Outlier("General", 0.05);
color="green";
};
R_Date("OxA-33548", 24090, 180)
{
Outlier("General", 0.05);
color="green";
};
R_Date("OxA-34767", 26400, 220)
{
Outlier("General", 0.05);
color="green";
};
R_Date("OxA-34768", 27380, 250)
{
Outlier("General", 0.05);
color="green";
};
R_Date("OxA-33546", 27330, 260)
{
Outlier("General", 0.05);
color="green";
};
R_Date("OxA-33834", 28020, 290)
{
Outlier("General", 0.05);
color="green";
};
Interval("Kz - Interval 4");
Date("Date layer 4");
};
Boundary("Kz - transition 4 to 3b");
Interval("Kz - Interval transition 4 (IVa) to 3b");
Phase("3b")
{
R_Date("OxA-35417", 23240, 180)
{
Outlier("General", 0.05);
color="green";
};
Interval("Kz - Interval 3b");
Date("Date layer 3b");
};
Boundary("Kz - end of 3b");
};
};
```

Model 5.

```
Plot()
 {
  Outlier_Model("General",T(5),U(0,4),"t");
  Outlier_Model("SSimple",N(0,2),0,"s");
  Sequence("Kz - Model 5")
  {
   Boundary("Kz - start level 6/7");
   Phase("6/7")
   {
    R_Date("OxA-24083", 37400, 500)
    {
     color="blue";
     Outlier("General", 0.05);
    };
    R_Date("OxA-34828", 44000, 1900)
    {
     Outlier("General", 0.05);
     color="green";
    };
    R_Date("OxA-22842", 41100, 750)
    {
     Outlier("General", 0.05);
     color="#5b92e5";
    };
    R_Date("OxA-34825", 43800, 1800)
    {
     Outlier("General", 0.05);
     color="green";
    };
    R_Date("OxA-X-2699-11", 42900, 1700)
    {
     Outlier("General", 0.05);
     color="green";
    };
    R_Date("OxA-34823", 43900, 1800)
    {
     Outlier("General", 0.05);
     color="green";
    };
    R_Date("GifA-101048", 29310, 320)
    {
     Outlier("General", 0.05);
     color="#5b92e5";
    };
    R_Date("GifA-101051", 43600, 1200)
    {
     Outlier("General", 0.05);
     color="#5b92e5";
    };
```

```
 R_Date("OxA-33555", 43700, 1900)
 {
  Outlier("General", 0.05);
  color="green";
 };
 R_Combine("Kz-109")
 {
  Outlier("General", 0.05);
  color="green";
  R_Date("OxA-34826", 39800, 1100)
  {
   Outlier("SSimple", 0.05);
   color="green";
  };
  R_Date("OxA-34827", 40900, 1300)
  {
   Outlier("SSimple", 0.05);
   color="green";
  };
 };
 Interval("Kz - Interval 6/7");
 Date("Date layer 6/7");
};
Boundary("Kz - transition 6/7 to 5c");
Interval("Kz - Interval transition 6/7 to 5c");
Phase("5c")
{
 R_Date("Gif/LSM-10994", 38700, 1400)
 {
  Outlier("General", 0.05);
  color="#5b92e5";
 };
 R_Date("OxA-25406", 37600, 500)
 {
  color="blue";
  Outlier("General", 0.05);
 };
 R_Date("OxA-34824", 37600, 900)
 {
  Outlier("General", 0.05);
  color="green";
 };
 R_Date("OxA-24802", 37650, 500)
 {
  color="blue";
  Outlier("General", 0.05);
 };
 R_Date("OxA-23975", 38050, 500)
 {
  color="blue";
  Outlier("General", 0.05);
```

```
 };
 R_Date("OxA-33835", 37500, 900)
 {
  Outlier("General", 0.05);
  color="green";
 };
 R_Date("OxA-33552", 37000, 800)
 {
  Outlier("General", 0.05);
  color="green";
 };
 R_Date("OxA-33553", 36800, 800)
 {
  Outlier("General", 0.05);
  color="green";
 };
 R_Date("GifA-99706", 36200, 540)
 {
  Outlier("General", 0.05);
  color="#5b92e5";
 };
 R_Date("OxA-24080", 36350, 400)
 {
  color="blue";
  Outlier("General", 0.05);
 };
 R_Date("OxA-35234", 37400, 800)
 {
  Outlier("General", 0.05);
  color="green";
 };
 R_Date("OxA-25405", 36900, 450)
 {
  color="blue";
  Outlier("General", 0.05);
 };
 R_Date("OxA-34769", 36550, 750)
 {
  Outlier("General", 0.05);
  color="green";
 };
 R_Date("OxA-24058", 32330, 260)
 {
  color="blue";
  Outlier("General", 0.05);
 };
 Interval("Kz - Interval 5c");
 Date("Date layer 5c");
};
Boundary("Kz - transition 5c to 5b");
Interval("Kz - Interval transition 5c to 5b");
```

```
Phase("5b")
{
 R_Date("OxA-24059", 36650, 450)
 {
  color="blue";
  Outlier("General", 0.05);
 };
 R_Date("OxA-22914", 36250, 450)
 {
  Outlier("General", 0.05);
  color="#5b92e5";
 };
 C_Date("CI", -37900, 140);
 R_Date("OxA-33554", 33650, 550)
 {
  Outlier("General", 0.05);
  color="green";
 };
 R_Date("OxA-33551", 32750, 500)
 {
  Outlier("General", 0.05);
  color="green";
 };
 R_Date("OxA-35575", 27830, 270)
 {
  Outlier("General", 0.05);
  color="green";
 };
 R_Date("OxA-35576", 28010,280)
 {
  Outlier("General", 0.05);
  color="green";
 };
 R_Date("OxA-24865", 28380, 170)
 {
  color="blue";
  Outlier("General", 0.05);
 };
 R_Date("GifA-99044", 26490, 270)
 {
  color="blue";
  Outlier("General", 0.05);
 };
 Interval("Kz - Interval 5b");
 Date("Date layer 5b");
};
Boundary("Kz - transition 5b to 5a");
Interval("Kz - Interval transition 5b to 5a");
Phase("5a")
{
 R_Date("OxA-33550", 27540, 270)
```

```
 {
  Outlier("General", 0.05);
  color="green";
 };
 R_Date("Gif-10992", 25650, 730)
 {
  color="blue";
  Outlier("General", 0.05);
 };
 R_Date("OxA-33549", 27290, 270)
 {
  Outlier("General", 0.05);
  color="green";
 };
 R_Date("OxA-24786", 26320, 190)
 {
  color="blue";
  Outlier("General", 0.05);
 };
 R_Date("OxA-34822", 25400, 200)
 {
  Outlier("General", 0.05);
  color="green";
 };
 Interval("Kz - Interval 5a");
 Date("Date layer 5a");
};
Boundary("Kz - transition 5a to 4");
Interval("Kz - Interval transition 5a to 4");
Phase("4")
{
 R_Date("OxA-25355", 25770, 140)
 {
  color="blue";
  Outlier("General", 0.05);
 };
 R_Date("OxA-25184", 27370, 190)
 {
  color="blue";
  Outlier("General", 0.05);
 };
 R_Date("OxA-35230", 26340, 220)
 {
  Outlier("General", 0.05);
  color="green";
 };
 R_Date("OxA-33547", 25800, 220)
 {
  Outlier("General", 0.05);
  color="green";
 };
```

```
 R_Date("OxA-33548", 24090, 180)
 {
  Outlier("General", 0.05);
  color="green";
 };
 R_Date("Gif/LSM-10677", 26120, 100)
 {
  color="blue";
  Outlier("General", 0.05);
 };
 R_Date("OxA-34767", 26400, 220)
 {
  Outlier("General", 0.05);
  color="green";
 };
 R_Date("OxA-34768", 27380, 250)
 {
  Outlier("General", 0.05);
  color="green";
 };
 R_Date("OxA-33546", 27330, 260)
 {
  Outlier("General", 0.05);
  color="green";
 };
 R_Date("OxA-33834", 28020, 290)
 {
  Outlier("General", 0.05);
  color="green";
 };
 Interval("Kz - Interval 4");
 Date("Date layer 4");
};
Boundary("Kz - transition 4 to 3b");
Interval("Kz - Interval transition 4 (IVa) to 3b");
Phase("3b")
{
 R_Date("OxA-35417", 23240, 180)
 {
  Outlier("General", 0.05);
  color="green";
 };
 R_Date("Gif-10674", 19770, 270)
 {
  color="blue";
  Outlier("General", 0.05);
 };
 Interval("Kz - Interval 3b");
 Date("Date layer 3b");
};
Boundary("Kz - end of 3b");
```

```
  };
 };
```

Model 6.

```
Plot()
 {
  Outlier_Model("General",T(5),U(0,4),"t");
  Outlier_Model("SSimple",N(0,2),0,"s");
  Sequence("Kz - Model 6")
  {
   Boundary("Kz - start level 6/7");
   Phase("6/7")
   {
    R_Date("OxA-24083", 37400, 500)
    {
     color="blue";
     Outlier("General", 0.05);
    };
    R_Date("OxA-34828", 44000, 1900)
    {
     Outlier("General", 0.05);
     color="green";
    };
    R_Date("OxA-22842", 41100, 750)
    {
     Outlier("General", 0.05);
     color="#5b92e5";
    };
    R_Date("OxA-34825", 43800, 1800)
    {
     Outlier("General", 0.05);
     color="green";
    };
    R_Date("OxA-X-2699-11", 42900, 1700)
    {
     Outlier("General", 0.05);
     color="green";
    };
    R_Date("OxA-34823", 43900, 1800)
    {
     Outlier("General", 0.05);
     color="green";
    };
    R_Date("GifA-101048", 29310, 320)
    {
     Outlier("General", 0.05);
     color="#5b92e5";
    };
    R_Date("GifA-101051", 43600, 1200)
    {
```

```
  Outlier("General", 0.05);
  color="#5b92e5";
 };
 R_Date("OxA-33555", 43700, 1900)
 {
  Outlier("General", 0.05);
  color="green";
 };
 R_Combine("Kz-109")
 {
  Outlier("General", 0.05);
  color="green";
  R_Date("OxA-34826", 39800, 1100)
  {
   Outlier("SSimple", 0.05);
   color="green";
  };
  R_Date("OxA-34827", 40900, 1300)
  {
   Outlier("SSimple", 0.05);
   color="green";
  };
 };
 Interval("Kz - Interval 6/7");
 Date("Date layer 6/7");
};
Boundary("Kz - transition 6/7 to 5c");
Interval("Kz - Interval transition 6/7 to 5c");
Phase("5c")
{
 R_Date("Gif/LSM-10994", 38700, 1400)
 {
  Outlier("General", 0.05);
  color="#5b92e5";
 };
 R_Date("OxA-25406", 37600, 500)
 {
  color="blue";
  Outlier("General", 0.05);
 };
 R_Date("OxA-34824", 37600, 900)
 {
  Outlier("General", 0.05);
  color="green";
 };
 R_Date("OxA-24802", 37650, 500)
 {
  color="blue";
  Outlier("General", 0.05);
 };
 R_Date("OxA-23975", 38050, 500)
```

```
 {
  color="blue";
  Outlier("General", 0.05);
 };
 R_Date("OxA-33835", 37500, 900)
 {
  Outlier("General", 0.05);
  color="green";
 };
 R_Date("OxA-33552", 37000, 800)
 {
  Outlier("General", 0.05);
  color="green";
 };
 R_Date("OxA-33553", 36800, 800)
 {
  Outlier("General", 0.05);
  color="green";
 };
 R_Date("GifA-99706", 36200, 540)
 {
  Outlier("General", 0.05);
  color="#5b92e5";
 };
 R_Date("OxA-24080", 36350, 400)
 {
  color="blue";
  Outlier("General", 0.05);
 };
 R_Date("OxA-35234", 37400, 800)
 {
  Outlier("General", 0.05);
  color="green";
 };
 R_Date("OxA-25405", 36900, 450)
 {
  color="blue";
  Outlier("General", 0.05);
 };
 R_Date("OxA-24058", 32330, 260)
 {
  color="blue";
  Outlier("General", 0.05);
 };
 Interval("Kz - Interval 5c");
 Date("Date layer 5c");
};
Boundary("Kz - transition 5c to 5b");
Interval("Kz - Interval transition 5c to 5b");
Phase("5b")
{
```

```
 R_Date("OxA-34769", 36550, 750)
 {
  Outlier("General", 0.05);
  color="green";
 };
 R_Date("OxA-24059", 36650, 450)
 {
  color="blue";
  Outlier("General", 0.05);
 };
 R_Date("OxA-22914", 36250, 450)
 {
  Outlier("General", 0.05);
  color="#5b92e5";
 };
 C_Date("CI", -37900, 140);
 R_Date("OxA-33554", 33650, 550)
 {
  Outlier("General", 0.05);
  color="green";
 };
 R_Date("OxA-33551", 32750, 500)
 {
  Outlier("General", 0.05);
  color="green";
 };
 R_Date("OxA-35575", 27830, 270)
 {
  Outlier("General", 0.05);
  color="green";
 };
 R_Date("OxA-35576", 28010,280)
 {
  Outlier("General", 0.05);
  color="green";
 };
 R_Date("OxA-24865", 28380, 170)
 {
  color="blue";
  Outlier("General", 0.05);
 };
 R_Date("GifA-99044", 26490, 270)
 {
  color="blue";
  Outlier("General", 0.05);
 };
 Interval("Kz - Interval 5b");
 Date("Date layer 5b");
};
Boundary("Kz - transition 5b to 5a");
Interval("Kz - Interval transition 5b to 5a");
```

```
Phase("5a")
{
 R_Date("OxA-33550", 27540, 270)
 {
  Outlier("General", 0.05);
  color="green";
 };
 R_Date("Gif-10992", 25650, 730)
 {
  color="blue";
  Outlier("General", 0.05);
 };
 R_Date("OxA-33549", 27290, 270)
 {
  Outlier("General", 0.05);
  color="green";
 };
 R_Date("OxA-24786", 26320, 190)
 {
  color="blue";
  Outlier("General", 0.05);
 };
 R_Date("OxA-34822", 25400, 200)
 {
  Outlier("General", 0.05);
  color="green";
 };
 Interval("Kz - Interval 5a");
 Date("Date layer 5a");
};
Boundary("Kz - transition 5a to 4");
Interval("Kz - Interval transition 5a to 4");
Phase("4")
{
 R_Date("OxA-25355", 25770, 140)
 {
  color="blue";
  Outlier("General", 0.05);
 };
 R_Date("OxA-25184", 27370, 190)
 {
  color="blue";
  Outlier("General", 0.05);
 };
 R_Date("OxA-35230", 26340, 220)
 {
  Outlier("General", 0.05);
  color="green";
 };
 R_Date("OxA-33547", 25800, 220)
 {
```

```
 Outlier("General", 0.05);
 color="green";
};
R_Date("OxA-33548", 24090, 180)
{
 Outlier("General", 0.05);
 color="green";
};
R_Date("Gif/LSM-10677", 26120, 100)
{
 color="blue";
 Outlier("General", 0.05);
};
R_Date("OxA-34767", 26400, 220)
{
 Outlier("General", 0.05);
 color="green";
};
R_Date("OxA-34768", 27380, 250)
{
 Outlier("General", 0.05);
 color="green";
};
R_Date("OxA-33546", 27330, 260)
{
 Outlier("General", 0.05);
 color="green";
};
R_Date("OxA-33834", 28020, 290)
{
 Outlier("General", 0.05);
 color="green";
};
Interval("Kz - Interval 4");
Date("Date layer 4");
};
Boundary("Kz - transition 4 to 3b");
Interval("Kz - Interval transition 4 (IVa) to 3b");
Phase("3b")
{
R_Date("OxA-35417", 23240, 180)
{
 Outlier("General", 0.05);
 color="green";
};
R_Date("Gif-10674", 19770, 270)
{
 color="blue";
 Outlier("General", 0.05);
};
Interval("Kz - Interval 3b");
```

```
    Date("Date layer 3b");
   };
   Boundary("Kz - end of 3b");
  };
 };
```

Model 7.

```
Plot()
 {
  Outlier_Model("General",T(5),U(0,4),"t");
  Outlier_Model("SSimple",N(0,2),0,"s");
  Sequence("Kz - Model 7")
  {
   Boundary("Kz - start layer 9a");
   Phase("9a")
   {
    Date("Koz7 OSL",N(2017-43000,3000))
    {
     Outlier("General", 0.05);
    };
    Date("Koz6 OSL",N(2017-49000,4000))
    {
     Outlier("General", 0.05);
    };
    Date("Date layer 9a");
    Interval("Kz - interval 9a");
   };
   Boundary("Kz - transition 9a to 6/7 ls/lp");
   Interval("Kz - interval transition 9a to 6/7 lslp");
   Phase("6/7 ls & 6/7 lp")
   {
    R_Date("OxA-34828", 44000, 1900)
    {
     Outlier("General", 0.05);
     color="green";
    };
    R_Date("OxA-34825", 43800, 1800)
    {
     Outlier("General", 0.05);
     color="green";
    };
    R_Date("OxA-X-2699-11", 42900, 1700)
    {
     Outlier("General", 0.05);
     color="green";
    };
    R_Date("OxA-34823", 43900, 1800)
    {
     Outlier("General", 0.05);
```

```
  color="green";
 };
 R_Date("OxA-33555", 43700, 1900)
 {
  Outlier("General", 0.05);
  color="green";
 };
 Interval("Kz - Interval 6/7 ls lp");
 Date("Date layer 6/7 ls/lp");
 Date("Koz5 OSL",N(2017-35000,2000))
 {
  Outlier("General", 0.05);
 };
 Date("Koz4 OSL",N(2017-33000,2000))
 {
  Outlier("General", 0.05);
 };
};
Boundary("Kz - transition 6/7 ls/lp to 6/7 lb");
Interval("Kz - Interval transition 6/7 ls lp to 6/7 lb");
Phase("6/7 lb")
{
 R_Combine("Kz-109")
 {
  Outlier("General", 0.05);
  color="green";
  R_Date("OxA-34826", 39800, 1100)
  {
   Outlier("SSimple", 0.05);
   color="green";
  };
  R_Date("OxA-34827", 40900, 1300)
  {
   Outlier("SSimple", 0.05);
   color="green";
  };
 };
 Interval("Kz - Interval 6/7 lb");
 Date("Date layer 6/7 lb");
};
Boundary("Kz - transition 6/7 lb to 5c");
Interval("Kz - Interval transition 6/7 lb to 5c");
Phase("5c")
{
 R_Date("OxA-34824", 37600, 900)
 {
  Outlier("General", 0.05);
  color="green";
 };
 R_Date("OxA-33835", 37500, 900)
 {
```

```
  Outlier("General", 0.05);
  color="green";
 };
 R_Date("OxA-33552", 37000, 800)
 {
  Outlier("General", 0.05);
  color="green";
 };
 R_Date("OxA-33553", 36800, 800)
 {
  Outlier("General", 0.05);
  color="green";
 };
 R_Date("OxA-35234", 37400, 800)
 {
  Outlier("General", 0.05);
  color="green";
 };
 R_Date("OxA-34769", 36550, 750)
 {
  Outlier("General", 0.05);
  color="green";
 };
 Date("Koz3 OSL",N(2017-33000,2000))
 {
  Outlier("General", 0.05);
 };
 Interval("Kz - Interval 5c");
 Date("Date layer 5c");
};
Boundary("Kz - transition 5c to 5b");
Interval("Kz - Interval transition 5c to 5b");
Phase("5b")
{
 C_Date("CI", -37900, 140)
 {
  Outlier("General", 0.05);
  color="#b7005c";
 };
 R_Date("OxA-33554", 33650, 550)
 {
  Outlier("General", 0.05);
  color="green";
 };
 R_Date("OxA-33551", 32750, 500)
 {
  Outlier("General", 0.05);
  color="green";
 };
 R_Date("OxA-35575", 27830, 270)
 {
```

```
  Outlier("General", 0.05);
  color="green";
 };
 R_Date("OxA-35576", 28010,280)
 {
  Outlier("General", 0.05);
  color="green";
 };
 Date("Koz2 OSL",N(2017-30000,2000))
 {
  Outlier("General", 0.05);
 };
 Interval("Kz - Interval 5b");
 Date("Date layer 5b");
};
Boundary("Kz - transition 5b to 5a");
Interval("Kz - Interval transition 5b to 5a");
Phase("5a")
{
 R_Date("OxA-33550", 27540, 270)
 {
  Outlier("General", 0.05);
  color="green";
 };
 R_Date("OxA-33549", 27290, 270)
 {
  Outlier("General", 0.05);
  color="green";
 };
 R_Date("OxA-34822", 25400, 200)
 {
  Outlier("General", 0.05);
  color="green";
 };
 Date("Koz1 OSL",N(2017-32000,2000))
 {
  Outlier("General", 0.05);
 };
 Interval("Kz - Interval 5a");
 Date("Date layer 5a");
};
Boundary("Kz - transition 5a to 4");
Interval("Kz - Interval transition 5a to 4");
Phase("4")
{
 R_Date("OxA-35230", 26340, 220)
 {
  Outlier("General", 0.05);
  color="green";
 };
 R_Date("OxA-33547", 25800, 220)
```

```
    {
     Outlier("General", 0.05);
     color="green";
    };
    R_Date("OxA-33548", 24090, 180)
    {
     Outlier("General", 0.05);
     color="green";
    };
    R_Date("OxA-34767", 26400, 220)
    {
     Outlier("General", 0.05);
     color="green";
    };
    R_Date("OxA-34768", 27380, 250)
    {
     Outlier("General", 0.05);
     color="green";
    };
    R_Date("OxA-33546", 27330, 260)
    {
     Outlier("General", 0.05);
     color="green";
    };
    R_Date("OxA-33834", 28020, 290)
    {
     Outlier("General", 0.05);
     color="green";
    };
    Interval("Kz - Interval 4");
    Date("Date layer 4");
   };
   Boundary("Kz - transition 4 to 3b");
   Interval("Kz - Interval transition 4 (IVa) to 3b");
   Phase("3b")
   {
    R_Date("OxA-35417", 23240, 180)
    {
     Outlier("General", 0.05);
     color="green";
    };
    Interval("Kz - Interval 3b");
    Date("Date layer 3b");
   };
   Boundary("Kz - end of 3b");
  };
 };
```

Model 8.

```
Plot()
```

```
{
 Outlier_Model("General",T(5),U(0,4),"t");
 Outlier_Model("SSimple",N(0,2),0,"s");
 Sequence("Kz - Model 8")
 {
  Boundary("Kz - start layer 9a");
  Phase("9a")
  {
   Date("Date layer 9a");
   Interval("Kz - interval 9a");
  };
  Boundary("Kz - transition 9a to 6/7 ls/lp");
  Interval("Kz - interval transition 9a to 6/7 lslp");
  Phase("6/7 ls & 6/7 lp")
  {
   R_Date("OxA-34828", 44000, 1900)
   {
    Outlier("General", 0.05);
    color="green";
   };
   R_Date("OxA-34825", 43800, 1800)
   {
    Outlier("General", 0.05);
    color="green";
   };
   R_Date("OxA-X-2699-11", 42900, 1700)
   {
    Outlier("General", 0.05);
    color="green";
   };
   R_Date("OxA-34823", 43900, 1800)
   {
    Outlier("General", 0.05);
    color="green";
   };
   R_Date("OxA-33555", 43700, 1900)
   {
    Outlier("General", 0.05);
    color="green";
   };
   Date("Date layer 6/7 ls/lp");
  };
  Boundary("Kz - transition 6/7 ls/lp to 6/7 lb");
  Interval("Kz - Interval transition 6/7 ls lp to 6/7 lb");
  Phase("6/7 lb")
  {
   R_Combine("Kz-109")
   {
    Outlier("General", 0.05);
    color="green";
    R_Date("OxA-34826", 39800, 1100)
```

```
  {
   Outlier("SSimple", 0.05);
   color="green";
  };
  R_Date("OxA-34827", 40900, 1300)
  {
   Outlier("SSimple", 0.05);
   color="green";
  };
 };
 Date("Date layer 6/7 lb");
};
Boundary("Kz - transition 6/7 lb to 5c");
Interval("Kz - Interval transition 6/7 lb to 5c");
Phase("5c")
{
 R_Date("OxA-34824", 37600, 900)
 {
  Outlier("General", 0.05);
  color="green";
 };
 R_Date("OxA-33835", 37500, 900)
 {
  Outlier("General", 0.05);
  color="green";
 };
 R_Date("OxA-33552", 37000, 800)
 {
  Outlier("General", 0.05);
  color="green";
 };
 R_Date("OxA-33553", 36800, 800)
 {
  Outlier("General", 0.05);
  color="green";
 };
 R_Date("OxA-35234", 37400, 800)
 {
  Outlier("General", 0.05);
  color="green";
 };
 Date("Date layer 5c");
};
Boundary("Kz - transition 5c to 5b");
Interval("Kz - Interval transition 5c to 5b");
Phase("5b")
{
 C_Date("CI", -37900, 140)
 {
  Outlier("General", 0.05);
  color="#b7005c";
```

```
 };
 R_Date("OxA-33554", 33650, 550)
 {
  Outlier("General", 0.05);
  color="green";
 };
 R_Date("OxA-33551", 32750, 500)
 {
  Outlier("General", 0.05);
  color="green";
 };
 R_Date("OxA-35575", 27830, 270)
 {
  Outlier("General", 0.05);
  color="green";
 };
 R_Date("OxA-35576", 28010,280)
 {
  Outlier("General", 0.05);
  color="green";
 };
 Interval("Kz - Interval 5b");
 Date("Date layer 5b");
};
Boundary("Kz - transition 5b to 5a");
Interval("Kz - Interval transition 5b to 5a");
Phase("5a")
{
 R_Date("OxA-33550", 27540, 270)
 {
  Outlier("General", 0.05);
  color="green";
 };
 R_Date("OxA-33549", 27290, 270)
 {
  Outlier("General", 0.05);
  color="green";
 };
 R_Date("OxA-34822", 25400, 200)
 {
  Outlier("General", 0.05);
  color="green";
 };
 Interval("Kz - Interval 5a");
 Date("Date layer 5a");
};
Boundary("Kz - transition 5a to 4");
Interval("Kz - Interval transition 5a to 4");
Phase("4")
{
 R_Date("OxA-35230", 26340, 220)
```

```
  {
   Outlier("General", 0.05);
   color="green";
  };
  R_Date("OxA-33547", 25800, 220)
  {
   Outlier("General", 0.05);
   color="green";
  };
  R_Date("OxA-33548", 24090, 180)
  {
   Outlier("General", 0.05);
   color="green";
  };
  R_Date("OxA-34767", 26400, 220)
  {
   Outlier("General", 0.05);
   color="green";
  };
  R_Date("OxA-34768", 27380, 250)
  {
   Outlier("General", 0.05);
   color="green";
  };
  R_Date("OxA-33546", 27330, 260)
  {
   Outlier("General", 0.05);
   color="green";
  };
  R_Date("OxA-33834", 28020, 290)
  {
   Outlier("General", 0.05);
   color="green";
  };
  Interval("Kz - Interval 4");
  Date("Date layer 4");
 };
 Boundary("Kz - transition 4 to 3b");
 Interval("Kz - Interval transition 4 (IVa) to 3b");
 Phase("3b")
 {
  R_Date("OxA-35417", 23240, 180)
  {
   Outlier("General", 0.05);
   color="green";
  };
  Interval("Kz - Interval 3b");
  Date("Date layer 3b");
 };
 Boundary("Kz - end of 3b");
};
```

```
 };
```

KDE Models

Model 0

```
Plot()
 {
  KDE_Model("Kozarnika KDE0", N(0,1), U(0,1))
  {
   R_Date("GifA-101051", 43600, 1200);
   R_Date("OxA-22842", 41100, 750);
   R_Date("GifA-101048", 29310, 320);
   R_Date("OxA-24083", 37400, 500);
   R_Date("Gif/LSM-10994", 38700, 1400);
   R_Date("OxA-23975", 38050, 500);
   R_Date("OxA-25406", 37600, 500);
   R_Date("OxA-24802", 37650, 500);
   R_Date("GifA-99706", 36200, 540);
   R_Date("OxA-25405", 36900, 450);
   R_Date("OxA-24080", 36350, 400);
   R_Date("OxA-24058", 32330, 260);
   R_Date("OxA-24059", 36650, 450);
   R_Date("OxA-22914", 36250, 450);
   R_Date("OxA-24865", 28380, 170);
   R_Date("GifA-99044", 26490, 270);
   R_Date("Gif-10992", 25650, 730);
   R_Date("OxA-24786", 26320, 190);
   R_Date("Gif/LSM-10677", 26120, 100);
   R_Date("OxA-25355", 25770, 140);
   R_Date("OxA-25184", 27370, 190);
   R_Date("Gif-10674", 19770, 270);
   R_Date("GifA-98345", 11550, 100);
  };
 };
```

Model 1

```
Plot()
 {
  KDE_Model("Kozarnika KDE1", N(0,1), U(0,1))
  {
   R_Date("OxA-35417", 23240, 180);
   R_Date("OxA-34767", 26400, 220);
   R_Date("OxA-33546", 27330, 260);
   R_Date("OxA-34768", 27380, 250);
   R_Date("OxA-33834", 28020, 290);
   R_Date("OxA-33548", 24090, 180);
   R_Date("OxA-33547", 25800, 220);
   R_Date("OxA-35230", 26340, 220);
```

```
  R_Date("OxA-34822", 25400, 200);
  R_Date("OxA-33549", 27290, 270);
  R_Date("OxA-33550", 27540, 270);
  R_Date("OxA-35575", 27830, 270);
  R_Date("OxA-35576", 28010,280);
  R_Date("OxA-33551", 32750, 500);
  R_Date("OxA-33554", 33650, 550);
  R_Date("OxA-35234", 37400, 800);
  R_Date("OxA-33553", 36800, 800);
  R_Date("OxA-33552", 37000, 800);
  R_Date("OxA-33835", 37500, 900);
  R_Date("OxA-34824", 37600, 900);
  R_Date("OxA-34826", 39800, 1100);
  R_Date("OxA-34827", 40900, 1300);
  R_Date("OxA-33555", 43700, 1900);
  R_Date("OxA-34823", 43900, 1800);
  R_Date("OxA-X-2699-11", 42900, 1700);
  R_Date("OxA-34825", 43800, 1800);
  R_Date("OxA-34828", 44000, 1900);
  R_Date("OxA-34769", 36550, 750);
 };
};
```

Model 2

```
Plot()
 {
  KDE_Model("Kozarnika KDE2", N(0,1), U(0,1))
  {
   R_Date("GifA-101051", 43600, 1200);
   R_Date("OxA-22842", 41100, 750);
   R_Date("GifA-101048", 29310, 320);
   R_Date("OxA-24083", 37400, 500);
   R_Date("Gif/LSM-10994", 38700, 1400);
   R_Date("OxA-23975", 38050, 500);
   R_Date("OxA-25406", 37600, 500);
   R_Date("OxA-24802", 37650, 500);
   R_Date("GifA-99706", 36200, 540);
   R_Date("OxA-25405", 36900, 450);
   R_Date("OxA-24080", 36350, 400);
   R_Date("OxA-24058", 32330, 260);
   R_Date("OxA-24059", 36650, 450);
   R_Date("OxA-22914", 36250, 450);
   R_Date("OxA-24865", 28380, 170);
   R_Date("GifA-99044", 26490, 270);
   R_Date("Gif-10992", 25650, 730);
   R_Date("OxA-24786", 26320, 190);
   R_Date("Gif/LSM-10677", 26120, 100);
   R_Date("OxA-25355", 25770, 140);
   R_Date("OxA-25184", 27370, 190);
   R_Date("Gif-10674", 19770, 270);
   R_Date("GifA-98345", 11550, 100);
   R_F14C("OxA-35417",0.05541,0.00126);
   R_F14C("OxA-33834",0.03057,0.00109);
   R_F14C("OxA-34767",0.03741,0.00105);
   R_F14C("OxA-34768",0.03309,0.00102);
   R_F14C("OxA-33546",0.03330,0.00109);
   R_F14C("OxA-35230",0.03768,0.00105);
   R_F14C("OxA-33547",0.04030,0.00110);
   R_F14C("OxA-33548",0.04983,0.00115);
   R_F14C("OxA-33549",0.03346,0.00111);
   R_F14C("OxA-33550",0.03246,0.00109);
   R_F14C("OxA-33551",0.01696,0.00105);
   R_F14C("OxA-33552",0.01000,0.00102);
   R_F14C("OxA-33835",0.00940,0.00101);
   R_F14C("OxA-34769",0.01054,0.00098);
   R_F14C("OxA-33553",0.01021,0.00103);
   R_F14C("OxA-33554",0.01513,0.00108);
   R_F14C("OxA-33555",0.00432,0.00101);
   R_F14C("OxA-34822",0.04237,0.00108);
   R_F14C("OxA-34823",0.00423,0.00097);
   R_F14C("OxA-X-2699-11",0.00481,0.001);
   R_F14C("OxA-34824",0.00926,0.00099);
   R_F14C("OxA-35234",0.00954,0.00098);
```

```
  R_F14C("OxA-35575",0.0313,0.00104);
  R_F14C("OxA-35576",0.03061,0.00105);
  R_F14C("OxA-34825",0.00427,0.00098);
  R_F14C("OxA-34826",0.00702,0.00098);
  R_F14C("OxA-34827",0.00614,0.00098);
  R_F14C("OxA-34828",0.00417,0.00097);
 };
};
```

Name	Unmodelled (BP)				Modelled (BP)				Indices Amodel 72.2 Aoverall 71.2	
	From 68.3 % prob.	*To 68.3 % prob.*	*From 95.4 % prob.*	*To 95.4% prob.*	*From 68.3 % prob.*	*To 68.3 % prob.*	*From 95.4 % prob.*	*To 95.4 % prob.*	*A*	C
Kz - end of 3b					27670	26060	27760	23960		97.9
Date layer 3b					28320	26670	30060	25460		98.3
Kz - Interval 3b					0	3300	0	5140		94.2
OxA-35417	27650	27330	27760	27240	27670	27340	27810	27210	101.1	99.5
3b										
Kz - Interval transition 4 (IVa) to 3b					0	800	0	2640		97.6
Kz - transition 4 to 3b					30180	27500	30700	27330		91.1
Date layer 4					31460	29460	31550	28120		97.8
Kz - Interval 4					1260	4030	730	4220		91.3
OxA-33834	32810	31610	33040	31340	31560	31200	31790	29650	28.1	99.3
OxA-33546	31550	31150	31790	31050	31400	31120	31610	31020	113.6	99.7
OxA-34768	31570	31170	31800	31080	31410	31140	31620	31040	111.8	99.6
OxA-34767	30910	30390	31070	30190	30920	30400	31080	30180	103.2	99.7
OxA-33548	28520	27980	28690	27830	30810	27890	31480	27810	66.5	91.7
OxA-33547	30310	29910	30770	29540	30370	29890	30870	29530	95.2	99.2
OxA-35230	30860	30340	31030	30150	30890	30360	31060	30140	103	99.7
4										
Kz - Interval transition 5a to 4					0	100	0	240		99.9
Kz - transition 5a to 4					31610	31350	31740	31220		99.6
Date layer 5a					31700	31410	31870	31270		99.8
Kz - Interval 5a					0	220	0	520		99.7
OxA-34822	29950	29330	30030	29210	31700	31410	31870	31270	5.5	99.7
OxA-33549	31540	31130	31790	31020	31680	31420	31810	31280	84.4	99.8
OxA-33550	31690	31230	32020	31100	31690	31420	31830	31290	118.1	99.8

5a										
Kz - Interval transition 5b to 5a					0	50	0	190		99.9
Kz - transition 5b to 5a					31790	31470	32030	31310		99.5
Date layer 5b					40180	31990	41110	31740		99.2
Kz - Interval 5b					9320	10340	8520	10600		99.3
OxA-35576	32800	31600	33010	31340	32810	31700	33090	31570	104.2	99.1
OxA-35575	32050	31370	32860	31190	32720	31590	32970	31500	94.4	99
OxA-33551	38030	36420	39020	36230	38130	36410	39120	36180	100.7	98.9
OxA-33554	39260	37680	39880	36980	39280	37640	40000	36890	100.9	98.8
Campanian ignimbrite	40000	39700	40140	39570	40000	39700	40160	39540	102.7	99.5
5b										
Kz - Interval transition 5c to 5b					940	2120	70	2270		99.5
Kz - transition 5c to 5b					41980	41050	42160	40240		98.8
Date layer 5c					42280	41470	42810	40800		99.6
OxA-35234	42370	41490	42780	40980	42230	41620	42480	41230	119.3	99.7
OxA-33553	42140	41160	42500	40480	42170	41530	42390	41080	117.8	99.7
OxA-33552	42210	41280	42570	40650	42180	41550	42430	41140	120	99.7
OxA-33835	42450	41460	43000	40840	42250	41610	42530	41200	122	99.7
OxA-34824	42510	41520	43070	40900	42270	41630	42550	41230	120.1	99.7
5c										
Kz - Interval transition 6/7 lb to 5c					0	200	0	770		99.8
Kz - transition 6/7 lb to 5c					42650	41890	43330	41530		99.2
Date layer 6/7 lb					44470	42500	45670	42020		99.7
OxA-34827	44850	42920	46560	42430						
OxA-34826	44040	42570	45030	42190						
Kz-109	44150	42920	44770	42530	44070	42900	44680	42540	105.2	99.7
6/7 lb										
Kz - Interval transition 6/7 ls lp to 6/7 lb					0	1290	0	2580		99.8
Kz - transition 6/7 ls/lp to 6/7 lb					45970	44190	46830	43200		99.2

Date layer 6/7 ls/lp					46860	44890	48500	44030		99.5
OxA-33555	48550	44550	54260	43240	46780	45000	48120	44410	135.3	99.5
OxA-34823	48500	44710	54340	43850	46790	45020	48100	44470	131.8	99.5
OxA-X-2699-11	47640	44240	50880	42920	46700	44940	47990	44320	130.2	99.5
OxA-34825	48420	44660	52360	43410	46770	45010	48110	44450	132.8	99.5
OxA-34828	48780	44690	54600	43950	46790	45030	48160	44470	132.2	99.5
6/7 ls & 6/7 lp										
Kz - interval transition 9a to 6/7 lslp					0	330	0	1390		99.8
Kz - transition 9a to 6/7 ls/lp					47910	45530	50020	44880		98.3
Kz - interval 9a					0	4410	0	12930		96.8
Date layer 9a					49940	45850	*55770*	45010		98
9a										
Kz - start layer 9a					*52550*	45760	60660	45220		*59.5*
Kz - Model 8										

Table S4: Model output for Model 8, our favoured model. C denotes Convergence. A denotes Agreement.

Element	Prior	Posterior	Model	Type	Element	Prior	Posterior	Model	Type
OxA-34828	5	3	General	t	OxA-33554	5	4	General	t
OxA-34825	5	3	General	t	OxA-33551	5	4	General	t
OxA-X-2699-11	5	3	General	t	OxA-35575	5	4	General	t
OxA-34823	5	3	General	t	OxA-35576	5	3	General	t
OxA-33555	5	3	General	t	OxA-33550	5	1	General	t
Kz-109	5	3	General	t	OxA-33549	5	1	General	t
OxA-34826	5	3	SSimple	s	OxA-34822	5	100	General	t
OxA-34827	5	3	SSimple	s	OxA-35230	5	3	General	t
OxA-34824	5	2	General	t	OxA-33547	5	3	General	t
OxA-33835	5	2	General	t	OxA-33548	5	36	General	t
OxA-33552	5	2	General	t	OxA-34767	5	2	General	t
OxA-33553	5	2	General	t	OxA-34768	5	4	General	t
OxA-35234	5	2	General	t	OxA-33546	5	3	General	t
Cl	5	3	General	t	OxA-33834	5	25	General	t
			General	t	OxA-35417	5	2	General	t

Table S5: Outlier probabilities for Model 8.

Supplement 2 to A Refined Chronology for the Middle–Upper Paleolithic Transition at Kozarnika Cave (Bulgaria) 40–50,000 Years Ago: New AMS Radiocarbon Dates and Implications for Early *Homo sapiens* in Europe

RACHEL HOPKINS
RLAHA, University of Oxford, Oxford, UNITED KINGDOM; and, Meow Wolf, Inc., 1352 Rufina Circle, Santa Fe, NM 87507, USA; rja.hopkins@protonmail.com

JEAN-LUC GUADELLI
PACEA-UMR 5199 CNRS, Université de Bordeaux, Allée Geoffroy St Hilaire, Bâtiment B2, CS 50023, 33615 Pessac cedex, FRANCE; jean-luc.guadelli@u-bordeaux.fr

DUSTIN WHITE
Department of Chemistry, University of York, UNITED KINGDOM; dustin.white@york.ac.uk

CHRIS STRINGER
Natural History Museum, Cromwell Road, London, UNITED KINGDOM; c.stringer@nhm.ac.uk

EMESE VÈGH
Department of Evolutionary Anthropology, University of Vienna, University Biology Building, Djerassiplatz 1, A-1030 Vienna; and, Human Evolution and Archaeological Science (HEAS) Network, Vienna, AUSTRIA; emese.vegh@univie.ac.at

MICHAEL BUCKLEY
Manchester Institute of Biotechnology, University of Manchester, M1 7DN, UNITED KINGDOM; M.Buckley@manchester.ac.uk

ALETA GUADELLI
Center for Underwater Archaeology, State Cultural Institute, Ministry of Culture, Str. Apollonia n°1, 8130 Sozopol, BULGARIA; aleta.guadelli@gmail.com

PHILIPPE FERNANDEZ
LAMPEA UMR 7269, CNRS, Aix Marseille Univ., Minist. Culture, MMSH, 5 Rue du Château de l'Horloge, F13094, Aix-en-Provence, FRANCE; philippe.fernandez@univ-amu.fr

NIKOLAI SIRAKOV
National Institute of Archaeology with Museum-Bulgarian Academy of Sciences, 2, Saborna Street, 1000, Sofia, BULGARIA; nikolaysirakov@gmail.com

TOM HIGHAM
Department of Evolutionary Anthropology, University of Vienna, University Biology Building, Djerassiplatz 1, A-1030 Vienna; and, Human Evolution and Archaeological Science (HEAS) Network, Vienna, AUSTRIA; thomas.higham@univie.ac.at

SUPPLEMENT 2

This supplement contains: Supplementary Dataset 1: the MALDI-ToF mass spectra processed using SpecieScan.

Sample	COL1_1_508_519	COL1_2_978_990	COL1_2_978_990_16	COL1a2_484__499	COL1a2_502__519	COL1a2_292__309	COL1a2_793__816	COL1a2_454__483	COL1a1_586__618	COL1a1_586__618_16	COL1a2_757__789	COL1a2_757__789_16	ZooMS_taxon	Family	Order	Correlation
Kz109	1105.6		1233.6	1453.7			2163.1		2853.4	2869.4			Ursus/Felis/Lynx	Ursidae/Felidae	Carnivora	0.172606442
Kz114	1105.6			1427.7		1648.8	2131.1			2899.4		3093.4	Capra/Rangifer	Bovidae/Cervidae	Artiodactyla	0.150302187
Kz03	1105.6			1427.7	1550.8	1648.8	2131.1		2883.4	2899.4			Cervus/Saiga/Gazella	Cervidae/Bovidae	Artiodactyla	0.21244812
Kz07	1105.6			1427.7	1550.8	1649.8	2145.1		2883.4				Equus	Equidae	Perissodactyla	0.186299389
Kz112	1105.6			1427.7	1550.8		2145.1		2883.4				Equus	Equidae	Perissodactyla	0.171484226
Kz116	1105.6	1182.6		1427.7	1550.8		2145.1		2883.4			2999.4	Equus	Equidae	Perissodactyla	0.201958379
Kz115	1105.6			1427.7	1550.8		2145.1			2899.4			Equus	Equidae	Perissodactyla	0.151944114
Kz82	1105.6			1427.7	1550.8	1648.8	2131.1		2883.4	2899.4		3033.4	Cervus/Saiga/Gazella	Cervidae/Bovidae	Artiodactyla	0.229381303
Kz85	1105.6			1427.7	1550.8		2145.1		2883.4				Equus	Equidae	Perissodactyla	0.134205303
Kz79	1105.6	1182.6		1427.7	1550.8		2145.1		2883.4				Equus	Equidae	Perissodactyla	0.176488376
Kz83	1105.6		1208.6	1427.7	1580.8	1648.8	2131.1		2853.4			3033.4	Bos/Bison	Bovidae	Artiodactyla	0.21244812
Kz93	1105.6	1182.6	1198.6	1427.7	1550.8		2145.1		2883.4	2899.4		2999.4	Equus	Equidae	Perissodactyla	0.219808732
Kz48	1105.6	1180.6	1196.6	1427.7	1580.8	1648.8	2131.1		2883.4				Capra/Ovis	Bovidae	Artiodactyla	0.231625357
Kz81	1105.6		1208.6	1427.7	1580.8	1648.8	2131.1		2853.4			3033.4	Bos/Bison	Bovidae	Artiodactyla	0.21547332
Kz88	1105.6			1427.7	1550.8	1648.8	2131.1		2883.4	2899.4		3033.4	Cervus/Saiga/Gazella	Cervidae/Bovidae	Artiodactyla	0.235389007
Kz38	1105.6			1453.7	1550.8	2145.1	2869.4						Rhinoceros	Rhinocerotidae	Perissodactyla	0.169107988
Kz116underscore1	1105.6		1198.6	1427.7			2145.1		2883.4	2899.4			Equus	Equidae	Perissodactyla	0.174499437
Kz87	1105.6	1192.6	1208.6	1427.7	1580.8	1648.8	2131.1		2853.4			3033.4	Bos/Bison	Bovidae	Artiodactyla	0.212991845
Kz80	1105.6		1208.6	1427.7	1580.8	1648.8	2131.1		2853.4	2869.4			Bos/Bison	Bovidae	Artiodactyla	0.251052542
Kz08	1105.6		1208.6	1427.7	1580.8	1648.8	2131.1		2853.4			3033.4	Bos/Bison	Bovidae	Artiodactyla	0.191271718
Kz110	1105.6		1208.6	1427.7	1580.8	1648.8	2131.1		2853.4	2869.4			Bos/Bison	Bovidae	Artiodactyla	0.247292972
Kz14	1105.6	1182.6		1427.7	1550.8	1649.8	2145.1		2883.4				Equus	Equidae	Perissodactyla	0.211835555
Kz111	1105.6		1198.6	1427.7	1550.8		2145.1		2883.4			2999.4	Equus	Equidae	Perissodactyla	0.216713939
Kz45	1105.6			1427.7	1550.8		2145.1		2883.4				Equus	Equidae	Perissodactyla	0.172039781

Supplement 3 to A Refined Chronology for the Middle–Upper Paleolithic Transition at Kozarnika Cave (Bulgaria) 40–50,000 Years Ago: New AMS Radiocarbon Dates and Implications for Early *Homo sapiens* in Europe

RACHEL HOPKINS
RLAHA, University of Oxford, Oxford, UNITED KINGDOM; and, Meow Wolf, Inc., 1352 Rufina Circle, Santa Fe, NM 87507, USA; rja.hopkins@protonmail.com

JEAN-LUC GUADELLI
PACEA-UMR 5199 CNRS, Université de Bordeaux, Allée Geoffroy St Hilaire, Bâtiment B2, CS 50023, 33615 Pessac cedex, FRANCE; jean-luc.guadelli@u-bordeaux.fr

DUSTIN WHITE
Department of Chemistry, University of York, UNITED KINGDOM; dustin.white@york.ac.uk

CHRIS STRINGER
Natural History Museum, Cromwell Road, London, UNITED KINGDOM; c.stringer@nhm.ac.uk

EMESE VÈGH
Department of Evolutionary Anthropology, University of Vienna, University Biology Building, Djerassiplatz 1, A-1030 Vienna; and, Human Evolution and Archaeological Science (HEAS) Network, Vienna, AUSTRIA; emese.vegh@univie.ac.at

MICHAEL BUCKLEY
Manchester Institute of Biotechnology, University of Manchester, M1 7DN, UNITED KINGDOM; M.Buckley@manchester.ac.uk

ALETA GUADELLI
Center for Underwater Archaeology, State Cultural Institute, Ministry of Culture, Str. Apollonia n°1, 8130 Sozopol, BULGARIA; aleta.guadelli@gmail.com

PHILIPPE FERNANDEZ
LAMPEA UMR 7269, CNRS, Aix Marseille Univ., Minist. Culture, MMSH, 5 Rue du Château de l'Horloge, F13094, Aix-en-Provence, FRANCE; philippe.fernandez@univ-amu.fr

NIKOLAI SIRAKOV
National Institute of Archaeology with Museum-Bulgarian Academy of Sciences, 2, Saborna Street, 1000, Sofia, BULGARIA; nikolaysirakov@gmail.com

TOM HIGHAM
Department of Evolutionary Anthropology, University of Vienna, University Biology Building, Djerassiplatz 1, A-1030 Vienna; and, Human Evolution and Archaeological Science (HEAS) Network, Vienna, AUSTRIA; thomas.higham@univie.ac.at

SUPPLEMENT 3

This supplement contains: Supplementary Dataset 2: contamination scanning (also assessed by SpecieScan) showing common laboratory contaminants and human keratin contamination.

Sample	contaminant	mass
Kz87_F1_Contaminants.csv	4HCCA Cluster	1060.0879
Kz87_F1_Contaminants.csv	Bovine Casein a-S1	1267.7045
Kz87_F1_Contaminants.csv	Keratin (Human)	1193.6161
Kz87_F1_Contaminants.csv	Porcine Trypsin, Methylated	2720.3634
Kz112_F1_Contaminants.csv	4HCCA Cluster	855.0714
Kz112_F1_Contaminants.csv	4HCCA Cluster	1060.0879
Kz112_F1_Contaminants.csv	Keratin	1315.6852
Kz112_F1_Contaminants.csv	Porcine Trypsin+Na	2305.16215
Kz112_F1_Contaminants.csv	Porcine Trypsin, Methylated	2720.3634
Kz85_F1_Contaminants.csv	4HCCA Cluster	855.0714
Kz85_F1_Contaminants.csv	4HCCA Cluster	1060.0879
Kz85_F1_Contaminants.csv	Porcine Trypsin, Methylated	2720.3634
Kz111_F1_Contaminants.csv	4HCCA Cluster	855.0714
Kz111_F1_Contaminants.csv	4HCCA Cluster	1060.0879
Kz111_F1_Contaminants.csv	Porcine Trypsin+Na	2305.16215
Kz110_F1_Contaminants.csv	4HCCA Cluster	1060.0879
Kz110_F1_Contaminants.csv	Bovine Casein a-S1	1267.7045
Kz110_F1_Contaminants.csv	Porcine Trypsin, Methylated	2720.3634
Kz14_F2_Contaminants.csv	4HCCA Cluster	855.0714
Kz14_F2_Contaminants.csv	4HCCA Cluster	1060.0879
Kz14_F2_Contaminants.csv	Porcine Trypsin, Methylated	2720.3634
Kz82_F1_Contaminants.csv	4HCCA Cluster	855.0714
Kz82_F1_Contaminants.csv	4HCCA Cluster	1060.0879
Kz82_F1_Contaminants.csv	Bovine Casein a-S1	1267.7045
Kz82_F1_Contaminants.csv	Keratin (Human)	2501.0672
Kz82_F1_Contaminants.csv	Keratin (Human)	2501.2518
Kz82_F1_Contaminants.csv	Porcine Trypsin, Methylated	2720.3634
Kz38_F1_Contaminants.csv	4HCCA Cluster	855.0714
Kz38_F1_Contaminants.csv	4HCCA Cluster	1060.0879
Kz38_F1_Contaminants.csv	Keratin	1315.6852
Kz38_F1_Contaminants.csv	Keratin (Human)	1765.7347
Kz38_F1_Contaminants.csv	Porcine Trypsin+Na	2233.086
Kz83_F1_Contaminants.csv	4HCCA Cluster	855.0714
Kz83_F1_Contaminants.csv	4HCCA Cluster	861.0794
Kz83_F1_Contaminants.csv	Bovine Casein a-S1	1267.7045
Kz83_F1_Contaminants.csv	Porcine Trypsin, Methylated	2720.3634
Kz114_F1_Contaminants.csv	4HCCA Cluster	855.0714
Kz114_F1_Contaminants.csv	4HCCA Cluster	1060.0879

Kz114_F1_Contaminants.csv	Bovine Casein a-S1	1267.7045
Kz114_F1_Contaminants.csv	Porcine Trypsin+Na	2233.086
Kz114_F1_Contaminants.csv	Porcine Trypsin, Methylated	2720.3634
Kz80_F1_Contaminants.csv	4HCCA Cluster	855.0714
Kz80_F1_Contaminants.csv	4HCCA Cluster	1060.0879
Kz80_F1_Contaminants.csv	Bovine Casein a-S1	1267.7045
Kz80_F1_Contaminants.csv	Porcine Trypsin, Methylated	2720.3634
Kz81_F1_Contaminants.csv	4HCCA Cluster	855.0714
Kz81_F1_Contaminants.csv	4HCCA Cluster	861.0794
Kz81_F1_Contaminants.csv	Bovine Casein a-S1	1267.7045
Kz81_F1_Contaminants.csv	Porcine Trypsin, Methylated	2720.3634
Kz115_F1_Contaminants.csv	4HCCA Cluster	855.0714
Kz115_F1_Contaminants.csv	4HCCA Cluster	1060.0879
Kz115_F1_Contaminants.csv	Keratin	1315.6852
Kz115_F1_Contaminants.csv	Keratin (Human)	973.5313
Kz115_F1_Contaminants.csv	Porcine Trypsin, Methylated	2720.3634
Kz03_F2_Contaminants.csv	4HCCA Cluster	855.0714
Kz03_F2_Contaminants.csv	4HCCA Cluster	1060.0879
Kz03_F2_Contaminants.csv	Bovine Casein a-S1	1267.7045
Kz03_F2_Contaminants.csv	Porcine Trypsin+Na	2233.086
Kz03_F2_Contaminants.csv	Porcine Trypsin, Methylated	2720.3634
Kz93_2_Contaminants.csv	4HCCA Cluster	855.0714
Kz93_2_Contaminants.csv	Keratin (Human)	1183.6157
Kz93_2_Contaminants.csv	Keratin (Human)	1329.6393
Kz109_1_F1_Contaminants.csv	4HCCA Cluster	855.0714
Kz109_1_F1_Contaminants.csv	4HCCA Cluster	1060.0879
Kz109_1_F1_Contaminants.csv	Bovine Casein a-S1	1267.7045
Kz109_1_F1_Contaminants.csv	Porcine Trypsin, Methylated	2720.3634
Kz48_F1_Contaminants.csv	4HCCA Cluster	855.0714
Kz48_F1_Contaminants.csv	4HCCA Cluster	1060.0879
Kz48_F1_Contaminants.csv	Bovine Casein a-S1	1267.7045
Kz48_F1_Contaminants.csv	Keratin (Human)	2501.0672
Kz48_F1_Contaminants.csv	Keratin (Human)	2501.2518
Kz116underscore1_F1_Contaminants.csv	4HCCA Cluster	855.0714
Kz116underscore1_F1_Contaminants.csv	4HCCA Cluster	1060.0879
Kz116underscore1_F1_Contaminants.csv	Porcine Trypsin, Methylated	2720.3634
Kz08_1_Contaminants.csv	Bovine Casein a-S1	1267.7045
Kz08_1_Contaminants.csv	Keratin (Human)	1329.6393
Kz08_1_Contaminants.csv	Porcine Trypsin, Methylated	2720.3634

Kz79_F2_Contaminants.csv	4HCCA Cluster	855.0714
Kz79_F2_Contaminants.csv	Keratin	2705.1611
Kz79_F2_Contaminants.csv	Porcine Trypsin, Methylated	2720.3634
Kz07_F1_Contaminants.csv	4HCCA Cluster	855.0714
Kz07_F1_Contaminants.csv	4HCCA Cluster	1060.0879
Kz07_F1_Contaminants.csv	Porcine Trypsin, Methylated	2720.3634
Kz45_F1_Contaminants.csv	4HCCA Cluster	855.0714
Kz45_F1_Contaminants.csv	4HCCA Cluster	861.0794
Kz45_F1_Contaminants.csv	4HCCA Cluster	1060.0879
Kz116_F2_Contaminants.csv	Porcine Trypsin, Methylated	2720.3634
Kz88_F3_Contaminants.csv	Bovine Casein a-S1	1267.7045
Kz88_F3_Contaminants.csv	Keratin (Human)	1707.7721
Kz88_F3_Contaminants.csv	Keratin (Human)	2566.2784
Kz88_F3_Contaminants.csv	Porcine Trypsin, Methylated	2720.3634